



저작자표시-비영리-변경금지 2.0 대한민국

이용자는 아래의 조건을 따르는 경우에 한하여 자유롭게

- 이 저작물을 복제, 배포, 전송, 전시, 공연 및 방송할 수 있습니다.

다음과 같은 조건을 따라야 합니다:



저작자표시. 귀하는 원저작자를 표시하여야 합니다.



비영리. 귀하는 이 저작물을 영리 목적으로 이용할 수 없습니다.



변경금지. 귀하는 이 저작물을 개작, 변형 또는 가공할 수 없습니다.

- 귀하는, 이 저작물의 재이용이나 배포의 경우, 이 저작물에 적용된 이용허락조건을 명확하게 나타내어야 합니다.
- 저작권자로부터 별도의 허가를 받으면 이러한 조건들은 적용되지 않습니다.

저작권법에 따른 이용자의 권리는 위의 내용에 의하여 영향을 받지 않습니다.

이것은 [이용허락규약\(Legal Code\)](#)을 이해하기 쉽게 요약한 것입니다.

[Disclaimer](#)

**A THESIS
FOR THE DEGREE OF DOCTOR OF PHILOSOPHY**

**Characterization of bioactive components from
arsenic-lower Jeju *Hizikia fusiforme***

Yu Lin Dai

DEPARTMENT OF MARINE LIFE SCIENCES

GRADUATE SCHOOL

JEJU NATIONAL UNIVERSITY

February, 2020

**Characterization of bioactive components from
arsenic-lower Jeju *Hizikia fusiforme***

Yu Lin Dai

(Supervised by Professor You-Jin Jeon)

A thesis submitted in partial fulfillment of the requirement for the degree of

DOCTOR OF PHILOSOPHY

February, 2020

The thesis has been examined and approved by




Thesis director, Choon-Bok Song (PhD), Professor of Marine life sciences,



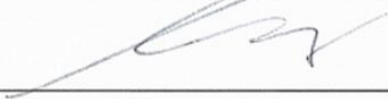
Gi-Young Kim (PhD), Professor of Marine life sciences,



You-Jin Jeon (PhD), Professor of Marine life sciences,



Bo-Mi Ryu (PhD), Research Professor of Marine Science Institute,



Jae-Young Oh (PhD), Research Professor of Marine Science Institute.

Date: 2020.02

DEPARTMENT OF MARINE LIFE SCIENCES

GRADUATE SCHOOL

JEJU NATIONAL UNIVERSITY

CONTENTS

SUMMARY	I
LIST OF TABLES	III
LIST OF FIGURES	IV

Part I. Acid- and hot water processing for arsenic-lower *Hizikia fusiforme*

1 Abstract	2
2 Introduction	3
3 Materials and methods	5
3.1 Materials	5
3.2 Hijiki origin and acid- hot water processing	5
3.3 Extraction of crude fucoidan (CF)	7
3.4 Extraction of alginic acid (HFA)	7
3.5 Fourier-transform infrared spectroscopy (FTIR) characterization	8
3.6 Liquid chromatography-electrospray ionization-mass spectrometry (LC-ESI-MS) analysis	8
3.7 Evaluation of heavy metal content	8
3.8 Chemical composition analysis	8
3.9 Statistical analysis	9
4 Results and Discussion	9
4.1 FTIR analysis	9
4.2 LC-ESI-MS analysis	11
4.3 Heavy metal ion content of Hijiki	11
4.4 Chemical compositions in processed and unprocessed Hijiki	18
5 Conclusion	18

Part II. Bioactivities of the polysaccharides from three collected-areas *Hizikia fusiforme*

1 Abstract	20
2 Introduction	22
3 <i>Materials and methods</i>	24
3.1 Materials	24
3.2 Extraction of active fractions from CF	24
3.3 Chemical analysis	25
3.3.1 Chemical composition	25

3.3.2 Analysis of the distribution of molecular weights	25
3.3.3 FTIR characterization.....	25
3.3.4 Nuclear Magnetic Resonance spectroscopy (NMR) analysis.....	25
3.3.5 LC-ESI-MS analysis.....	25
3.4 Screening anticancer effect of three locations Hijiki	26
3.4.1 Cell culture and cell viability.....	26
3.4.2 Apoptotic and necrotic body formation.....	26
3.4.3 Apoptosis analysis by flow cytometry	27
3.4.4 Determination of mitochondrial membrane potential	27
3.4.5 Measurement of cytochrome c release	27
3.4.6 Western blot analysis.....	27
3.5 Antioxidant effect of JHCF4	28
3.5.1 Radical scavenging assays by using electron spin resonance (ESR) spectrometer.....	28
3.5.2 Cell culture.....	28
3.5.3 Antioxidant activity against AAPH-induced cellular damage.....	28
3.5.4 Nuclear staining with Hoechst 33342	28
3.5.5 Apoptosis analysis by flow cytometry	29
3.5.6 Western blot analysis.....	29
3.5.7 Analysis of oxidative stress in AAPH treated zebrafish in 72 h post-fertilization (hpf).....	29
3.6 Hepato-effective effect of JHCF4	30
3.6.1 Cell culture.....	30
3.6.2 Protective effect of JHCF4 against ethanol-induced cellular damage	30
3.6.3 Nuclear staining with Hoechst 33342	30
3.6.4 Apoptosis analysis by flow cytometry	31
3.6.5 Western blot analysis.....	31
3.6.6 Analysis of oxidative stress in ethanol treated zebrafish (72 hpf)	31
3.6.7 Measurement of steatosis contents in ethanol treated zebrafish (128 hpf).....	32
3.6.8 Measurement of malondialdehyde (MDA), and glutathione (GSH) contents in ethanol treated zebrafish in 128 hpf.....	32
3.7 Anti-inflammatory effect of HFA against Fine dust (FD).....	33
3.7.1 Cell culture.....	33
3.7.2 Measurement of cell viability and ROS production.....	33
3.7.3 Nuclear staining with Hoechst 33342	33
3.7.4 Evaluation of inflammatory responses	34
3.7.5 Evaluation of heavy metal content in FD-treated keratinocytes.....	34
3.7.6 Enzyme immunoassay analysis.....	35

3.7.7 Western blot analysis.....	35
3.7.8 Analysis of inflammatory responses in FD treated zebrafish in 72 hpf	35
3.8 Statistical analysis	36
4 Results and Discussion.....	36
4.1 Screening anticancer effects for three locations Hijiki	36
4.2 Antioxidant effects of JHCFuc	56
4.3 Hepato-protective effect of JHCFuc against ethanol-induced damage.....	65
4.4 Anti-inflammatory potential of HFA against FD-induced inflammatory responses.....	75
5 Conclusion	92

Part III. Anti-inflammatory potential of the fucoxanthin-rich fraction from *Hizikia fusiforme* against fine dust-induced inflammatory responses *in vitro* and in a zebrafish model

1 Abstract	94
2 Introduction	95
3 Materials and methods	96
3.1 Preparation of FxRF	96
3.2 Chemical analysis of FxRF.....	96
3.3 Cell culture	97
3.4 Nuclear staining and ROS measurement.....	97
3.5 Evaluation of inflammatory responses	97
3.6 Western blot analysis	98
3.7 Zebrafsh embryo experiments	99
3.8 Statistical analysis	99
4 Results and Discussion.....	100
4.1 HPLC and RRLC-MS analysis of FxRF	100
4.2 Measurement of FxRF against FD-induced inflammatory responses in keratinocytes	103
4.3. Protective effect of FxRF against FD-induced apoptotic body formation in keratinocytes.....	103
4.4 Measurement of FxRF against FD-induced inflammatory responses in RAW 264.7 macrophages	107
4.5 Inflammatory responses in RAW 264.7 macrophages induced with a culture medium collected from FD-induced FxRF treatment keratinocytes	110
4.6 The anti-inflammatory effects of FxRF on the FD-induced zebrafish embryo model	113
5 Conclusion	117

Part IV. Isolation of saringosterol acetate from *Hizikia fusiforme* and its bioactivities

1 Abstract	119
2 Introduction	120
3 Materials and Methods	121
3.1 Preparation and identification of saringosterol acetate (SA).....	121
3.1.1 Preparation of hexane extracts from Hijiki.....	121
3.1.2 Isolation and identification of SA	121
3.2 Anticancer effect of SA against on MCF-7 cancer cells	121
3.2.1 Cell culture.....	121
3.2.2 Measurement of cell viability	122
3.2.3 Apoptotic and necrotic body formation.....	122
3.2.4 Apoptosis analysis by flow cytometry	122
3.2.5 Western blot analysis.....	122
3.3 Anti-obesity effect of SA against adipogenesis in adipocytes.....	123
3.3.1 Cell culture and adipocyte differentiation	123
3.3.2 Measurement of lipid accumulation	123
3.3.3 Measurement of triglyceride contents	123
3.3.4 Western blot analysis.....	124
3.4 Statistical analysis	124
4 Results and Discussion.....	124
4.1 Isolation and identification SA from Hijiki.....	124
4.2 Anticancer effect of SA against on MCF-7 cancer cells	126
4.2.1 Cytotoxicity of SA	126
4.2.2 Apoptosis morphology of SA on MCF-7 cancer cells	126
4.2.3 Apoptosis pathway regulated by SA	126
4.3 Anti-obesity effect of SA against adipogenesis in adipocytes.....	131
4.3.1 SA suppresses adipocyte differentiation	131
4.3.2 SA regulates adipogenesis-related factors in adipocytes.....	131
4.3.3 SA regulates AMPK and ACC factors in adipocytes.....	131
5 Conclusion	136
REFERENCE	137
ACKNOWLEDGEMENT	157

SUMMARY

Traditional medical application becomes potential supplement which is widely used as therapies for avoiding diseases in oriental countries [1]. Ocean is regarded as a life blood of all living creature with more than 70% of water mass surrounded on earth [2]. There are predicts 2.2 million eukaryotic species living under the water [3], hence marine product is a promising resource for medical application [4]. Seaweed, also named algae, refers to three types, Rhodophyta (red seaweed), Phaeophyta (brown seaweed), and Chlorophyta (green seaweed) [5]. *Hizikia fusiforme*, Hijiki, is a well-known brown seaweed that has been consumed as a marine resource for hundred years in Korea, Japan, and China [6, 7]. Hijiki is used as functional food because of its widely range of bioactivities [8, 9]. It is rich in nutrients including polysaccharides and mineral elements, and shows beneficial effects such as anticancer, immunomodulating activities, and anti-mutagenic effects [10-12].

Hijiki contains higher amounts of mineral elements than other foods [13]. At certain doses, most of mineral elements are regarded as nutrition, but some metals are human toxicants such as inorganic arsenic (iAs). iAs tend to be more toxic than organic arsenic, and the concentrations of iAs in Hijiki are as high as hundreds of ppm. It is indicated that the As concentration is greatly exceeds the limit stated under the provisional tolerable weekly intake, as advised by the World Health Organization (WHO) [14]. Chronic and acute exposure to arsenic leads to cancer, neurological disorders, liver disease, renal disease, and other health disorders [15, 16]. Acid-wash and hot water cooking are the most widely used methods to iAs removal [17-20], and the level of iAS intake allows the limits recommended by the WHO.

In this work, one percentage of citric acid- and hot water processing was performed to remove AS in Hijiki. The As-lower Hijiki was used for separated and isolated different bioactive fractions depend on their polarity. There are three active fractions: polysaccharides, saringosterol acetate, and fucoxanthin, which were isolated from water, hexane, and chloroform extraction, respectively. In water extraction, polysaccharides are the high amounts and bioactivities fractions. In polysaccharides, alginic acid and fucoidan are the two major active compounds. Alginic acid is a protonized water-insoluble polysaccharide, and comprises a family of unbranched binary copolymers of (1→4) linked β -D-mannuronic acid and α -L-guluronic acid [21]. Fucoidan is a sulfate-rich polysaccharide [22], which have been investigated its biological properties such as antioxidant, antiviral, anticancer, anti-inflammatory, anti-coagulant,

anti-angiogenic, and anti-adhesive effects [23-27]. In seaweeds, the molecular weight, sulfate content, and monosaccharide composition are the three main factors linked to the biological activity of fucoidan [28]. Moreover, the structural characteristics of fucoidan differ depending on the extract method, seaweed species, harvest season, geographic area, and algal maturity [24, 29-31]. Therefore, in the present work, the bioactivities of polysaccharides from AS-lower Hijiki were evaluated. In hexane extraction, saringosterol acetate was isolated by using centrifugal partition chromatography, and the anticancer and anti-obesity effects of saringosterol acetate were evaluated. In chloroform extraction, fucoxanthin-riched fraction was isolated and evaluated its anti-inflammatory effect against FD-induced inflammatory responses. Taken together, the aim of this study is to explore and discover the various properties of compounds of AS-lower Hijiki from different collected locations.

LIST OF TABLES

Table 1-1 Metal ion compositions in unprocessed and citric acid-processed Jeju Hijiki (JH).

Table 1-2 Metal ion compositions in unprocessed and citric acid-processed Wando Hijiki (WH).

Table 1-3 Metal ion compositions in unprocessed and citric acid-processed Chinese Zhejiang Hijiki (CH).

Table 1-4 Proximate compositions of general components in unprocessed and acid-processed JH.

Table 2-1 Chemical compositions of crude polysaccharides (JHCP), fucoidan (JHCFuc) and its fractions (JHCF1-JHCF4).

Table 2-2 Scavenging activities of crude polysaccharide (CP) and fucoidan (CF) from JH against DPPH, hydroxyl, and alkyl radical.

Table 2-3 Chemical composition of the purified HFA.

HFA: alginic acid of *Hizikia fusiforme*.

Table 2-4 Elemental metal composition of keratinocytes.

LIST OF FIGURES

Figure 1-1 Acid- and hot water processing of three locations Hijiki, JH, CH, and WH.

Figure 1-2 FT-IR spectroscopic analysis of structural features of JHCFucs. JHCFuc-acetic acid processing: crude fucoidan isolated from 1% acetic acid washed JH; JHCFuc-citric acid processing: crude fucoidan isolated from 1% citric acid washed JH; JHCFuc-unprocessing: crude fucoidan isolated from JH.

Figure 1-3 FT-IR spectroscopic analysis of structural features of HFAs. HFA-acetic acid processing: alginic acid isolated from 1% acetic acid washed JH; HFA-citric acid processing: alginic acid isolated from 1% citric acid washed JH; HFA-unprocessing: alginic acid isolated from JH.

Figure 1-4 Total Ion Chromatograms (TICs) of 1% citric acid-processed and unprocessed JHCFuc.

Figure 2-1 Percentages of cell viability as a measure of cell proliferation after treatment with different concentrations of JHCPs from three locations Hijiki in sample 24 h treatment. (a) Vero, (b) A549, (c) HT-29, (d) HL-60, (e) B16F10, (f) MCF-7, and (g) Hep3B cells. JHCP: The crude polysaccharide extract of Hijiki harvested from Jeju-Korea. WHCP: The crude polysaccharide extract of Hijiki harvested from Wando-Korea. CHCP: The crude polysaccharide extract of Hijiki harvested from Zhejiang-China. All experiments were performed in triplicate, and each value represents the mean \pm SE. * $p < 0.05$, ** $p < 0.001$ were considered as significant compared to the control.

Figure 2-2 DEAE-cellulose chromatogram of the fucoidan separated from the extract of acid-processed JH.

Figure 2-3 Percentage of cell viability as a measure of cell proliferation after treatment with different concentrations of fractions. (a) Cytotoxicity of JHCFuc and four active fractions were determined by MTT assay with Vero cells. (b) Cytotoxicity of JHCF4 was determined by MTT assay with Hep3B cells in 24 h and 48 h JHCF4 treatment. All experiments were performed in triplicate, and each value represents the mean \pm SE. * $p < 0.05$, ** $p < 0.001$ were considered as significant compared to the control.

Figure 2-4 Characterization of the structural features of commercial fucoidan, JHCP, JHCFuc, and

JHCF4 using FT-IR and monosaccharide analysis. (a) Monosaccharide content of JHCF4 was analyzed using an HPAE-PAD spectrum compared with black line standard monosaccharide mixture and red line HPAE-PAD spectrum for the monosaccharide content of JHCF4. (b) The approximate molecular weight distribution of JHCF4. (c) FT-IR spectra of JHCF1-JHCF4, processed and unprocessed JHCP, JHCFuc were compared to commercial fucoidan for the spectral analysis.

Figure 2-5 Chemical analysis of JHCF4. (a) ESI Q-TOF MS spectrum JHCF4, and (b) spectrum of ^1H NMR.

Figure 2-6 Apoptosis effects of JHCF4. (a) The anticancer effects of JHCF4 induce apoptotic bodies in Hep3B cells using Hoechst 33342 after 48 h incubation. (b) The anticancer effects of JHCF4 induce apoptotic bodies in Hep3B cells using acridine orange/ethidium bromide (AO/EtBr) staining after 48 h incubation.

Figure 2-7 Anticancer effects of JHCF4 induced apoptotic bodies in Hep3B cells by flow cytometry. Cell cycle analysis was performed by propidium iodide (PI) staining. All experiments were performed in triplicate, and each value represents the mean \pm SE. * $p < 0.05$, ** $p < 0.001$ were considered as significant compared to the control.

Figure 2-8 Induction of reactive oxygen species (ROS) generation, the integrity of mitochondrial membrane, and cytochrome c release by JHCF4-induced apoptosis in Hep3B cells. (a) Hep3B cells were treated with 50 $\mu\text{g}/\text{mL}$ JHCF4 for 24 and 48 h, incubated with 2', 7'-dichlorofluorescein diacetate (DCFH-DA) for 30 min. (b) Hep3B cells were treated with JHCF4 (50 $\mu\text{g}/\text{mL}$) for 24 and 48 h, incubated with Rhodamine 123 (200 nM) for 30 min in the dark, then analyzed by flow cytometry. Data are presented as fluorescence intensity. (c) Hep3B cells were treated with JHCF4 (50 $\mu\text{g}/\text{mL}$) for the indicated durations. All experiments were performed in triplicate, and a representative experiment is presented.

Figure 2-9 Induction of apoptosis-related proteins degradation by JHCF4. (a) Hep3B cells were treated with different concentrations of JHCF4 at 48 h. (b) Hep3B cells were treated with JHCF4 (50 $\mu\text{g}/\text{mL}$) with different incubation periods. All experiments were performed in triplicate, and each value represents the mean \pm SE. * $p < 0.05$, ** $p < 0.001$ were considered as significant compared to the control.

Figure 2-10 Evaluation of the four fractions for toxicity and intracellular ROS scavenging activities

against AAPH-induced oxidative stress in Vero cells. (a) Toxicity assessment of the sample. (b) Protective activity of four fractions against AAPH-induced cytotoxicity. (c) Scavenging activity of four fractions on AAPH induced intracellular ROS. Results represent the percentage (%) of cell viability and intracellular ROS levels. Experiments were performed in triplicate and the data are expressed as the mean \pm SE. * $p < 0.05$, ** $p < 0.001$.

Figure 2-11 Protective effects of JHCF4 against AAPH-induced Vero cells. (a) Effect of JHCF4 on cellular ROS levels and apoptotic body formation induced by AAPH. Apoptotic body formation was observed under a fluorescence microscope after Hoechst 33342 staining. (b) Dysregulation of cell cycle progression was indicated by flow cytometric analysis of the apoptotic sub-G1 cell population in Vero cells. (c) Western blot analyses of Vero cells for measuring the expression of Bax, Bcl-xL, and caspase-3. Results are reproducible based on three independent determinations. Experiments were performed in triplicate and the data are expressed as the mean \pm SE. * $p < 0.05$, ** $p < 0.001$.

Figure 2-12 Protective effects of JHCF4 against AAPH-induced ROS production and lipid peroxidation in zebrafish embryo model. Microscopic fluorescence images of the embryos stained with DCFH-DA and DPPP in the ROS production and lipid peroxidation assay, respectively. The relative fluorescence intensities indicate the level in the stained embryos. Experiments were performed in triplicate and the data are expressed as the mean \pm SE. * $p < 0.05$, ** $p < 0.001$.

Figure 2-13 Protective effects of JHCF4 against ethanol-induced Chang liver cells. (a) Cytotoxicity of different concentrations of ethanol in Chang liver cells. (b) Protective effects of JHCF4 against ethanol-induced damage by MTT assay in Chang liver cells. (c) Protective effect of JHCF4 apoptotic body formation induced by ethanol in Chang liver cells. Apoptotic body formation was observed using a fluorescence microscope after Hoechst 33342 staining. (d) Chang liver cells were treated with or without the indicated concentrations of JHCF4 for 24 h. The percentage of apoptotic cells was subsequently analyzed by flow cytometry. (e) Western blot analyses of Chang liver cells for measuring the expression of Bax, Bcl-xL, and caspase-3. Results are reproducible based on three independent determinations. Experiments were performed in triplicate and the data are expressed as the mean \pm SE. * $p < 0.05$, ** $p < 0.001$.

Figure 2-14 Protective effects of JHCF4 against ethanol-induced in zebrafish. (a) Cell death, (b) ROS

production, and (c) Lipid peroxidation in zebrafish embryo model (72 hpf). (d) Acute ethanol exposure reduces viability of zebrafish larvae (128 hpf). Outline of the ethanol treatment protocol. Ethanol exposure began at 96 hpf and continued for up to 32 h (96-128 hpf). (e) Larvae treated with 0-3% ethanol were scored for mortality, and the average of three clutches is plotted during 32 h of exposure; error bars show the SE value. (f) Ethanol exposure results for steatosis after treatment with various concentrations of JHCF4 and alteration of lipid metabolism in zebrafish embryo model (128 hpf). Whole-mount Oil red O staining of larvae after exposure in the presence or absence of 2% ethanol for 32 h reveals steatosis; yellow dotted line denotes the liver. The percent of larvae with steatosis analyzed by Oil red O staining of 15 clutches, with an average of 20 larvae per treatment per clutch. (g) MDA content and (h) total GSH content of ethanol-induced liver tissues of zebrafish treated with various concentrations of JHCF4. (i) Western blot analysis of p53 in the liver tissues of ethanol-induced zebrafish treated with various concentrations of JHCF4 for 32 h and untreated controls. Experiments were performed in triplicate and the data are expressed as the mean \pm SE. * $p < 0.05$, ** $p < 0.001$.

Figure 2-15 FT-IR spectroscopic analysis of structural features of HFA. HFA-processing: alginic acid isolated from 1% citric acid washed Hijiki; HFA-unprocessing: alginic acid isolated from original Hijiki.

Figure 2-16 Approximate molecular weight distribution of HFA.

Figure 2-17 Efficacy of HFA against inflammation induced by FD in HaCaT keratinocytes. (a) Analyses of HaCaT cell viability and intracellular ROS levels; (b) Western blot analyses of cyclooxygenase (COX)-2 expressions; and (c) ELISA of prostaglandin E₂ (PGE₂) and pro-inflammatory cytokines (IL-1 β , IL-6, and TNF- α). Pre-seeded cells (1×10^5 cells/mL) were treated with different HFA concentrations after 24 h and stimulated with FD after 30 min. Cells were harvested after 24 h to measure inflammatory mediators (COX-2 and PGE₂) and pro-inflammatory cytokines (IL-1 β , IL-6, and TNF- α). Apoptotic body formation was observed under a fluorescence microscope after (d) DCFH-DA treatment and (e) Hoechst 33342 staining. Graphical representations are means \pm SE based on three replications. * $p < 0.05$ and ** $p < 0.01$ indicate that the values of sample treated groups were significantly different from those for the FD-treated group.

Figure 2-18 Efficacy of HFA against inflammation induced by FD in RAW 264.7 macrophages. (a) Analyses of RAW cell viability and intracellular ROS levels; (b) Western blot analyses of inducible nitric

oxide synthases (iNOS) and COX-2 expressions; and (c) ELISA of PGE₂ and pro-inflammatory cytokines (IL-1 β , IL-6, and TNF- α). Pre-seeded cells (1×10^5 cells/mL) were treated with different HFA concentrations after 24 h and stimulated with FD after 30 min. Cells were harvested after 24 h to measure inflammatory mediators (COX-2 and PGE₂) and pro-inflammatory cytokines (IL-1 β , IL-6, and TNF- α). Graphical representations are means \pm SE based on three replications. *p < 0.05 and **p < 0.01 indicate that the values of sample treated groups were significantly different from those for the FD-treated group.

Figure 2-19 Inflammatory stimulation of the RAW 264.7 macrophages by the culture medium of FD-induced HaCaT cells and the anti-inflammatory effects of HFA. (a) nitric oxide (NO) production and cytotoxicity, (b) Analysis of iNOS and COX-2 levels, and (c) inflammatory mediators, including tumor necrosis factor α (TNF- α), interleukin (IL)-1 β , IL-6, and PGE₂. The HaCaT cells were pre-seeded in culture plates (1×10^5 cells/mL), incubated for 24 h, and treated with different concentrations of HFA. After 1 h, the cells were treated with FD (125 μ g/mL) and 24 h later, the culture medium were treated to each pre-seeded RAW 264.7 macrophages culture well plates in real time. The evaluations were made after a 24 h. Experiments were carried out in triplicate, and the results are represented as means \pm SE. *p < 0.05 and **p < 0.01 indicate that the values of sample treated groups were significantly different from those for the FD-treated group. H-FD: The cultured medium of FD-stimulated in keratinocytes

Figure 2-20 Inflammatory stimulation of zebrafish larvae by FD and anti-inflammatory effects of HFA. The anti-inflammatory properties were evaluated by measuring NO and ROS production, and cell death in the zebrafish embryo model. Experiments were carried out in triplicate, and the results are represented as means \pm SE. *p < 0.05 indicate that the values of sample treated groups were significantly different from those for the FD-treated group.

Figure 3-1 Chemical information of fucoxanthin-rich fraction (FxRF) from Hijiki. (a) Extraction and isolation scheme for FxRF, 0M: The separated active fraction from elution of CHCl₃-MeOH mixture (100:0); 10M: The separated active fraction from elution of CHCl₃-MeOH mixture (90:10); 20M: The separated active fraction from elution of CHCl₃-MeOH mixture (80:20); 30M: The separated active fraction from elution of CHCl₃-MeOH mixture (70:30); 40M: The separated active fraction from elution of CHCl₃-MeOH mixture (60:40); 50M: The separated active fraction from elution of CHCl₃-MeOH

mixture (50:50). (b) The HPLC chromatographs of Fx standard and FxRF. The mobile phases used in the isocratic elution consisted of eluent: 0.1% formic acid water and 95% methanol. The flow rate was 0.3 mL/min and UV detection was observed at 445 nm. (c) The mass spectrum of fucoxanthin from FxRF.

Figure 3-2 Efficacy of FxRF against inflammation induced by FD in HaCaT keratinocytes. (a) Analyses of HaCaT cell viability and intracellular ROS levels; (b) Western blot analyses of COX-2 expressions; (c) Levels of key molecular mediators in the MAPK pathways; and (d) ELISA of PGE₂ and pro-inflammatory cytokines (IL-1 β , IL-6, and TNF- α). Pre-seeded cells (1×10^5 cells/mL) were treated with different FxRF concentrations after 24 h and stimulated with FD after 30 min. Cells were harvested after 24 h to measure inflammatory mediators (COX-2 and PGE₂) and pro-inflammatory cytokines (IL-1 β , IL-6, and TNF- α). Apoptotic body formation was observed under a fluorescence microscope after (e) DCFH-DA treatment and (f) Hoechst 33342 and PI staining. Graphical representations are means \pm SE based on three replications. * $p < 0.05$ and ** $p < 0.01$ indicate that the values of sample treated groups were significantly different from those for the FD-treated group.

Figure 3-3 Efficacy of FxRF against inflammation induced by FD in RAW 264.7 macrophages. (a) Analyses of RAW cell viability and intracellular ROS levels; (b) Western blot analyses of iNOS and COX-2 expressions; and (c) ELISA of PGE₂ and pro-inflammatory cytokines (IL-1 β , IL-6, and TNF- α). Pre-seeded cells (1×10^5 cells/mL) were treated with different FxRF concentrations after 24 h and stimulated with FD after 30 min. Cells were harvested after 24 h to measure inflammatory mediators (COX-2 and PGE₂) and pro-inflammatory cytokines (IL-1 β , IL-6, and TNF- α). Graphical representations are means \pm SE based on three replications. * $p < 0.05$ and ** $p < 0.01$ indicate that the values of sample treated groups were significantly different from those for the FD-treated group.

Figure 3-4 Inflammatory stimulation of the RAW 264.7 macrophages by the culture medium of FD-induced HaCaT cells and the anti-inflammatory effects of FxRF. (a) NO production and cytotoxicity, and (b) Analysis of iNOS and COX-2 levels and (c) Inflammatory mediators, including tumor necrosis factor α (TNF- α), interleukin (IL)-1 β , IL-6, and PGE₂. The HaCaT cells were pre-seeded in culture plates (1×10^5 cells/mL), incubated for 24 h, and treated with different concentrations of FxRF. After 1 h, the cells were treated with FD (125 μ g/mL) and 24 h later, the culture medium were treated to each pre-seeded RAW 264.7 macrophages culture well plates in real time. The evaluations were made

after a 24 h. Experiments were carried out in triplicate, and the results are represented as means \pm SE. * $p < 0.05$ and ** $p < 0.01$ indicate that the values of sample treated groups were significantly different from those for the FD-treated group. H-FD: The cultured medium of FD-stimulated in keratinocytes.

Figure 3-5 Inflammatory stimulation of zebrafish larvae by FD and anti-inflammatory effects of FxRF. The anti-inflammatory properties were evaluated by measuring NO and ROS production, and cell death in the zebrafish embryo model. Experiments were carried out in triplicate, and the results are represented as means \pm SE. Values are significantly different from the positive control (FD treated group) at * $p < 0.05$ and ** $p < 0.001$.

Figure 4-1 Preparation of SA of *H. fusiformis*. (a) TLC of SA collected from hexane extract of *H. fusiformis* by CPC. SA is indicated by black line, and (b) ESI-MS spectrum of SA. CPC condition: Stationary phase: upper organic phase; mobile phase: lower aqueous phase; flow rate: 2 mL/min; rotation speed: 1000 rpm; sample: 500 mg dissolved in 6 mL mixture of lower phase and upper phase (1:1, v/v) of the solvent system.

Figure 4-2 Cytotoxicity of SA on MCF-7 cancer cells and Vero kidney normal cells. Cells were treated to indicate concentrations of SA and measured by MTT assay. Experiments were performed in triplicate and the data are expressed as the mean \pm SE. * $p < 0.05$, ** $p < 0.001$.

Figure 4-3 Apoptosis effects of SA. (a) Effect of SA on the induction of apoptotic bodies, and (b) flow cytometry analysis of SA on the nuclear morphology in three cancer cells. Cells were stained with PI and Annexin V-FITC. Experiments were performed in triplicate and the data are expressed as the mean \pm SE. * $p < 0.05$, ** $p < 0.001$.

Figure 4-4 Apoptosis effects of SA on apoptosis-related proteins on MCF-7 cancer cells. Cells were treated with SA at the indicated concentration for 24 h. Experiments were performed in triplicate and the data are expressed as the mean \pm SE. * $p < 0.05$, ** $p < 0.001$.

Figure 4-5 Anti-obesity effect of SA in 3T3-L1 adipocytes. (a) Cytotoxicity of SA on cell viability of 3T3-L1 adipocytes for 2 days, 4 days, 6 days, and 8 days differentiation, and (b) SA inhibits intracellular lipid accumulation in 3T3-L1 adipocytes. (c) Lipid accumulation was determined by Oil Red O staining and (d) triglyceride levels. Experiments were performed in triplicate and the data are expressed as the

mean \pm SE. * $p < 0.05$, ** $p < 0.001$.

Figure 4-6 Anti-obesity effect of SA on signal factors in 3T3-L1 adipocytes. (a) Effect of SA treatment on adipogenic-related protein levels in 3T3-L1 adipocytes. (b) Effect of SA on phosphorylation of adipogenic-specific proteins in 3T3-L1 adipocytes. Experiments were performed in triplicate and the data are expressed as the mean \pm SE. * $p < 0.05$, ** $p < 0.001$.

Figure 4-7 SA suppresses activation of p-AMPK α in 3T3-L1 pre-adipocytes. Experiments were performed in triplicate and the data are expressed as the mean \pm SE. * $p < 0.05$, ** $p < 0.001$.

**Part I. Acid- and hot water processing for
arsenic-lower *Hizikia fusiform***

1 Abstract

The aim of this part is to optimize AS removed method for three regional *Hizikia fusiforme* (Zhejiang-China [CH], Jeju-Korea [JH], and Wando-Korea [WH]) in East Asia. CH, JH, and WH were processed using different acids (one percentage citric acid or one percentage acetic acid) and hot water to decrease heavy metal level and measured by using inductively coupled plasma optical emission spectrometry (ICP-OES). The crude fucoidan (CF) and alginic acid (HFA) were extracted from acids processed Hijiki and their structures were analyzed by using fourier-transform infrared spectroscopy (FTIR) and liquid chromatography-electrospray ionization-mass spectrometry (LC-ESI-MS). Our results indicate the chemical structures of CFs in two acids processed Hijiki were no significant difference compared to unprocessed Hijiki. However, compared to the unprocessed Hijiki, the structure of HFA from acetic acid processed Hijiki was strongly affected by acid-processing. Therefore, one percentage citric acid and hot water processing was selected as the appropriate AS removed method. These results may explain why the contents and structures of Hijiki were slightly affected by acid-processing.

2 Introduction

Seaweed has strongly bio-ability to uptake heavy metals [32]. Last century, the bio-ability of seaweed was used for cleaning waste water [33] and regarded as economical sorbents for industrial metals removal [34]. Previous study highlight that an application of seaweed *Sargassum* was used in heavy metals removal in rainwater runoff [35]. Recently, a new promising technology of seaweed for sequester heavy metals was developed [36]. Except bio-sorption of these biomasses, seaweeds with high nutritional value were used as folk medical application for hundred years and they exhibited a wide range of bioactivities such as anticancer, antioxidant, and anti-inflammatory effects [37-39]. For human, appropriate concentrations of metals such as potassium, sodium, and calcium are necessary to sustain their blood pressure [40] and bone function [41], whereas high amount of heavy metals such as lead, copper, and AS are observed to induce high risk health [42]. In algae, the high nutritional value and the high levels of heavy metal like “a double-edged sword”. High concentrations of heavy metals in edible seaweed becomes an obstacle for functional food development [43]. Therefore, seaweeds could be used as functional food with limited heavy metal contents.

AS, a metalloid, is located in the 33rd position in the Periodic Table [44], which is one of the most harmful metals for seaweed dietary [45]. Scientists have determined that arsenic trioxide (As_2O_3) is the strongest toxicity form, and iAS is regarded as an toxic marker in determination of food poison [46]. iAS can inactivate to more than two hundreds enzymes and further induce DNA synthesis disorder [47]. In cellular mitochondria, iAS stimulates morphological changes and increases cell oxidative stress [15]. Chronic and acute exposure to AS leads to cancer, neurological disorder, renal disease, and other health disorders [16].

The different regions have their strictly standard to control the uptake dose of AS. The intake AS standard of WHO in drinking water is recommended a maximum contaminant level of 10 ppb [48]; the AS standard of Asia Pacific Region is 50 ppb [49]; the AS national standard of US is 10 ppb [50]; the AS national standard of China is 50 ppb [51]; the AS national standard of Indian is 10 ppb [46]; and AS national standard of Bangladesh is 50 ppb [52]. For seaweed, only a few developed Western countries including US, Australia, Spain, and New Zealand have published their national guidelines in high risk of toxic metals, and a limitation for seaweed iAS is not allowed above a level of 1 ppm [53-55]. In 2019, the

Ministry of Food and Drug Safety in Korea allows AS should be no more than 4 ppm for food additives [56].

H. fusiformis, synonym Hijiki, is a popular food in East Asian countries, unfortunately, also presented in the highest level of iAS among all marine algae [57]. In 2004, the British Food Standard Agency issued that consumers are not suggested to consume Hijiki because of high levels of AS [58]. It was observed that As is reached more than hundreds ppm in Hijiki, indicating As concentration greatly exceeds the limit stated under the provisional tolerable weekly intake, as advised by the WHO [14]. As dietary, Hijiki is believed to induce cancer for Japanese population because of high AS accumulation [59]. A previous study showed that five species of seaweed, *Hizikia fusiformis*, *Laminaria japonica*, *Porphyra tenera*, *Undaria pinnatifida*, and *Palmaria palmate* have the different levels of heavy metals. These studies showed that seaweed dietary is associates with human health because of AS [60]. Thus, researchers are engaged to find an effective and low-cost way to remove heavy metals in seaweed.

In traditional method, washing- and soaking Hijiki was frequently used to reduce AS in Japan [17], and the temperature plays a key factor in iAS removal [61]. Japanese cooking method for dried Hijiki was performed as 20 times volumes of water for different treated time from 20 to 360 min without cooking. The result was observed that more than 50% of AS was diminished in long period processing [20]. Another pre-cook processing was used by soaking Hijiki in water, and cooking. It was found that the cooking is an effective method for AS removal [19].

In modern study, a better iAS removal condition was selected as pH 4, temperature 50°C, removal time at 8 h. It was observed that more than 95% AS removal, unfortunately, with more than 50% polysaccharides decreased [62]. A previous report was undertaken that aims to decrease more iAS content and keep more nutritional compositions. The method was set to citric acid concentration of 0.6%, temperature of 50°C. Following 2 h processing, the content of moisture, lipid, and protein in processed seaweed was relatively stable than those of unprocessed seaweed. The removal of AS was reached 89.6% [63]. Interestingly, a recent Korean study was developed a novel method; Hijiki was innovatively performed to heat (90°C for 5 min) and 2% NaCl solution to reduce AS concentration. The result met the national standard of marine functional food [64].

Taken together, acid- and hot water processing are the most widely used methods to decrease iAs

concentrations, and the intake of AS concentrations could adhere to the limits of the provisional tolerable weekly intake recommended by the WHO. In this work, the aim is to find an appropriate method to reduce AS content from different harvest locations of Hijiki.

3 Materials and methods

3.1 Materials

Heavy metal salts, potassium permanganate, and nitric acid were purchased from Sigma-Aldrich, USA. Multi-element Calibration Standard and calibration blank containing one percentage HNO₃ for PerkinElmer OPTIMA 7300DV inductively coupled plasma optical emission spectroscopy (ICP-OES) was purchased from Perkin Elmer Inc. USA. Ultrapure deionized water used as the blank and solvents were obtained from Millipore Milli-Q purifier. All other chemicals were analytical grade and obtained from commercial.

3.2 Hijiki origin and acid- hot water processing

H. fusiforme was harvested from Jeju-Korea (JH), Zhejiang-China (CH), and Wando-Korea (WH) in May 2017. The collected positions of JH, CH, and WH are 33°25'24.1"N/ 126°55'22.7"E, 27°50'27.9"N/ 121°02'53.9"E, 34°18'03.9"N/ 126°46'53.7"E, respectively. Repositories were deposited in Jeju National University (Jeju, Korea). In Fig. 1-1, it is observed that the appearances of fresh JH, CH, and WH were showed different color. Sample processed method was followed previous study with a slight modification [62]. The obtained Hijiki was cleaned with tap water and freeze dried. The dried Hijiki was washed by one percentage citric acid or acetic acid for 30 min separately. The two acids processing Hijiki were adjusted the pH 7.0 using distilled water. The samples were cooked in 90°C hot water for 10 min for removing heavy metals, and the boiled seaweeds were freeze dried and grounded into powder.

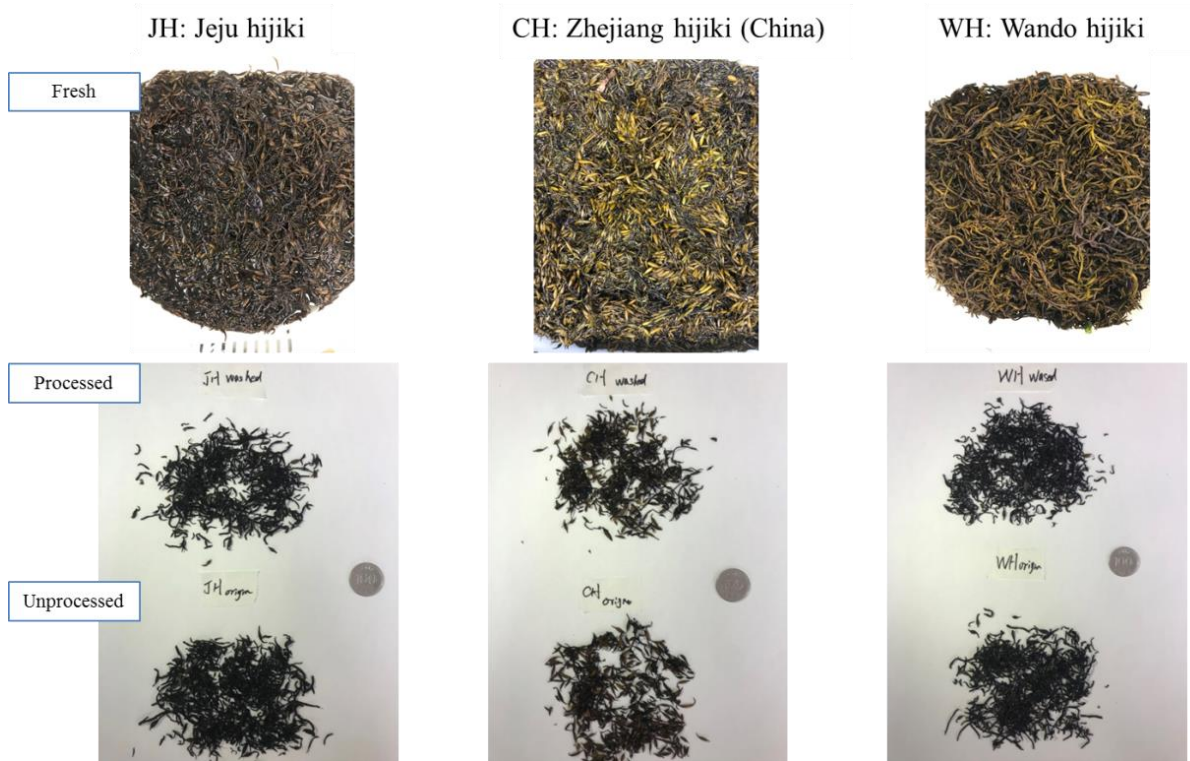


Figure 1-1 Acid- and hot water processing of three locations Hijiki, JH, CH, and WH.

3.3 Extraction of crude fucoidan (CF)

In order to evaluate two acids (citric acid and acetic acid) processing whether influence polysaccharide structure, we were extracted two main polysaccharides (fucoidan and alginic acid) and identified their compositions and structures.

The Hijiki powders (JH, CH, and WH) were separately homogenized with distilled water for 24 h at 50°C for water extraction. The water extract was evaporated under vacuum at 37°C and the precipitated product was obtained by centrifugation after adding 95% ethanol. The precipitated was re-dissolved in distilled water, dialyzed (MWCO, 10-12 kDa) against water at 4°C for 72 h with changing fresh distilled water each 12 h, and then finally lyophilized. The product was considered as crude polysaccharide (CP).

Fucoidan was isolated and separated from CP according to the previous protocol with a slight modification [65]. The CP solution adjusted to pH 8.0 for the 0.5% Alcalase assisted hydrolysis of proteins. Subsequently the solution was treated with 4 M CaCl₂ in pH 5.0 for purification. The precipitated product was clarified and the resultant supernatant was treated with ethanol to precipitate and then dialyzed and lyophilized. The product was considered as crude fucoidan (CF).

3.4 Extraction of alginic acid (HFA)

Alginic acid was extracted according to the previously protocol with slight modifications [66]. The dry sample powder was de-pigmented with 95% ethanol. The de-pigmented powder was immersed in 10% formaldehyde for 8 h, filtered through a wire sieve, and washed with 95% ethanol to remove any remaining formaldehyde. The powder was then air-dried and lyophilized. It was then immersed in dilute HCl (pH 4.0). HCl was added to sustain the pH value at 4.0. The suspension was agitated at 30°C for 24 h, filtered through a wire sieve, and washed with cold distilled water. It was then immersed in 5% Na₂CO₃ (w/v) and agitated at 30°C for 24 h to extract the alginic acid. The extract was filtered through a wire sieve and centrifuged at 4°C (10,000 × g for 10 min). The supernatant was then recovered. The mixture was adjusted to pH 6.0 by gradual additions of HCl. A saturated CaCl₂ solution was added to the mixture to precipitate the alginic acid as calcium alginic acid. The pellet was separated by centrifugation, suspended in 10% HCl for 2 h, and recovered by centrifugation. This acid wash was repeated 6 times. After the final washing, the pellet was suspended in distilled water and neutralized with NaOH. The dialyzed and lyophilized was powder considered as *H. fusiforme* alginic acid (HFA).

3.5 Fourier-transform infrared spectroscopy (FTIR) characterization

Samples were analyzed using a Thermo Scientific Nicolet 6700 FTIR spectrometer (MA, USA). Spectral measurements were taken within the frequency range of 500-2000 cm^{-1} .

3.6 Liquid chromatography-electrospray ionization-mass spectrometry (LC-ESI-MS) analysis

Samples were hydrolyzed with 0.2 M Trifluoroacetic acid (TFA) at 100 °C for 3 h, and then co-evaporated excess TFA with menthol, which of this method was followed by previous study [67]. The hydrolysate was dissolved with 0.5 mL of distilled water and filtrated through 0.45 μm filter, then analyzed by LC-MS.

ESI-MS spectra were performed by an ACQUITY UPLC system coupled with SYNAPT G2-Si HDMS (Waters, Manchester, UK) with an electrospray-ionization source in the negative-ion mode. The column was used as Waters Acquity BEH C18 1.7 μm (2.1 \times 100 mm), and column Temp was set to 40°C. The mobile phase system was: 0.1% formic acid in H₂O (A), and: 0.1% FA in acetonitrile (B). The flow rate was set to 0.3 mL/min, and the injection volume was set to 5 μL . The capillary was set to 2 kV; the cone voltage of 10V; the source temperature of 110°C; the desolvation temperature of 400°C. The MS Scan range was set to 100-2000 Da.

3.7 Evaluation of heavy metal content

Three locations Hijiki were ashed in muffle furnace. Subsequently the samples were incorporated 0.1mL of nitro hydrochloric acid mixture HCl: HNO₃=3:1 to each 1 mg of ash, and carried out the digestion at 100°C for 1h. Finally, the supernatants were filtered and diluted to concentration of 1 ppm using 3% HNO₃. All the solutions were analyzed using ICP-OES. The equipment was calibrated to perform the analysis using a multi-element calibration standard (PerkinElmer N9300233) including 10 ppm of Ag, Al, As, Ba, Be, Bi, Ca, Cd, Co, Cr, Cs, Cu, Fe, Ga, In, K, Li, Mg, Mn, Na, Ni, Pb, Rb, Se, Sr, Tl, U, V and Zn. Each element was detected at least by using three non-overlapping wavelengths.

3.8 Chemical composition analysis

The uronic acid and sulfate contents of the samples were estimated by Bitter *et al.*[68] and Dodgson *et al.*[69], respectively. The protein content was analyzed by the Lowry method [70]. The monosaccharide compositions of fractions were detected by HPLC [71].

3.9 Statistical analysis

All assays were made in three independent experiments. Values were expressed as the mean \pm standard error (SE). One-way ANOVA was used to analyze the mean values in GraphPad prism 5 software.

4 Results and Discussion

Acid- and hot water processing may influence the structure of polysaccharides. As the two main active polysaccharides, CF and HFA were extracted by two kinds of acids processed Hijiki to confirm whether the structure of them influenced by acid-processing. Based on these results, we selected a more “soft” acid processing as the used method.

4.1 FTIR analysis

FTIR is a widely used analytical technology to investigate and identify structural compounds or unknown mixtures [72]. Fig. 1-2 shows the FTIR spectrum of CF in JH (JHCFuc) from processed and unprocessed Hijiki. The observed peaks at 1261, 1230, 1056, and 802 cm^{-1} indicated the presence of C=O stretching vibration of an *O*-acetyl group, CH vibration of the polysaccharides composed of fucose, D-glucose, D-mannose, D-xylose, and galacturonic acid, CH_3 (fucose, *O*-acetyl), S=O stretching vibration, and S=O stretching of alkyl sulfoxide and anomeric region of carbohydrate. The peaks at 543 cm^{-1} reflect the C-O-S secondary axial sulfate group at C-4 of fructopyranose residue. In FTIR, the peaks between 1120 and 1270 cm^{-1} of two acid processed JHCFucs showed lower relative abundances compared to unprocessed crude fucoidan, while those of two different acids processing no different were observed. Thus, the sulfate content of processed sample was lower than in unprocessed sample. However, citric acid and acetic acid processed JHCFucs showed a slightly difference.

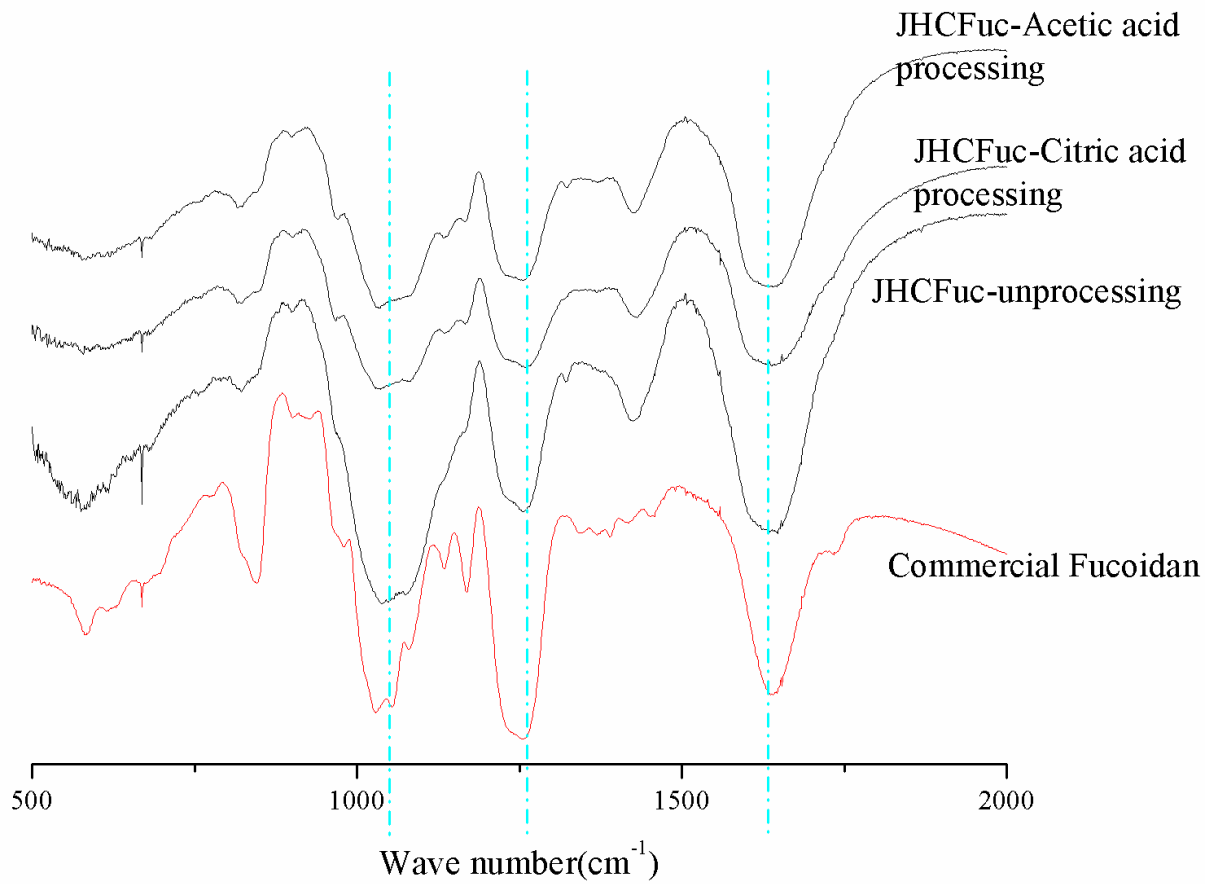


Figure 1-2 FT-IR spectroscopic analysis of structural features of JHCFucs. JHCFuc-acetic acid processing: crude fucoidan isolated from 1% acetic acid washed JH; JHCFuc-citric acid processing: crude fucoidan isolated from 1% citric acid washed JH; JHCFuc-unprocessing: crude fucoidan isolated from JH.

Fig. 1-3 shows the FTIR spectrums of two acid processed HFAs from processed and unprocessed Hijiki. The peaks were observed at wave numbers 3625 cm^{-1} , 1680 cm^{-1} , 1420 cm^{-1} , and 1035 cm^{-1} in both commercial sodium alginate and in the unprocessed and two acid processed HFAs spectra. Importantly, it is observed that the peaks of HFA in acetic acid processing much lower than those of citric acid processed HFA. We deduced that acetic acid was strongly influence to the structure of HFA. Thus, coupled with the spectrums of JHCFuc and HFA, the citric acid processing was selected as the final method to remove AS.

4.2 LC-ESI-MS analysis

Citric acid-processed and unprocessed JHCFucs were further analyzed by LC-ESI-MS, and their Total Ion Chromatograms (TICs) were exhibited good separation. It is observed that more ion peaks in TIC of unprocessed JHCFuc than processed JHCFuc. That means the unprocessed JHCFuc contained more detectable compounds than those of processed JHCFuc in LC-ESI-MS (Fig. 1-4). We suspected that the numbers of peaks in acid-processing lower than unprocessed JHCFuc because these small units were flowed away by acid processing. However, it is observed that more than 80% peaks were same in TICs of acid processed and unprocessed JHCFucs, illustrating that JHCFuc slightly influenced by acid-processing.

4.3 Heavy metal ion content of Hijiki

According to the FTIR and LC-MS spectrums, JH, CH, and WH were processed by 1% citric acid- and hot water. The metal contents of JH, WH, and CH are shown in Table 1-1, Table 1-2, and Table 1-3, respectively. In Table 1-1, the unprocessed JH contained the following metal elements at decreasing concentrations in the indicated order, K, Ca, Na, Mg, Sr, Fe, Al, and Zn, and these elements are naturally occurring nutrients in the human body. Heavy metals such as As are toxic and its concentration was significantly lower in acid-washed sample than in the unprocessed sample. AS concentration was markedly lower in acid-processed Hijiki (22 ppm) than in the unprocessed sample (89 ppm), illustrating iAS concentration in citric acid-processed Hijiki as a functional food ingredient adhere to the heavy metal intake limit standard published by the WHO. The AS contents in processed WH and CH also showed a significant decrease compared those of unprocessed Hijiki. According to these data, we found that JH showed the lowest AS content among the three locations acid-processed Hijiki.

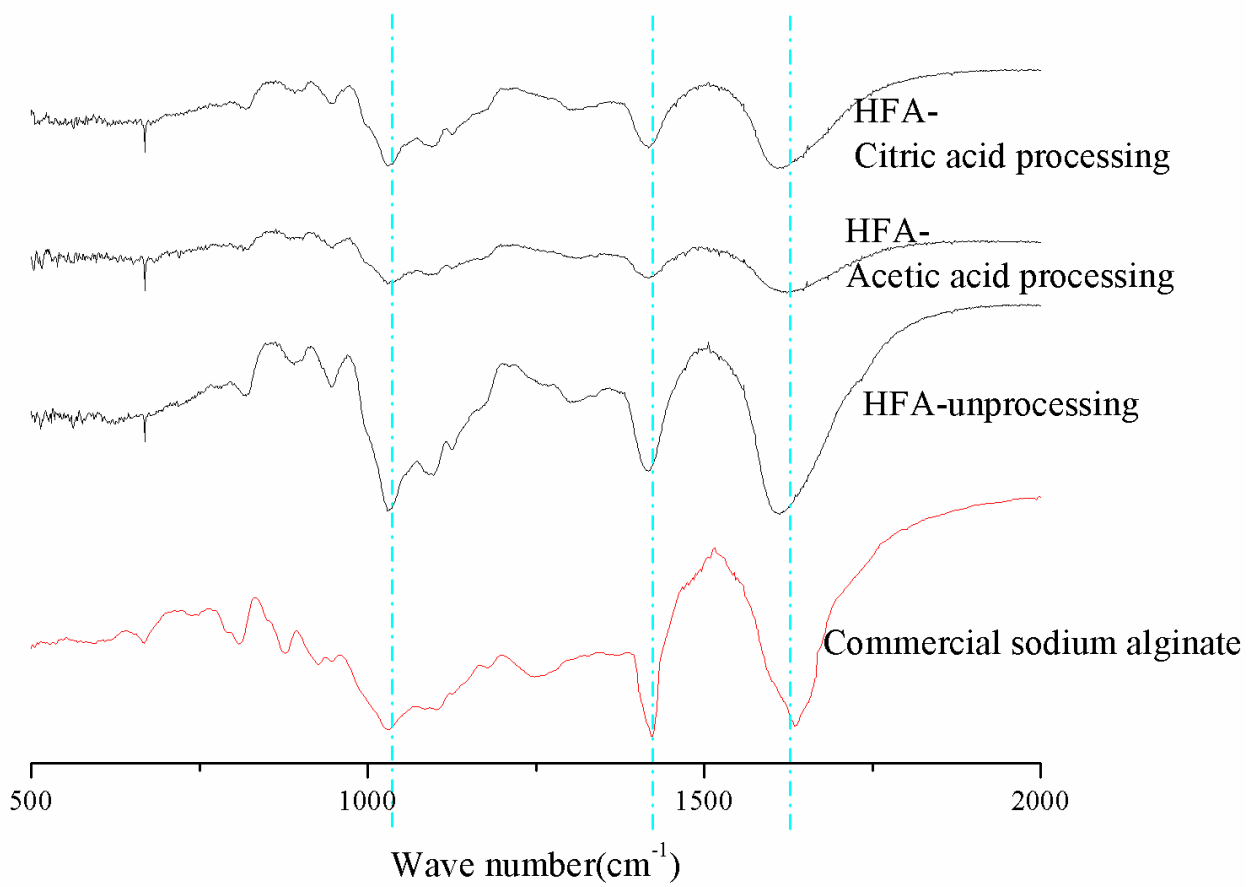


Figure 1-3 FT-IR spectroscopic analysis of structural features of HFAs. HFA-acetic acid processing: alginic acid isolated from 1% acetic acid washed JH; HFA-citric acid processing: alginic acid isolated from 1% citric acid washed JH; HFA-unprocessing: alginic acid isolated from JH.

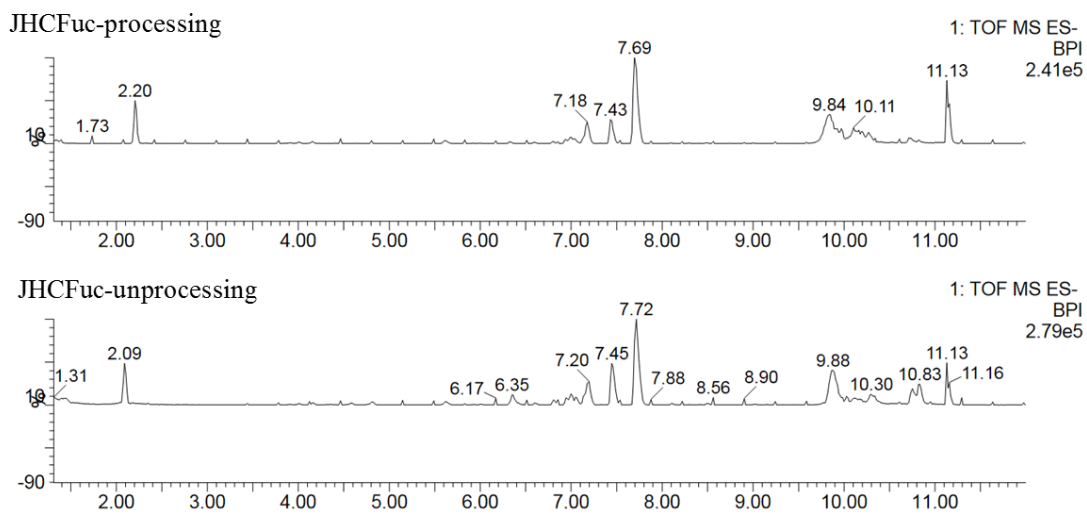


Figure 1-4 Total Ion Chromatograms (TICs) of 1% citric acid-processed and unprocessed JHCFuc.

Table 1-1 Metal ion compositions in unprocessed and citric acid-processed Jeju Hijiki (JH).

Metal ion (ppm)	Unprocessing	Acid-processing
K	28583.65	13267.62
Ca	11411.04	10788.79
Na	8067.29	4162.76
Mg	6424.56	5587.62
Sr	1296.38	1181.23
Fe	331.92	145.17
Al	55.18	45.07
As	89.75	22.64
Zn	N.D.	N.D.
Mn	N.D.	N.D.
Pb	N.D.	N.D.
Cu	N.D.	N.D.
Cr	N.D.	N.D.
Ni	N.D.	N.D.
Cd	N.D.	N.D.
Co	N.D.	N.D.
V	N.D.	N.D.

N.D. represents for not detect

Table 1-2 Metal ion compositions in unprocessed and citric acid-processed Wando Hijiki (WH).

Metal ion (ppm)	Unprocessing	Acid-processing
K	18249.24	9232.57
Ca	10132.54	8702.56
Na	13003.81	6180.68
Mg	5667.21	4590.52
Sr	1214.02	1020.37
Fe	871.33	312.53
Al	50.95	43.86
As	95.98	30.64
Zn	6.29.	4.79
Mn	N.D.	N.D.
Pb	N.D.	N.D.
Cu	5.12	3.25.
Cr	N.D.	N.D.
Ni	N.D.	N.D.
Cd	N.D.	N.D.
Co	N.D.	N.D.
V	N.D.	N.D.

N.D. represents for not detect

Table 1-3 Metal ion compositions in unprocessed and citric acid-processed Chinese Zhejiang Hijiki**(CH).**

Metal ion (ppm)	Unprocessing	Acid-processing
K	15325.42	10254.93
Ca	11703.59	10032.59
Na	8067.64	4162.76
Mg	6195.2	5422.95
Sr	853.51	625.21
Fe	472.21	321.83
Al	78.57	55.76
As	83.24	26.37
Zn	196.24	169.24
Mn	1.71	N.D.
Pb	N.D.	N.D.
Cu	2.34	N.D.
Cr	N.D.	N.D.
Ni	N.D.	N.D.
Cd	N.D.	N.D.
Co	N.D.	N.D.
V	N.D.	N.D.

N.D. represents for not detect

Table 1-4 Proximate compositions of general components in unprocessed and acid-processed JH.

Component (%)	Unprocessing*	Acid-processing*
Ash	15.2±0.05	11.1±0.06
Moister	5.26±0.23	5.34±0.39
Carbohydrate	59.7±3.25	50.3±4.01
Polyphenol	1.3±0.02	1.23±0.01
Protein	13.5±1.02	12.6±0.95

*Each value represents mean ±standard error (SE).

4.4 Chemical compositions in processed and unprocessed Hijiki

In JH, the extract of unprocessed sample showed higher ash content compared with the acid-processed sample in Table 1-4. The values of polyphenol, carbohydrate, and protein were higher in unprocessed samples than in processed samples. The carbohydrate content showed the largest decrease of 15% because hot water was used in processing, and carbohydrates easily dissolve in hot water. However, the extent of the decrease in carbohydrates was not as much as that of iAs content (75%).

In Korea, Wando Island is a well-known marine cultivate farmland [73]. Jeju Island is the largest Island in Korea with its famous marine products as well [74]. An investigation of AS content for different harvested locations seaweeds in Korea was performed by using HPLC-ICP-MS [75]. China has the biggest marine food market in the world and also the top country in seafood producing and consuming [76]. We have concluded these traditional and modern methods in AS removal in different countries. In the present study, we collected three locations Hijiki samples from Korea and China, combined these removed AS methods and selected an appropriate method to reduce AS content. Our results indicate acetic acid was strongly influence the structure of HFA, and JH showed the lowest AS content among these three areas citric acid processed Hijiki. It is also indicates that low loss of nutritional compositions in citric acid processing was observed. Therefore, in the next following Parts, citric acid processing was used for remove AS content in Hijiki.

5 Conclusion

AS exist high level in Hijiki and induces high risk in health. Citric acid- and hot water processing was used to remove AS in Hijiki, indicating a markedly reduction of AS. Additionally, the most concentrations of nutritional compounds were stay in processed Hijiki. JH showed the lowest AS content among three locations processed Hijiki. Therefore, JH could be a potential marine product for further investigation.

**Part II. Bioactivities of the polysaccharides from
three collected-areas *Hizikia fusiforme***

1 Abstract

The aim of this part is to investigate the various effects of polysaccharides from three regional AS-lower Hijiki (CH, JH, and WH). In Part I, Hijiki was selected to decrease heavy metal content by using 1% citric acid and 90°C hot water processing and JH showed lowest AS level among three samples.

In screening anticancer effects Hijiki, crude polysaccharide from JH (JHCP) was selected the best activity among three locations CPs. Further, the crude fucoidan from JH (JHCFuc) was separated using diethylaminoethyl (DEAE)-cellulose-ion exchange chromatography to obtain four active fractions (JHCF1-JHCF4) and their monosaccharide composition was detected using high-performance liquid chromatography (HPLC). The structure of JHCFuc and four fractions was analyzed using nuclear magnetic resonance (NMR), liquid chromatography-electrospray ionization-mass spectrometry (LC-ESI-MS), and fourier-transform infrared spectroscopy (FTIR). Moreover, in anticancer effects of these fractions, JHCF4 decreased Hep3B cell growth in 48 h with a half-maximal inhibitory concentration of $33.53 \pm 2.50 \mu\text{g/mL}$, which represented the strongest anticancer activity. Nuclear staining with Hoechst 33342 and acridine orange-ethidium bromide (AO/EtBr) staining demonstrated that the anticancer activity of JHCF4 was mediated by apoptosis. Moreover, JHCF4 downregulated B-cell lymphoma extra-large (Bcl-xL), while upregulating Bcl-2-associated X protein (Bax), caspase-3, and apoptotic bodies to different degrees in Hep3B cells. JHCF4 induced apoptosis via the generation of ROS along with the concurrent loss of mitochondrial membrane potential, indicating the potential role of the mitochondria-mediated pathway.

According to the results in anticancer effect of JHCF4, the antioxidant effect of JHCF4 was evaluated. Among fractions, JHCF4 showed the highest sulfate content and the lowest half-maximal inhibitory concentration (IC_{50}) scavenging activity against 2,2-diphenyl-1-picrylhydrazyl (DPPH), alkyl, and hydroxyl radicals, as well as protected against reactive oxygen species (ROS) in 2,2'-azobis(2-amidinopropane) dihydrochloride (AAPH)-treated Vero cells. Further, JHCF4 showed protective activity against AAPH-induced apoptosis, as observed by nuclear staining with Hoechst 33342. JHCF4 showed upregulated Bcl-xL and downregulated Bax, and caspase-3 in the background of increasing AAPH concentrations in Vero cells. JHCF4 induced apoptosis via a mitochondria-mediated pathway. Additionally, JHCF4 was selected for further *in vivo* analysis in a zebrafish model, which

markedly decreased ROS generation and lipid peroxidation. Thus, JHCF4 showed potential protective activity against AAPH-induced ROS both *in vitro* and in the zebrafish model.

In hepato-protective effect of JHCF4 study, the protective effects of JHCF4 against ethanol-induced cell damage and oxidative stress were investigated *in vitro* and *in vivo*. Furthermore, the low cytotoxicity and high cell viability of JHCF4 against ethanol-induced cell damage, as well as protection against ethanol-induced cell apoptosis, was observed via nuclear staining with Hoechst 33342 in Chang liver cells. Additionally, the treatment of the 72 h post-fertilization (hpf) zebrafish model with JHCF4 increased the ethanol-stimulated survival rate and decreased oxidative stress, lipid peroxidation, and cell death level. JHCF4 was found to significantly decrease steatosis production in the 128 hpf zebrafish model by Oil red O staining, and markedly attenuated the malondialdehyde (MDA) and glutathione (GSH) content compared to the blank group.

Other active polysaccharide isolated from *Hizikia fusiforme*, alginic acid (HFA), showed anti-inflammatory effects against Fine dust (FD)-induced inflammation. FD pollution is a serious environmental issue in industrial countries and causes disorders of the respiratory system and skin in humans. The structures of processed and unprocessed HFA were then analyzed by FT-IR, revealing little influence after citric acid-processing. HFA had a protective effect and inhibited the production of ROS, cyclooxygenase (COX)-2, prostaglandin E₂ (PGE₂), interleukin (IL)-1 β , and IL-6 in FD-induced HaCaT keratinocytes, and the expression of nitric oxide (NO), inducible nitric oxide synthases (iNOS), PGE₂, tumor necrosis factor- α (TNF- α) expression in FD-induced RAW 264.7 macrophages. Further, the inflammatory potential of the culture medium of FD-induced keratinocytes in macrophages and the expression of NO, iNOS, PGE₂, and pro-inflammatory cytokines was evaluated. HFA treatment significantly attenuated the inflammatory responses, indicating its effectiveness in suppressing inflammatory responses.

JHCF4 showed potential antioxidant, anticancer, and hepato-protective effects both *in vitro* and *in vivo*. HFA showed an anti-inflammatory effect by decreasing NO, ROS production, and cell death in FD-stimulated cells and zebrafish embryos.

2 Introduction

Cancer is a severe disease and the second leading cause of death worldwide [77]. The American Cancer Society reported that liver cancer is much more common in sub-Saharan African and Southeast Asian countries than it is in the US [78]. There are many risk factors associated with the development of cancer including heavy alcohol consumption, excess body weight, physical inactivity, and poor nutrition [79]. Cancer screening and precision medicine have become the most effective therapies in recent years. Although numerous synthetic anticancer drugs are developed yearly, most are unfortunately associated with toxicity and side effects [80]. Metabolic disorder sometimes caused by excessed oxidative stress [81]. Antioxidants from natural resources have protective effects against cellular death caused by free radicals and reactive oxygen species (ROS) [82]. Therefore, people living in developing countries are more inclined to consume natural antioxidant and anticancer functional foods than those in developed countries to prevent cancer.

Alcoholic liver disease (ALD) is a major cause of liver disease worldwide, as well as promoting the progression of nonalcoholic fatty liver disease and other liver diseases [83]. Alcohol dependence or abuse may cause depressive episodes, severe anxiety, insomnia, and abuse of other drugs [84]. Due to the high rate of incidence between ALD and other diseases, a series studies of the relationship between high alcohol consumption and risk of heart failure [85], atrial fibrillation [86], and coronary artery disease [87] have been carried out. Alcohol intake is strongly correlated with an increased stroke morbidity [88], and has been found to induce ALD via direct and indirect pathways [89]. Excessive alcohol drinking also disturbs metabolism of acetaldehyde and results in a wide range of health problems, including hangovers, liver damage, or even cancer.

Air contaminants have become an environmental issue of increasing concern especially in developing countries. Fine dust (FD) particles are the major contributors in air pollution, and exert detrimental effects in organisms [90]. The relationship between air pollution and daily mortality was surveyed in Beijing, China, dating back to the 1980s [91]. Over the last two decades, China's dramatic economic rise has been accompanied with the occurrence of haze or smog episodes, due to increased usage of coal-burning power, vehicles, and a series of agricultural activities [92]. FD with potentially toxic metals in aerosols is often present at concentrations well above the natural environmental conditions

in Asia [93, 94]. High risk of diseases including lung cancer, chronic respiratory and heart disease, weakening of the immune system, and reduction in lung function is associated with FD [95]. These particles have proved to have an adverse effect in respiratory complications and are believed to elicit allergic reactions and inflammatory responses in RAW 264.7 macrophages [96, 97]. Some studies have described the potential toxicological mechanisms and gene expression associated with FD and skin using human epidermal keratinocytes [98, 99]. Highly exposed parts of the human body such as the face, neck, and arms are easily infected by diseases. Foreign agents could cause alterations in the growth and differentiation patterns of exposed human tissues. These might result in the activation of inflammation or immune suppression that compromises the appearance of skin [100].

Fucoidan is a complex sulfate-rich polysaccharide in seaweed [22]. Previous reports have been investigated the biological properties of fucoidan, such as antioxidant, antiviral, anticancer, anti-inflammatory, anticoagulant, anti-angiogenic, and anti-adhesive effects [23-27]. In different seaweeds, molecular weight, sulfate content, and monosaccharide composition are the three main factors linked to the biological activity of fucoidan [28]. Moreover, the structural characteristics of fucoidan differ depending on the extraction method, seaweed species, harvest season, geographic area, and algal maturity [24, 29-31]. Some studies have examined fucoidan isolated and characterized from *H. fusiformis* [101, 102]. The antioxidant protective effect of fucoidan from Hijiki against diesel exhaust particles was investigated [103]. Previous studies have recovered on hepato-protective agents from natural products, including *Rhizoma Polygonati*, *Astragalus membranaceus* Bge., and *Herba Artemisiae Scopariae* [104]. Moreover, fucoidan extracted from seaweed has been found to have high antioxidant properties, and may therefore have the potential to be used as a natural hepato-protective agent [105, 106]. In addition, water extracts from fifty types of seaweed were screened for hepato-protective effects against alcohol in Korea [107]. In another study, the ethanol extracts from twenty types of algae against ethanol-induced oxidative damage *in vitro* and in an *in vivo* zebrafish model were investigated [108].

In the last decade, studies have found that antioxidant effects are associated with hepato-protective effects, providing an opportunity for the discovery of new agents against ALD from natural products [109]. A moderate correlation was found between the anticancer activity and the free radical scavenging properties of fucoidan [110]. Our study observed a potential antioxidant, anticancer, and

hepato-protective effects of active fraction (JHCF4) separated from crude fucoidan in AS-lower Hijiki (JHCFuc).

Alginic acid is a protonized water-insoluble polysaccharide [21]. It forms hydrogels, chelates metals and may possess antioxidant and anti-inflammatory effects [111-113]. Previous studies have examined the protective effect of alginic acid isolated from *Sargassum horneri* against urban aerosol-induced inflammatory responses [66]. Although some studies have investigated the effects of FD on the skin and respiratory system, the possible effects of alginic acid from *H. fusiforme* (HFA) remain sparsely studied. In this study, the protective effect of HFA against FD-induced inflammatory responses in keratinocytes and macrophages were evaluated. Our study observed a protective effect of HFA against FD-induced inflammatory responses as well.

Taken together, the aim of this study is to discover the various properties of polysaccharide extract of AS-low *H. fusiforme*.

3 Materials and methods

3.1 Materials

Potassium bromide, 1-phenyl-3-methyl-5-pyrazolone (PMP), monosaccharide standards (mannose, galactose, xylose, fucose, glucuronic acid), commercial fucoidan, heavy metal salts, potassium permanganate, hydrogen peroxide, and nitric acid were purchased from Sigma-Aldrich, USA. Dextran standards (788, 404, 212, 112, 47.3, 11.8, and 5.9 kDa) were purchased from Shodex (Tokyo, Japan). PL aquagel-OH column (300 mm × 8 mm, 8 μm) was purchased from Perkin Elmer (Massachusetts, USA). The fine dust was collected from Beijing, China (collected from 1996-2005; Certified Reference Material No. 28). Commercial sodium alginate was purchased from DaeJung chemicals metals Co., LTD, Korea. All other chemicals were obtained commercially and were of analytical grade.

3.2 Extraction of active fractions from CF

Crude polysaccharide (CP) from *H. fusiforme* was extracted and its method was showed in “Part I”. CPs were carried out for the screening of anticancer effect initially.

CF was separated and purified by anion-exchange chromatography. A diethylaminoethyl (DEAE)-cellulose column (17 cm × 2.5 cm) was pre-equilibrated with 50.0 mM sodium acetate buffer (pH 5.0). Column separation was performed with a gradient elution starting with 0 M to 2 M NaCl in

sodium acetate buffer. The column eluates were obtained as each 15.0 mL into 120 tubes. The polysaccharide content in each tube was measured by phenol-H₂SO₄ assay [114]. The positive tubes were pooled into different fractions and lyophilized. Then, each fraction was subjected to dialysis membranes to remove ionic contaminants and lyophilized.

3.3 Chemical analysis

3.3.1 Chemical composition

The uronic acid and sulfate contents of the samples were estimated by Bitter *et al.*[68] and Dodgson *et al.*[69], respectively. The protein content was analyzed by the Lowry method [70]. The monosaccharide compositions of fractions were detected by HPLC [71].

3.3.2 Analysis of the distribution of molecular weights

Samples were analyzed by agarose gel electrophoresis protocol with slightly modifications [115]. Samples and markers (1 mg/mL) were electrophoresed in 1% agarose gels using a Tris-Borate-EDTA running buffer (pH 8.3). The used molecular weight markers are Dextran sulfate MW 50-500 kDa (D8906 Sigma), chondroitin 6-sulfate MW≈60 kDa (C4384 Sigma), and Dextran sulfate MW≈8 kDa (D4911 Sigma). Electrophoresis was carried out for 20 min at 100V. The gel was stained with 0.02% o-Toluidine in 3% acetic acid containing 0.5% Triton X-100 and destained in 3% acetic acid.

3.3.3 FTIR characterization

Samples were analyzed using a Thermo Fisher Scientific Nicolet 6700 FTIR spectrometer (MA, USA). Spectral measurements were taken within the frequency range of 500-2000 cm⁻¹.

3.3.4 Nuclear Magnetic Resonance spectroscopy (NMR) analysis

NMR spectrum of samples were determined using a JEOL JNMECX 400, 400 MHz spectrometer (Japan) at 33 k. Samples were dissolved in deuterium oxide (4.65 ppm) and mixed with 1 μL of deuterated methanol (3.35, 4.78 ppm) as the internal standard. Proton NMR spectra were acquired with 128 scans.

3.3.5 LC-ESI-MS analysis

Samples were hydrolyzed with TFA followed by “Part I”. ESI-MS spectra were performed by an ACQUITY UPLC system coupled with SYNAPT G2-Si HDMS (Waters, Manchester, UK) with an electrospray-ionization source in the negative-ion mode. The column was used as Waters Acquity BEH

C18 1.7 μm ($2.1 \times 100 \text{ mm}$), and column Temp was set to 40°C . The mobile phase system was: 0.1% formic acid in H_2O (A), and: 0.1% FA in acetonitrile (B). The flow rate was set to 0.3 mL /min , and the injection volume was set to $5 \mu\text{L}$. The capillary was set to 2kV , the cone voltage of 10V , the source temperature of 110°C , the desolvation temperature of 400°C . The MS Scan range was set to $100\text{-}2000 \text{ Da}$.

3.4 Screening anticancer effect of three locations Hijiki

3.4.1 Cell culture and cell viability

MCF-7 human breast cancer, Hep3B human liver cancer, B16F10 Mus musculus skin melanoma, HL-60 human leukemia, HT-29 human colon cancer, A549 human lung cancer, and Vero monkey kidney epithelial cell lines were purchased from Korean Cell Line Bank (KCLB, Seoul, Korea). Roswell Park Memorial Institute medium (RPMI) Dulbecco's modified Eagle's medium (DMEM), penicillin/streptomycin (P/S), and fetal bovine serum (FBS) were obtained from Gibco Inc. (Grand Island, NY, USA). B16F10, MCF-7, and HT-29 cells were maintained in DMEM medium, Vero, A549, Hep3B, and HL-60 cells were cultured in RPMI medium; both medium contained 10% FBS and 1% P/S mixture. Cells were cultured at 37°C with a 5% CO_2 humidified condition. The cells were seeded at the density of 1×10^5 cells/mL in 96-well culture plates. After 24 h, the cells were treated with each sample at various concentrations. The cell survival rate was evaluated by 3-(4, 5-dimethylthiazol-2-yl)-2, 5-diphenyltetrazolium bromide (MTT) assay 24 h after sample treatment [116]. Based on the initial bioactivities screening results, JHCF4 was selected for the following study.

3.4.2 Apoptotic and necrotic body formation

3.4.2.1 Nuclear staining with Hoechst 33342

Cells were considered viable after stained nuclei homogeneously, while the observation of chromatin condensation and fragmentation indicating apoptosis [117]. Cells were seeded the density as 1×10^5 cells/mL in 24-well culture plates and added to various concentrations JHCF4 after 24 h. Then Hoechst 33342 (stock 1 mg/mL) was treated into each well for $10 \mu\text{L}$ after 48 h. Cells stained in 10 min with Hoechst 33342 in the dark and images were obtained using a fluorescence microscope equipped with a CoolSNAP-Pro color digital camera (Meyer Instruments, Inc., Houston, TX, USA).

3.4.2.2 Nuclear staining with acridine orange-ethidium bromide (AO/EtBr)

Cells were seeded at the density of 1×10^5 cells/mL in 24-well culture plates and treated with

different concentrations of JHCF4. After 48 h, 10 μ L of 100 μ g/mL AO/EtBr (Sigma-Aldrich) was added into each well. Cells were stained for 10 min. The double stain was washed twice using phosphate-buffered saline (PBS) and images were captured by a fluorescence microscope as the described above.

3.4.3 Apoptosis analysis by flow cytometry

Apoptotic cells were measured by FACS Calibur flow cytometric analysis. Treatment of JHCF4 with increasing concentrations in cells (2×10^5 cells/mL), and maintained in incubator for 48 h. Cells were collected and kept in 70% ethanol and washed with 2 mM EDTA in PBS, and continually stained with 100 μ g/mL PI and RNase for 30 min in dark. Data were analyzed using Cell Quest Pro software (Becton Dickinson, San Jose, CA, USA).

3.4.4 Determination of mitochondrial membrane potential

Rhodamine 123 is used for monitoring mitochondrial membrane, which preferentially partitions into active mitochondria depend on the negative mitochondrial membrane potential [118]. Rhodamine 123 solution was added to cells after the treatment with JHCF4 (50 μ g/mL) in different incubation periods. The Hep3B cells were harvested and washed with PBS in 30 min at 37°C in dark and then analyzed by flow cytometry.

3.4.5 Measurement of cytochrome c release

Mitochondrial and cytosolic fractions were isolated followed the previous protocol [119]. Briefly, cells were treated with JHCF4 (50 μ g/mL) in various incubation periods, washed twice in PBS and then resuspended in homogenizing buffer. Hep3B cells were kept in 30 min on ice, and then passed through a needle 10 times. Undamaged cells were continuously pelleted and obtained by centrifugation (750 g for 20 min). The content of cytochrome c was expressed by Western blotting as follows.

3.4.6 Western blot analysis

Cells (2×10^5 cells/mL) were seeded in single culture plates and incubated for 24 h, treatment of JHCF4 in order and obtained cells after 48 h. Cells were homogenized and centrifuged to remove precipitation, and protein supernatants were collected and determined by BCA protein kit (Thermo Fisher Scientific, MA, USA). Polyacrylamide gels (12%) were carried out to load 30 μ g of proteins of each sample with lysis buffer, and protein bands separated depend on molecular weight by using

electrophoresis method. The separated proteins were transferred onto nitrocellulose membranes. The membranes were blocked by 5% non-fat milk and incubated with primary antibodies and secondary antibodies by step. The membranes were treated by chemiluminescent substrate (Cyanagen Srl, Bologna, Italy) and the fluorescence images were carried out a FUSION SOLO Vilber Lourmat system (FUSION, Paris, France) [120]. Intensity of bands was calculated using Image J software.

3.5 Antioxidant effect of JHCF4

3.5.1 Radical scavenging assays by using electron spin resonance (ESR) spectrometer

The 2, 2-diphenyl-1-picrylhydrazyl (DPPH), alkyl, and hydroxyl free radical scavenging properties of four fractions were measured by ESR (JESFA200; Jeol, Tokyo, Japan), as followed by Nanjo, Hiramoto and Finkelstein, respectively [121-123].

3.5.2 Cell culture

Vero monkey kidney epithelial cell lines were purchased from Korean Cell Line Bank (KCLB, Seoul, Korea). Cultured condition of Cells and MTT assay are same as the described in “3.4.1”.

3.5.3 Antioxidant activity against AAPH-induced cellular damage

MTT assay was performed with measure cell survival rate, and ROS level assay was carried out with detect fluorescence intensity using a fluorescent probe dye in oxidation-sensitive, 2', 7'-dichlorofluorescein diacetate (DCFH-DA) in AAPH-induced Vero cells [124]. The Vero cells were seeded at a density of 1×10^5 cells/mL in 96-well culture plates. Three concentrations (37.5, 75 and 150 $\mu\text{g/mL}$) of JHCF4 were added to the cells after 24 h seeding. Following 1 h of incubation, cells were treated with AAPH; untreated cells were used as control. The MTT concentration was used as 2 mg/mL and the DCFH-DA concentration was used as 5 $\mu\text{g/mL}$ dissolved in PBS solution. The survival rate and ROS level of cells were measured after 48 h seeding.

3.5.4 Nuclear staining with Hoechst 33342

Cells were considered viable after stained nuclei homogeneously, while the observation of chromatin condensation and fragmentation indicating apoptosis [117]. Cells were seeded the density as 1×10^5 cells/mL in 24-well culture plates and added to various concentrations JHCF4 or 10 mM of AAPH solution after 24 h. Cells stained in 10 min with Hoechst 33342 in the dark and imaged using a fluorescence microscope as the described above.

3.5.5 Apoptosis analysis by flow cytometry

Apoptotic cells were measured by FACS Calibur flow cytometric analysis (Becton Dickinson, San Jose, CA, USA). Treatment of JHCF4 with increasing concentrations in cells (2×10^5 cells/mL), spiked with or without 10 mM AAPH 1 h later, and maintained in incubator for 24 h. Cells were collected and kept in 70% ethanol and washed with 2 mM EDTA in PBS, and continually stained with 100 μ g/mL propidium iodide (PI) and RNase for 30 min in dark. Data were analyzed and detected instrument as the described above.

3.5.6 Western blot analysis

Vero cells (2×10^5 cells/mL) were seeded in single culture plates and incubated for 24 h, treatment of increasing concentrations of JHCF4 and 10 mM of AAPH in order (the control were not treated with either JHCF4 or AAPH), and obtained cells after 24 h. Cells were homogenized and centrifuged to remove precipitation, and protein supernatants were collected and determined by BCA protein kit (Thermo Fisher Scientific, MA, USA). Polyacrylamide gels (12%) were carried out to load 30 μ g of proteins of each sample with lysis buffer, and protein bands separated depend on molecular weight by using electrophoresis technique. The separated proteins were transferred onto nitrocellulose membranes. The membranes were blocked by 5% non-fat milk and incubated with primary antibodies and secondary antibodies by step. The membranes were treated by chemiluminescent substrate and the fluorescence images were carried out a FUSION SOLO Vilber Lourmat system as the described above.

3.5.7 Analysis of oxidative stress in AAPH treated zebrafish in 72 h post-fertilization (hpf)

Zebrafish assay was carried out using the methods described previously [125]. DCFH-DA, an oxidant-sensitive fluorescent probe dye, was used to determine the generation of ROS in embryos. Diphenyl-1-pyrenylphosphine (DPPP) was used for measure the levels of lipid peroxidation, and acridine orange staining, a nucleic acid selective metachromatic dye, was used to evaluate the cell death in live embryos.

Adult zebrafish were supplied by a pet shop in Jeju, South Korea. Zebrafish were cultured in water with a 14/10 h light/dark cycle at 28.5°C. Embryos were collected by natural fertilization. At 7 h post-fertilization (hpf), the embryos were treated with or without the indicated concentrations of JHCF4 (25, 50, and 100 μ g/mL) and incubated 1 h. Fresh medium containing 15 mM AAPH was then added to

each well. After 24 h of incubation, the embryos were added fresh medium before separating and transferring randomly into 24-well plates. The embryos were then supplemented with fresh medium containing DCFH-DA solution (20 $\mu\text{g}/\text{mL}$), DPPP solution (25 $\mu\text{g}/\text{mL}$), and acridine orange solution (7 $\mu\text{g}/\text{mL}$), respectively. The embryos were incubated at 28.5°C for 1 h in the dark. The spectrofluorometer (Perkin-Elmer LS-5B, Austria) was used to calculate the fluorescence intensity of embryos. The CoolSNAP-Pro color digital fluorescent microscope (Olympus, Japan) was used to calculate the expressions of stained embryos.

3.6 Hepato-effective effect of JHCF4

3.6.1 Cell culture

Chang liver cells were purchased from Korean Cell Line Bank (KCLB, Seoul, Korea). Chang liver cells were cultured in DMEM medium. Cells cultured condition and MTT assay as the described above.

3.6.2 Protective effect of JHCF4 against ethanol-induced cellular damage

MTT assay was performed with measure cell survival rate in and ethanol-induced Chang liver cells [124]. The Chang liver cells were seeded at a density of 1×10^5 cells/mL in 96-well culture plates. Different concentrations of ethanol (1.25%, 2.5%, 4%, and 5%) were added to the cells. Three concentrations (37.5, 75 and 150 $\mu\text{g}/\text{mL}$) of JHCF4 were added to the cells after 24 h seeding. Following 1 h of incubation, cells were treated with ethanol (2.5%); untreated cells were used as control. Following incubation for 24 h, cells were treated in 50 μL PBS containing MTT (2 mg/mL). Cells were incubated for 3 h in the dark, and then a 200 μL of dimethyl sulfoxide (DMSO) was replaced excess medium in each well. The optical density of cells was measured at 540 nm. The survival rate of cells was measured after 48 h seeding.

3.6.3 Nuclear staining with Hoechst 33342

To determine the hepato-protective effects of JHCF4 after ethanol-induced nuclear morphology changes in Chang liver cells, Hoechst 33342 staining was used. Cells were considered viable after staining the nuclei homogeneously, while evidence of chromatin condensation and fragmentation indicated apoptosis [117]. Chang liver cells (1×10^5 cells/mL) were pre-seeded in 24-well culture plates and treated with different concentrations of JHCF4 and ethanol (2.5%) following incubation for 24 h. The control was not treated with either JHCF4 or ethanol. After 24 h, the cells were treated with 10 μL PBS

containing Hoechst 33342 (1 mg/mL) for 10 min at 37°C in the dark. After staining, images were obtained using a fluorescence microscope equipped with a CoolSNAP-Pro color digital camera as the described above.

3.6.4 Apoptosis analysis by flow cytometry

Apoptotic Chang liver cells were confirmed using a FACS Calibur flow cytometer (Becton Dickinson, San Jose, CA, USA). Chang liver cells were seeded at a density of 2×10^5 cells/mL for 24 h before treating with the indicated concentrations of JHCF4. Following 1 h of incubation, ethanol (2.5%) was spiked into each well and incubated for 24 h. Cells were harvested and preserved in 70% ethanol, then washed with PBS containing 2 mM EDTA. Subsequently, PBS solution containing PI (100 µg/mL) and RNase (20 µg/mL) was added to the cells for 30 min at 37°C in the dark. Data were analyzed using Cell Quest Pro software (BD Biosciences, San Jose, CA, USA). Data were analyzed and detected instrument as the described above.

3.6.5 Western blot analysis

Chang liver cells were seeded at a density of 2×10^5 cells/mL in culture plates for 24 h, then treated with JHCF4 and ethanol (2.5%) (The control was not treated with either JHCF4 or ethanol). Following 24 h of incubation, cells were harvested and homogenized using lysis buffer before centrifuging to remove any residues. The supernatants of the lysates were measured for their protein content using a BCA protein kit (Thermo Fisher Scientific, MA, USA). The loading samples containing 30 µg proteins and lysis buffer were loaded on 12% polyacrylamide gels, and bands were separated by using electrophoresis technique. Following transfer the gel onto nitrocellulose membranes, the membranes were blocked by 5% nonfat milk, and incubated with specific primary antibodies and secondary antibodies in sequence. In assay of signaling protein in 128 hpf zebrafish, total hepatic protein were separated on electrophoresis technique. The membranes blocked, primary antibodies and second antibodies treated were followed described above. The blots were developed by chemiluminescent substrate and the fluorescence images were performed by FUSION SOLO Vilber Lourmat system as the described above [120]. Expressions of blots were calculated using Image J software.

3.6.6 Analysis of oxidative stress in ethanol treated zebrafish (72 hpf)

Zebrafish assay was carried out and the method was followed previous studies [125]. Adult zebrafish

were supplied by a pet shop in Jeju, South Korea. Zebrafish were cultured in water with a 14/10 h light/dark cycle at 28.5°C. Embryos were collected by natural fertilization. At 7 h post-fertilization (hpf), the embryos were treated with or without the indicated concentrations of JHCF4 (25, 50, and 100 µg/mL) and incubated 1 h. Fresh medium containing 0.3% ethanol was then added to each well. After 24 h of incubation, the embryos were added fresh medium before separating and transferring randomly into 24-well plates. The DCFH-DA, DPPP, and acridine orange solutions were stained to the embryos, which those concentrations, treated time, and calculation of fluorescence intensity were followed “3.5.7”.

3.6.7 Measurement of steatosis contents in ethanol treated zebrafish (128 hpf)

The liver functions in 120 hpf zebrafish have been previously established, and were analyzed using multiple techniques [126]. Different concentrations of ethanol in zebrafish are associated with different survival rates. In our study, the survival rate was measured in 96 hpf zebrafish larvae treated with the indicated concentrations ethanol (0%, 0.5%, 1.5%, and 3%). Oil Red O staining was performed to measure the levels of steatosis in larvae according to a previous study, with slight modifications [127]. Whole larvae were fixed with PBS containing 4% formaldehyde. The fixed larvae was then washed with PBS and infiltrated with increase concentrations of 2-propanol. After staining the larvae with 2-propanol containing 0.5% Oil Red O overnight, the larvae were washed with decreasing concentrations of 2-propanol and transferred to 80% glycerol. The images of steatosis were obtained using a fluorescence microscope equipped with a CoolSNAP-Pro color digital camera (Meyer Instruments, Inc., Houston, TX, USA).

3.6.8 Measurement of malondialdehyde (MDA), and glutathione (GSH) contents in ethanol treated zebrafish in 128 hpf

The lipid peroxidation of the liver tissues were measured according the content of MDA [128] using a glutathione assay kit (MAK085; Sigma-Aldrich, MO, USA). Briefly, a 5 mg of dried whole larvae (approximates 30 larvae) were homogenized in 100 µL of iced MDA lysis buffer containing 1µL of BHT (100×), then centrifuged at 13,000 × g for 10 min. The supernatant was added to 300 µL MDA-thiobarbituric acid (TBA) adduct. A ratio of 1:3 of supernatant and MDA-TBA was obtained. The sample was incubated at 95°C for 60 min, and then allows cooling on ice. The absorbance of the solution was measured at 532 nm. A standard curve was prepared with MDA standard.

The measurement of total GSH levels was performed according to a previous study [129]. A glutathione assay kit (CS0260; Sigma-Aldrich, MO, USA) was used for the measurement. A total of 5 mg of dried whole larvae were homogenized in iced 5% 5-sulfosalicylic acid (SSA) and centrifuged at 10,000 $\times g$ for 10 min at 4°C. After removing the pellet, the supernatant was incubated with working solutions (1 \times assay buffer, glutathione reductase, and 5, 5'-dithio-bis-[2-nitrobenzoic acid] solution) at room temperature for 5 min. Following treatment with 0.16 mg/mL of NADPH, the GSH value was measured according to its kinetic read at 412 nm for 5 min. A standard curve was prepared using reduced form GSH.

3.7 Anti-inflammatory effect of HFA against Fine dust (FD)

3.7.1 Cell culture

RAW 264.7 macrophages and HaCaT keratinocytes were purchased from Korean Cell Line Bank (KCLB, Seoul, Korea). The cells were maintained in DMEM medium; both medium contained 10% FBS and 1% P/S mixture. Cells cultured condition was performed as the described above.

3.7.2 Measurement of cell viability and ROS production

Cells (1×10^5 cells/mL) were seeded in 96-well culture plates and treated in the presence or absence of indicated concentrations (25, 50 and 100 $\mu\text{g/mL}$) of HFA. After 1 h incubation, the cells were substituted in fresh medium before treated FD (125 $\mu\text{g/mL}$) for 30 min incubation. The cells untreated with HFA and FD was considered as control. Following incubation for 24 h, cells were treated in 50 μL PBS containing MTT (2 mg/mL) for detection of cell death. The cells were incubated for 3 h in the dark, and then a 200 μL of DMSO was replaced excess medium in each well. The MTT assay is recognized as a colorimetric assay, heavy metals strongly influence the value of cell viability. To avoid the influence of heavy metals in cell viability, DMSO containing formazan was centrifuged (10,000 $\times g$ for 10 min) and the supernatant was collected and measured under 540 nm. For ROS production, after incubation with samples for 24 h, cells were treated in 10 μL PBS containing 5 $\mu\text{g/mL}$ of DCFH-DA, and incubated for 10 min in the dark. The ROS productions of cells were detected using a fluorescence microscope equipped with CoolSNAP-Pro color digital camera (Meyer Instruments, Inc., Houston, TX, USA).

3.7.3 Nuclear staining with Hoechst 33342

Keratinocytes were seeded the density as 1×10^5 cells/mL in 24-well culture plates and added to

various concentrations HFA or FD (125 $\mu\text{g}/\text{mL}$) after 24 h. Then Hoechst 33342 (stock 1 mg/mL) was treated into each well for 10 μL after 24 h. Cells stained in 10 min with Hoechst 33342 in the dark and imaged by the fluorescence microscope. The fluorescence microscope was followed the described above.

3.7.4 Evaluation of inflammatory responses

RAW 264.7 macrophages and HaCaT keratinocytes were pre-seeded separately in different 24-well plates and incubated for 24 h. The different concentrations of HFA were then treated to each well. Following incubation for 1 h, cells was added to the presence or absence of the FD at concentration of 125 $\mu\text{g}/\text{mL}$. The wells were rinsed with fresh DMEM after additional 30-min incubation. The culture plates were continuously incubated for 24 h. The cell medium was harvested to analyze the inflammatory mediators and the pro-inflammatory cytokines. In HaCaT keratinocytes, cell viability, intracellular ROS production, the inflammatory mediators, and the pro-inflammatory cytokines were evaluated using MTT assay, DCFH-DA assay and commercial kit [130]. The metal ions contents of cells were harvested and analyze by PerkinElmer OPTIMA 7300DV inductively coupled plasma optical emission spectroscopy (ICP-OES). In macrophages, cell viability, NO production, the inflammatory mediators, and the pro-inflammatory cytokines were evaluated followed the previous protocols [131].

The pre-seeded keratinocytes was treated different concentrations of HFA and induced inflammation by FD for additional 30 min incubation. The wells were replenished with fresh DMEM and incubated for 24 h. The culture medium of FD-induced keratinocytes (H-FD) were treated with the pre-seeded macrophages in real time and analyzed for all the inflammatory mediators and the pro-inflammatory cytokines after 24 h incubation.

3.7.5 Evaluation of heavy metal content in FD-treated keratinocytes

The FD-induced keratinocytes were performed same as the described in “3.7.4”, and then the harvested keratinocytes were heated in 110 $^{\circ}\text{C}$ oven for 24 h. Subsequently the dried samples were incorporated 0.1 mL of nitro hydrochloric acid mixture $\text{HCl}:\text{HNO}_3=3:1$ to each 1 mg of sample and carried out the digestion at 100 $^{\circ}\text{C}$ for 1h. Finally, the supernatants were filtered and diluted to concentration of 1 ppm using 3% HNO_3 . Ultrapure deionized water used as the blank and solvents were obtained from Millipore Milli-Q purifier. The equipment was calibrated to perform the analysis using a multi-element calibration standard (PerkinElmer N9300233) including 10 ppm of Ag, Al, As, Ba, Be, Bi,

Ca, Cd, Co, Cr, Cs, Cu, Fe, Ga, In, K, Li, Mg, Mn, Na, Ni, Pb, Rb, Se, Sr, Tl, U, V and Zn. Each element was detected at least by using three non-overlapping wavelengths.

3.7.6 Enzyme immunoassay analysis

The medium was recovered and determined by commercial ELISA kits to evaluate the levels of pro-inflammatory cytokines and inflammatory mediators. The kits were purchased from Thermo Fisher Scientific (Waltham, MA, USA), R&D Systems (Minneapolis, MN, USA), Becton Dickinson & Co. (Franklin Lakes, NJ, USA), and Invitrogen (Carlsbad, CA, USA). The analysis method was followed the manufacturer's guidelines.

3.7.7 Western blot analysis

Cells (2×10^5 cells/mL) were seeded in single culture plates and incubated for 24 h, treatment of HFA and FD in order and obtained cells after 24 h. Cells were homogenized and centrifuged to remove precipitation, and protein supernatants were collected and determined by BCA protein kit (Thermo Fisher Scientific, MA, USA). Polyacrylamide gels (12%) were carried out to load 30 μ g of proteins of each sample with lysis buffer, and protein bands separated depend on molecular weight by using electrophoresis method. The separated proteins were transferred onto nitrocellulose membranes. The membranes were blocked by blocking buffer and incubated with primary antibodies and secondary antibodies by step. The membranes were treated by chemiluminescent substrate and the fluorescence images were carried out a FUSION SOLO Vilber Lourmat system as the described above.

3.7.8 Analysis of inflammatory responses in FD treated zebrafish in 72 hpf

Adult zebrafish were supplied by a pet shop in Jeju, South Korea. Zebrafish were cultured in water with a 14/10 h light/dark cycle at 28.5°C. Embryos were collected by natural fertilization. The experiments of FD-induced ROS, NO production, and cell death in embryos were evaluated. According to the our previous protocol [131], the treated concentration of FD at 10 μ g/mL was used in embryo viability assay. In brief, the embryos were transferred to 12-well plates and treated with different concentrations HFA followed by FD treatment. Following incubation for 72 h, the hatched larvae were stained by 4-Amino-5-methylamino-2', 7'-difluorofluorescein diacetate (DAF-FM DA), DCFH-DA and acridine orange respectively to identify NO productions, ROS levels, and cell death in the dark. The spectrofluorometer (Perkin–Elmer LS-5B, Austria) was performed to calculate the fluorescence intensity

of each embryo and intensity of stained embryos was calculated using Image J software.

3.8 Statistical analysis

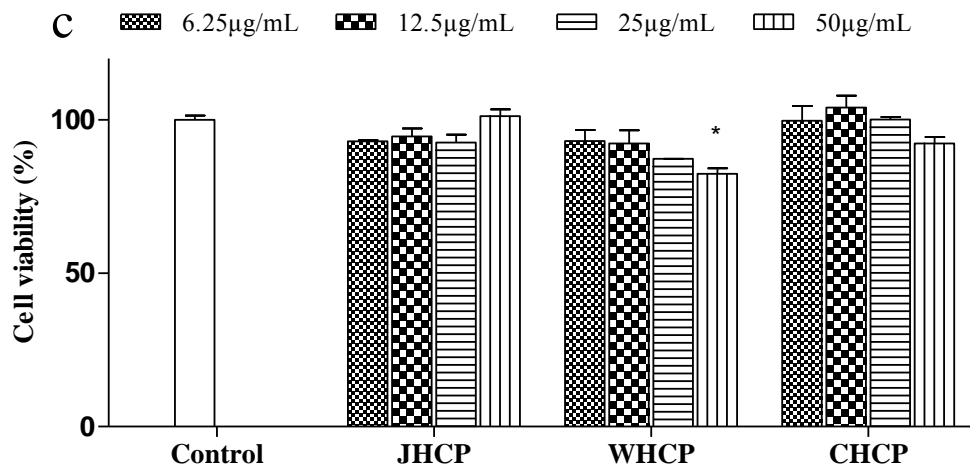
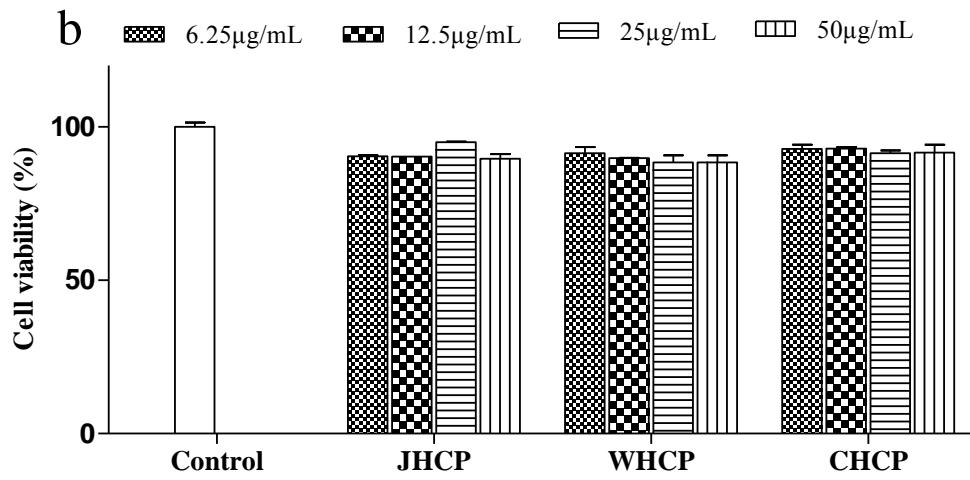
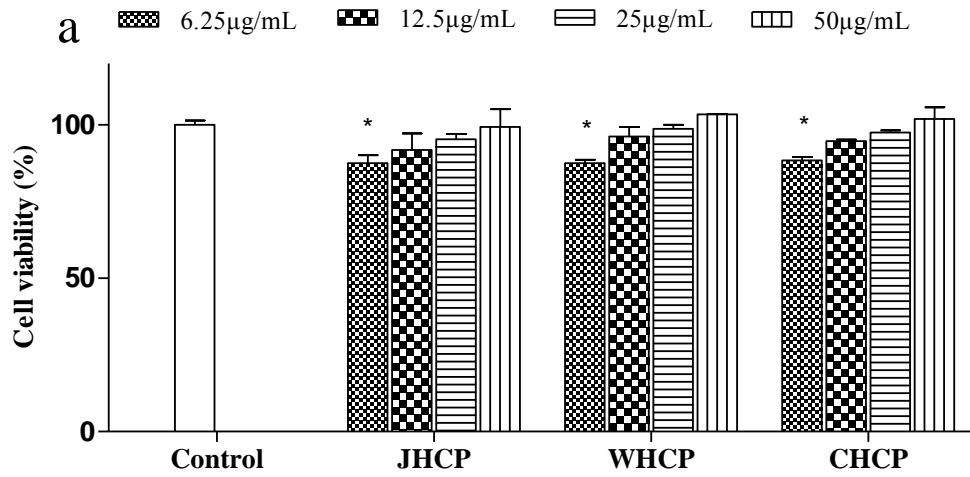
All assays were made in three independent experiments. Values were expressed as the mean \pm SE. One-way ANOVA was used to analyze the mean values in GraphPad prism 5 software. Student's t-test (* $p < 0.05$ and ** $p < 0.01$) was used to analyze the means of the parameters of significant differences.

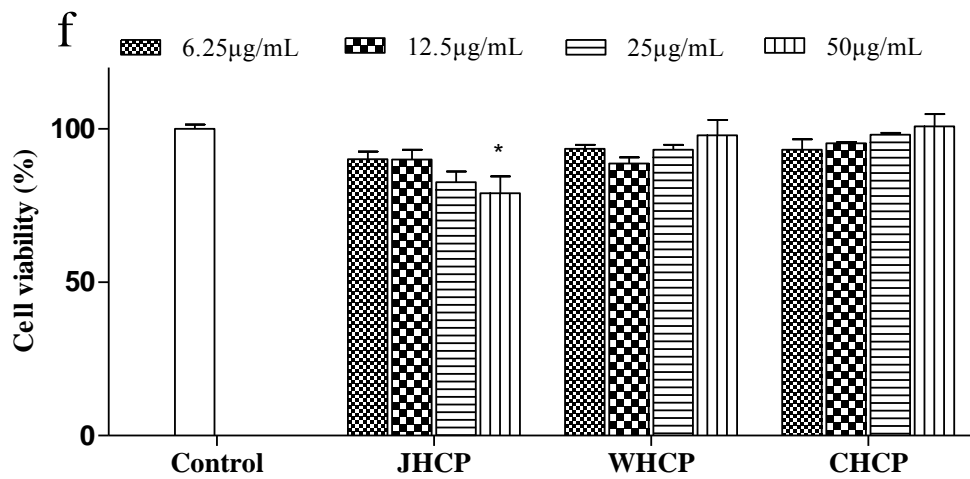
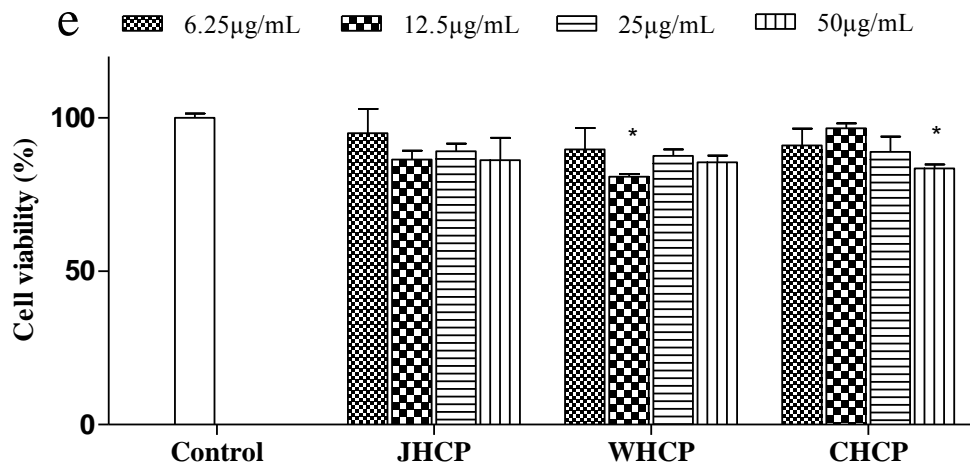
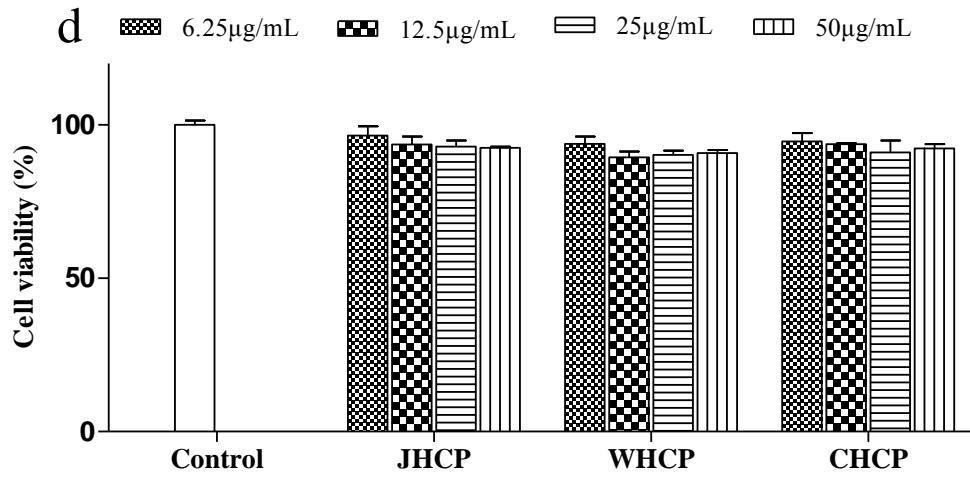
4 Results and Discussion

4.1 Screening anticancer effects for three locations Hijiki

4.1.1 Screening anticancer effects of CPs

Fucoidan is one of the main components in crude polysaccharide. Therefore, we were initially screening the anticancer effects of CPs to three locations Hijiki. Fig. 2-1a-g shows the effects of CPs from three different harvest areas on the cell death rate of Vero (kidney epithelial), A549 (lung cancer), HT-29 (colon cancer), HL-60 (leukemia), B16F10 (mouse skin cancer), MCF-7 (breast cancer), and Hep3B (liver cancer) cell lines. The CPs reduced B16F10, Hep3B, and HT-29 cell survival rates in a concentration-dependent manner. The normal Vero cell line had a higher survival rate after treatment with each concentration than the six malignant cell lines did. Furthermore, in the anticancer activity screening, JHCP exhibited the strongest antiproliferative effects and decreased the survival rate of Hep3B cells. In contrast, Vero cells exposed to CPs showed survival rates above 85% at each concentration. Hence, active fractions from JH were selected for further biological investigation.





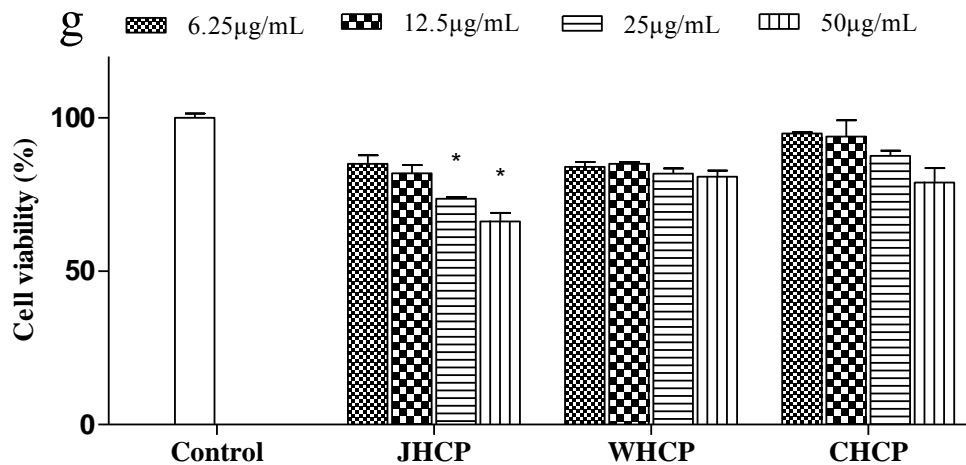


Figure 2-1 Percentages of cell viability as a measure of cell proliferation after treatment with different concentrations of JHCPs from three locations Hijiki in sample 24 h treatment. (a) Vero, (b) A549, (c) HT-29, (d) HL-60, (e) B16F10, (f) MCF-7, and (g) Hep3B cells. JHCP: The crude polysaccharide extract of Hijiki harvested from Jeju-Korea. WHCP: The crude polysaccharide extract of Hijiki harvested from Wando-Korea. CHCP: The crude polysaccharide extract of Hijiki harvested from Zhejiang-China. All experiments were performed in triplicate, and each value represents the mean \pm SE. * $p < 0.05$, ** $p < 0.001$ were considered as significant compared to the control.

4.1.2 Isolation of active fraction and cell cytotoxicity

JHCFuc was separated using DEAE-cellulose with sodium chloride (NaCl, 0-2 M) as the elutant. Four different positive fractions (JHCF1, JHCF2, JHCF3, and JHCF4) were selected based on their ionic characteristics at different molarities of NaCl (Fig. 2-2).

Vero cells exposed to JHCFuc and the four active fractions showed survival rates above 85% at each concentration (Fig. 2-3a). Based on the known anticancer activity of JHCP, we treated Hep3B cells with JHCF4 and the results showed that it reduced Hep3B cell survival rates in a concentration-dependent manner after sample treatment for 24 h. Similarly, JHCF4 significantly decreased Hep3B cell survival rates with a half-maximal inhibitory concentration (IC_{50}) of $33.53 \pm 2.50 \mu\text{g/mL}$ after sample treatment for 48 h (Fig. 2-3b).

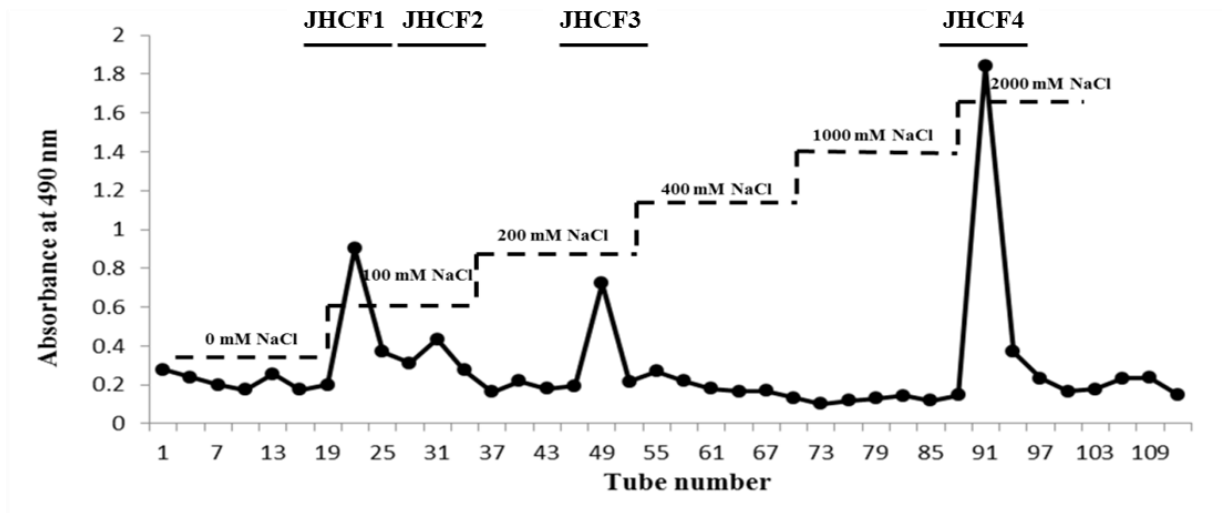


Figure 2-2 DEAE-cellulose chromatogram of the fucoidan separated from the extract of acid-processed JH.

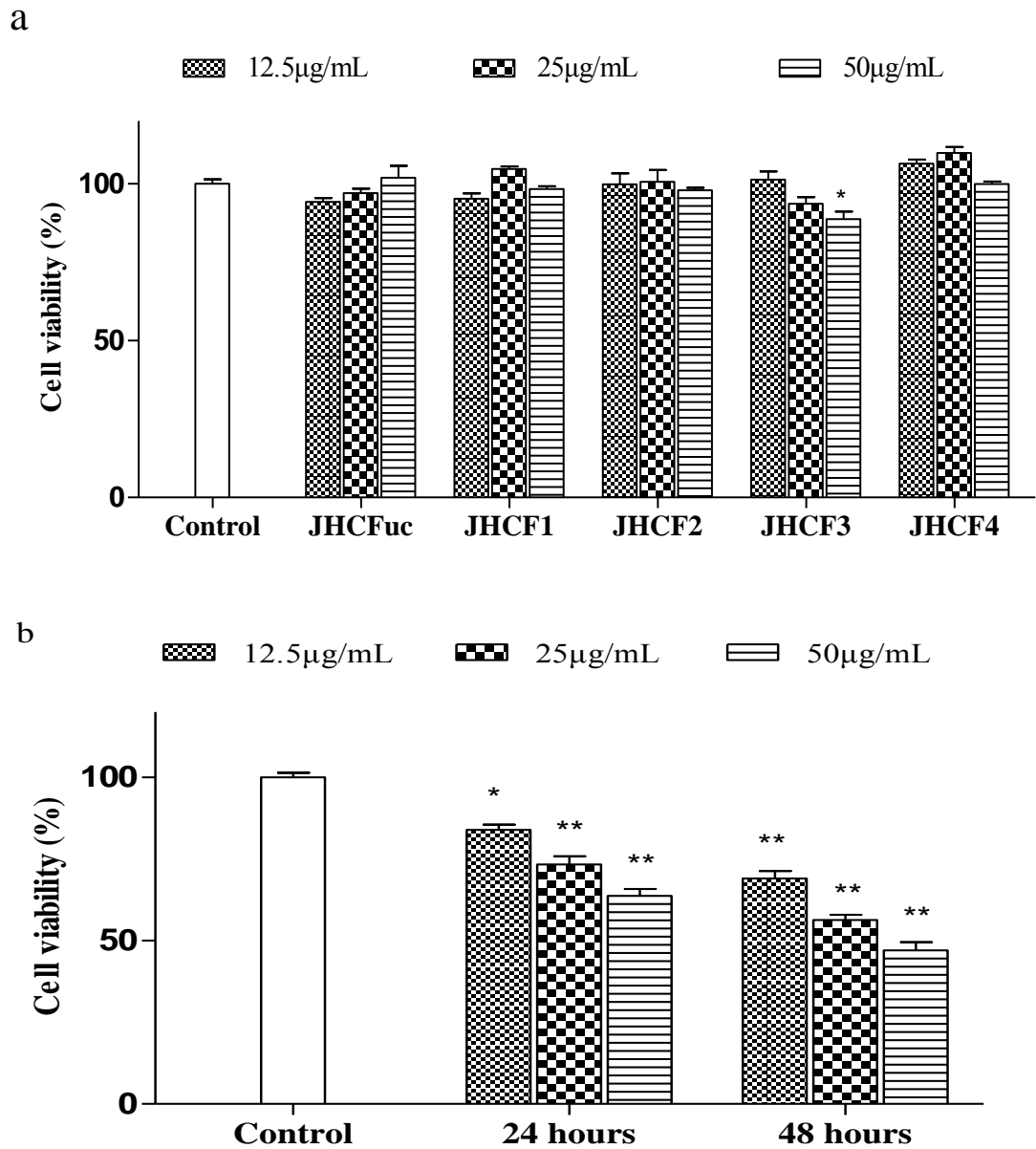


Figure 2-3 Percentage of cell viability as a measure of cell proliferation after treatment with different concentrations of fractions. (a) Cytotoxicity of JHCFuc and four active fractions were determined by MTT assay with Vero cells. (b) Cytotoxicity of JHCF4 was determined by MTT assay with Hep3B cells in 24 h and 48 h JHCF4 treatment. All experiments were performed in triplicate, and each value represents the mean \pm SE. * $p < 0.05$, ** $p < 0.001$ were considered as significant compared to the control.

4.1.3 Composition and structure of active fraction

4.1.3.1 Monosaccharide composition

The monosaccharide composition and the other major components, uronic acids, sulfate, and protein of JHCP, JHCFuc and JHCF4 from JH are shown in Table 2-1 and Fig. 2-4a. Monosaccharide composition analysis showed that fucose (37.56%), mannose (22.55%), and galactose (38.43%) were the major sugars in fucoidan with minor amounts of rhamnose (1.05%) and arabinose (0.40%). The sulfate content of fractions JHCF1, JHCF2, JHCF3, and JHCF4 was $5.4 \pm 0.24\%$, $1.74 \pm 0.13\%$, $5.75 \pm 0.32\%$, and $17.6 \pm 0.36\%$, respectively. The result of the analysis of the separated fractions was in agreement with previously reported findings [102].

4.1.3.2 Agarose gel electrophoresis

Among the isolated fractions, the monosaccharide and sulfate contents of JHCF4 showed the highest yields. A positive correlation was found between sulfate content and bioactivity [132]. Compared to the polysaccharide molecular weight markers, the approximate molecular weight distribution of JHCF4 was in the range of 60-150 kDa as shown in Fig. 2-4b. Therefore, JHCF4 was selected for further anticancer analysis.

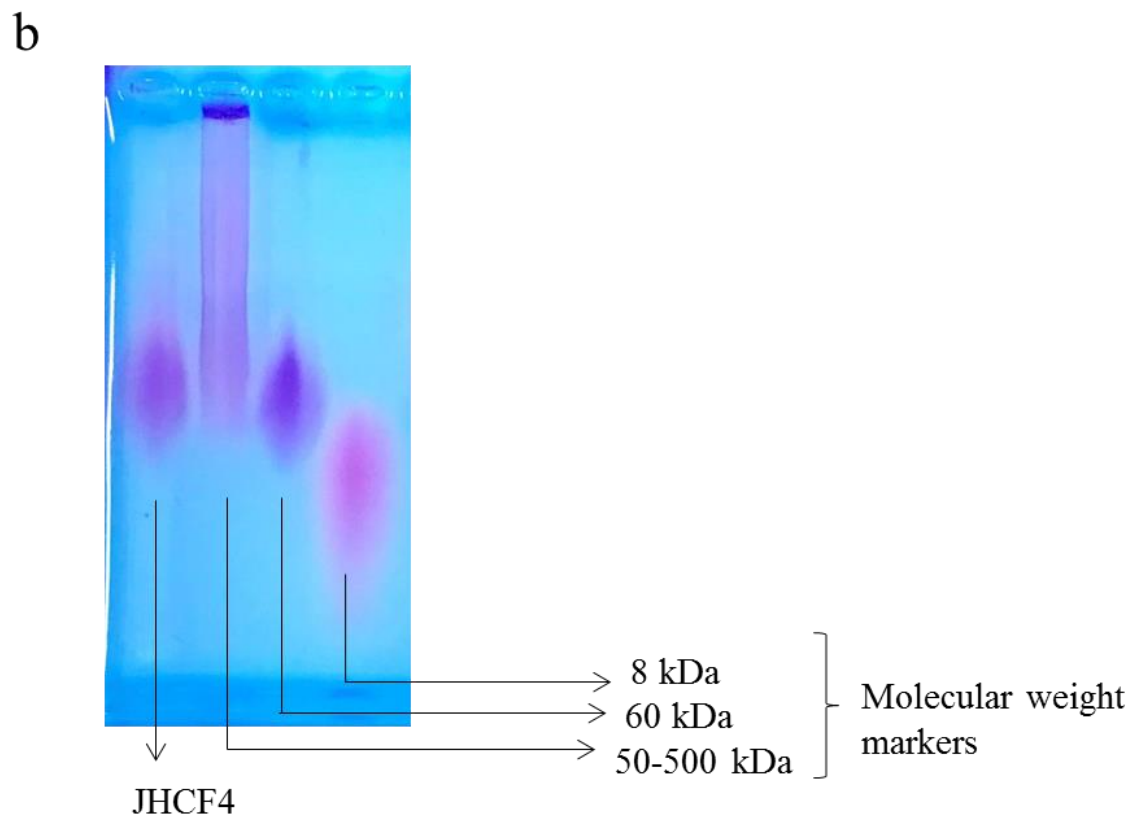
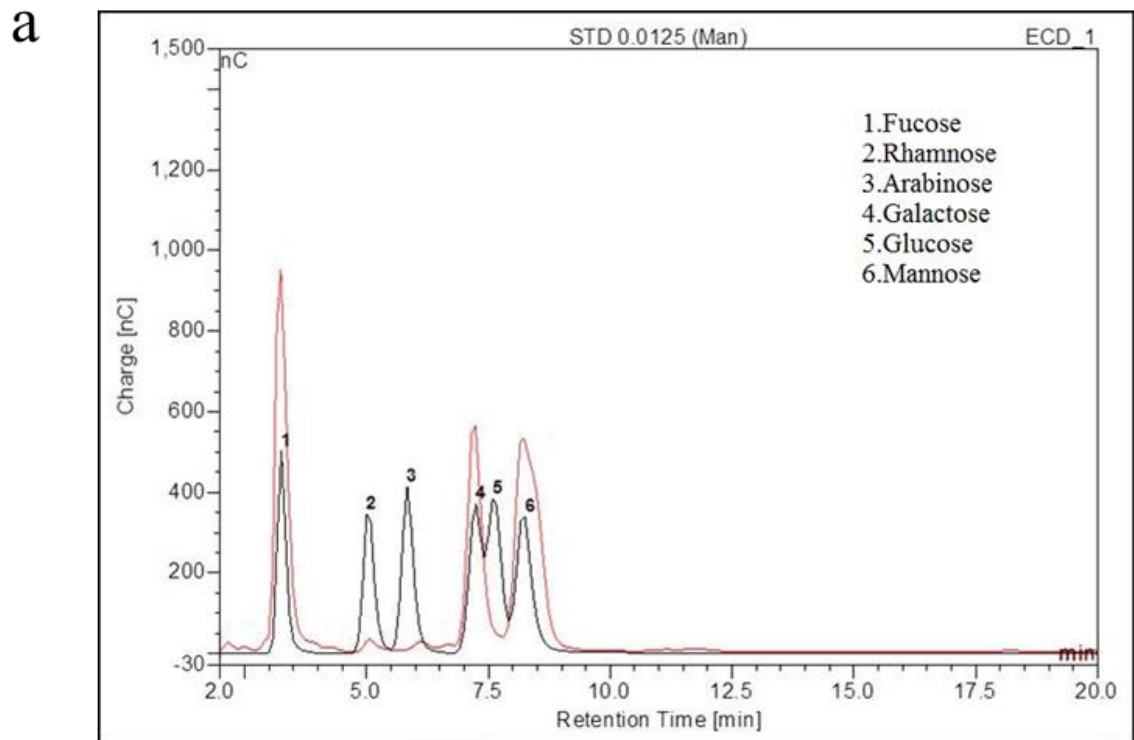
4.1.3.3 FTIR analysis

Fig. 2-4c shows the FTIR spectrums of JHCFuc from processed and unprocessed Hijiki. The observed peaks at 1261, 1230, 1056, and 802 cm^{-1} indicated the presence of C=O stretching vibration of an *O*-acetyl group, CH vibration of the polysaccharides composed of fucose, D-glucose, D-mannose, D-xylose, and galacturonic acid, CH_3 (fucose, *O*-acetyl), S=O stretching vibration, and S=O stretching of alkyl sulfoxide and anomeric region of carbohydrate. The peaks at 543 cm^{-1} reflect the C-O-S secondary axial sulfate group at C-4 of fructopyranose residue. Similar findings were observed in previous studies [110]. In FTIR spectrum, the peaks between 1120 and 1270 cm^{-1} of the processed JHCFuc showed lower relative abundances compared to unprocessed JHCFuc. Thus, the sulfate content of processed sample was lower than in unprocessed sample. However, JHCF4 showed the highest sulfate content among all four fractions.

Table 2-1 Chemical compositions of crude polysaccharides (JHCP), fucoidan (JHCFuc) and its fractions (JHCF1-JHCF4).

Sample	Uronic acid	Protein	Sugar (%)					Sulfate (%)*
			Fucose	Rhamnose	Arabinose	Galactose	Mannose	
JHCP	15.1	9.5	46.76	3.14	0.80	25.59	23.69	0.31±0.00
JHCFuc	18.9	1.9	37.56	1.05	0.40	38.43	22.55	13.30±0.50
JHCF1	26.7	1.5	41.88	1.11	2.35	27.78	26.86	5.4±0.24
JHCF2	19.4	2.3	22.25	2.94	8.16	26.73	39.89	1.74±0.13
JHCF3	20.6	1.6	43.40	0.62	0.71	23.51	31.73	5.75±0.32
JHCF4	16.9	1.2	46.32	1.17	1.13	27.36	24.00	17.6±0.36

*Each value represents mean ±SE of three determinants of each fraction.



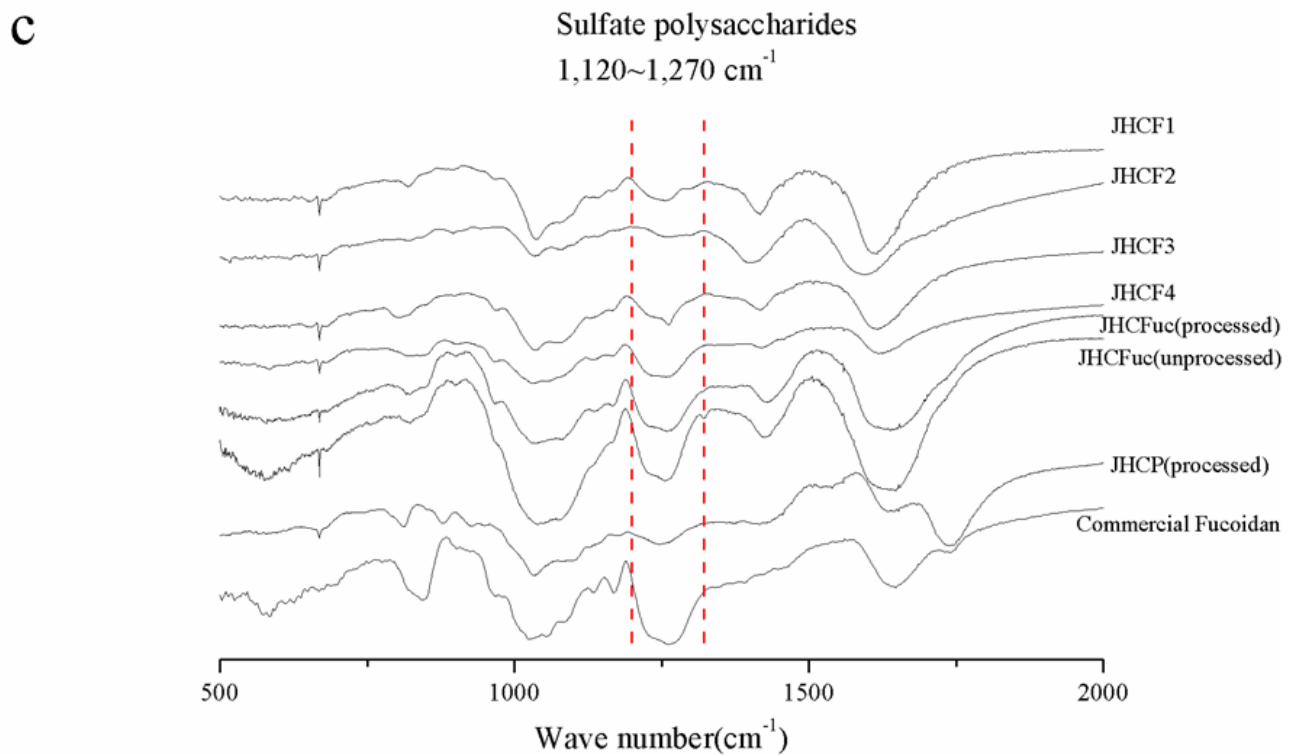


Figure 2-4 Characterization of the structural features of commercial fucoidan, JHCP, JHCFuc, and JHCF4 using FT-IR and monosaccharide analysis. (a) Monosaccharide content of JHCF4 was analyzed using an HPAE-PAD spectrum compared with black line standard monosaccharide mixture and red line HPAE-PAD spectrum for the monosaccharide content of JHCF4. (b) The approximate molecular weight distribution of JHCF4. (c) FT-IR spectra of JHCF1-JHCF4, processed and unprocessed JHCP, JHCFuc were compared to commercial fucoidan for the spectral analysis.

4.1.3.4 LC-ESI-MS analysis

The results observed that a sugar unites from hydrated JHCF4. According to a recent study [67], the LC-MS spectrum of ion (m/z 339.0930) was assigned as [FucGal]⁻, and its spectrum was shown in Fig. 2-5a. Based on the previous results in JHCF4, the percentage of monosaccharide compositions for fucose (37.56%) and galactose (38.43%) were ranking in the first and third largest among all the monosaccharide, respectively. Thus, we deduced that a large amount of fucose/Galactose unites is existed in JHCF4.

4.1.3.5 ¹H NMR analysis

Fig. 2-5b shows the proton ¹H NMR analysis of JHCF4 with characteristic peaks of fucoidan as previously reported [16]. Peaks between 5.0 and 5.6 ppm represented the anomeric protons of -l-fucopyranosyl units and the broad methyl peak at 0.9-1.3 ppm, which of them were corresponded to α -l-fucopyranosyl units. Moreover, an observed peak at 4.65 ppm corresponded to H₄ of 4-sulfated fucose. Sulfated polysaccharides have complex and heterogeneous structures that lack regularity.

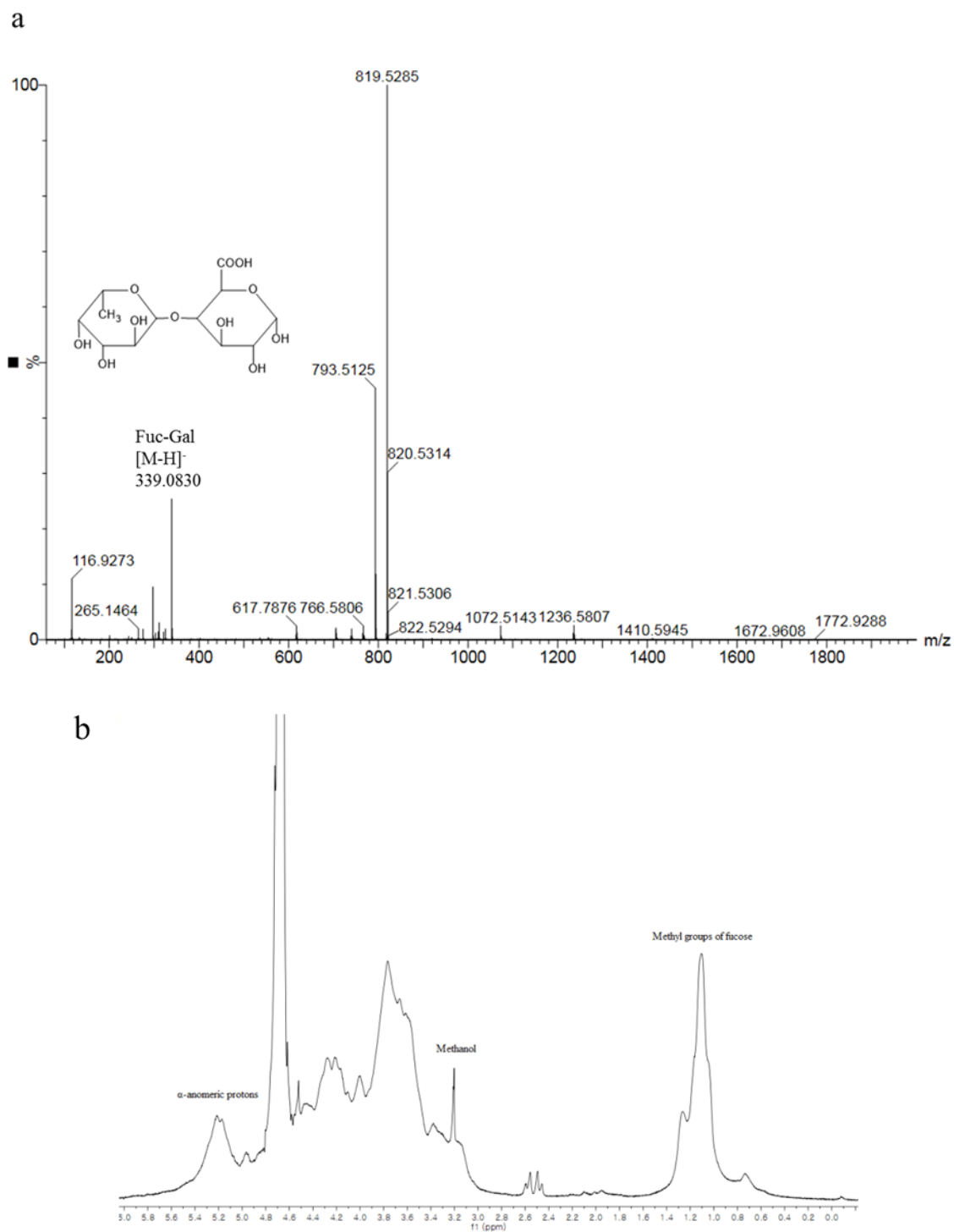


Figure 2-5 Chemical analysis of JHCF4. (a) ESI Q-TOF MS spectrum JHCF4, and (b) spectrum of ^1H NMR.

4.1.4 JHCF4 induced apoptotic morphology of Hep3B cells

4.1.4.1 Nuclear staining with Hoechst 33342

To evaluate the anticancer effect of JHCF4 against nuclear morphological changes in Hep3B cells, the cell-permeable DNA dye Hoechst 33342 was used. Cells were considered viable if nuclei were stained homogeneously, while chromatin condensation and fragmentation indicated apoptosis [117]. JHCF4 was selected for further studies to investigate its potential in inducing apoptotic bodies because it showed the lowest IC_{50} . Subsequently, cell nuclear morphology was observed using fluorescence microscopy. Apoptotic body formation was clearly identified in JHCF4-treated Hep3B cells (Fig. 2-6a). In addition, the observed apoptotic bodies increased with increasing concentration of JHCF4.

4.1.4.2 Nuclear staining with AO/EtBr

The AO/EtBr staining protocol identifies early and late apoptotic cells and necrotic cells [133], and was performed to characterize cell morphology [134]. Viable cells showed green homogeneous nuclei, whereas early apoptotic cells were characterized by fragmented green patches. Late apoptotic cells were characterized by both green and orange or orange particulate matter, and necrotic cells were characterized by damaged cytoplasmic membranes and appeared homogeneously red [135]. Fig. 2-6b shows the effects of JHCF4 on Hep3B cells, which were characterized by increased apoptotic body formation that occurred in a dose-dependent manner. Small amounts of low-concentration JHCF4 (12.5 $\mu\text{g/mL}$) induced early apoptotic body formation in cells 48 h after treatment, with few cells in the late apoptotic and necrotic stages. At medium and high concentrations (25 and 50 $\mu\text{g/mL}$), an increasing number of late apoptotic body forms was observed, as well as a few necrotic cells.

We treated Hep3B cells with different concentrations of JHCF4, resulting in the induction of apoptotic body formation in a dose-dependent manner (Fig. 2-7).

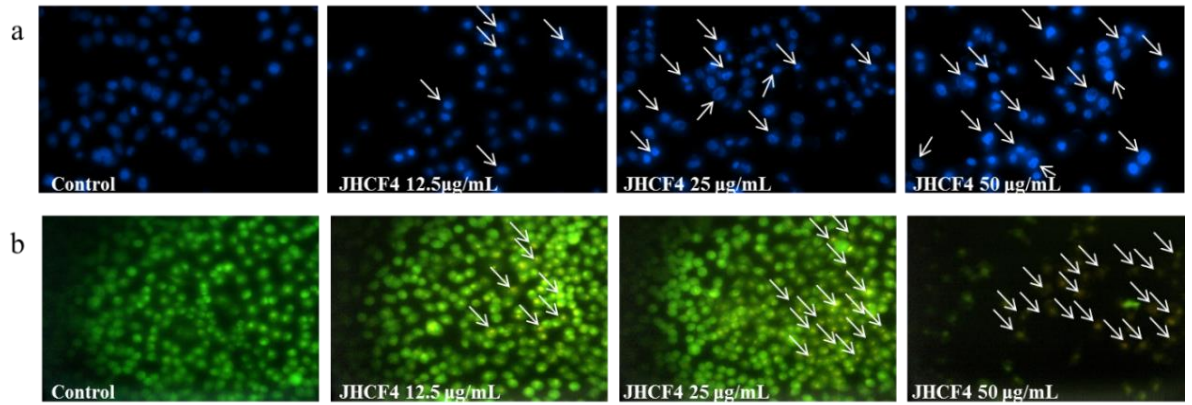


Figure 2-6 Apoptosis effects of JHCF4. (a) The anticancer effects of JHCF4 induce apoptotic bodies in Hep3B cells using Hoechst 33342 after 48 h incubation. (b) The anticancer effects of JHCF4 induce apoptotic bodies in Hep3B cells using acridine orange/ethidium bromide (AO/EtBr) staining after 48 h incubation.

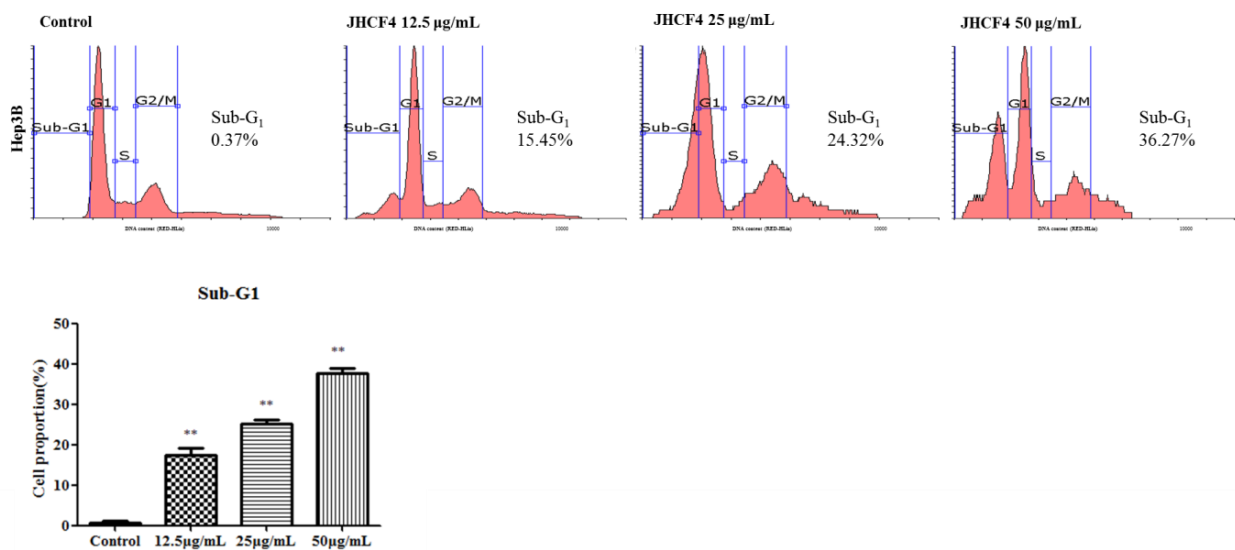


Figure 2-7 Anticancer effects of JHCF4 induced apoptotic bodies in Hep3B cells by flow cytometry.

Cell cycle analysis was performed by PI staining. All experiments were performed in triplicate, and each value represents the mean \pm SE. * $p < 0.05$, ** $p < 0.001$ were considered as significant compared to the control.

4.1.5 Induction of ROS generation, mitochondrial membrane potential, and cytochrome c release in JHCF4-induced apoptosis

ROS generation is related to JHCF4-induced apoptosis, and therefore ROS levels were analyzed in Hep3B cells. The results showed that JHCF4 induced ROS production in Hep3B cells in a time-dependent manner (Fig. 2-8a).

In cells, almost ninety percentage of the energy generation is associated with mitochondria, which plays a key role in regulating apoptosis. The mitochondrial integrity is disrupted in early apoptosis stage. The effects of JHCF4 on mitochondrial membrane potential were analyzed using Rhodamine 123. The reduction of fluorescence intensity in the 24 h treatment group indicated that the mitochondrial membrane potential was markedly decreased (Fig. 2-8b). Pretreatment with JHCF4 (50 $\mu\text{g}/\text{mL}$) induced mitochondrial membrane potential, increasing the Rhodamine 123 negative cells to 37.68% after 48 h.

Mitochondrion is an organelle including an outer layer and an inner layer separated by an inter-layer space. Cytochrome c is a proapoptotic protein in the mitochondria. These data illustrate that JHCF4 treatment gradually increased the release of cytochrome c into the cytosol of Hep3B cells (Fig. 2-8c). The excessive generation of ROS and the decrease of mitochondrial membrane potential indicate the activation of apoptosis [136]. Accumulation of ROS disrupted the mitochondrial membrane potential, which is associated with the release of apoptosis-related factors [137]. We found that JHCF4 reduced the depolarization of mitochondrial membrane potential in a time-dependent manner, which may be associated with its activation of the intracellular accumulation of ROS. This observation suggests that JHCF4 induces apoptosis in Hep3B cells via the mitochondrial pathway.

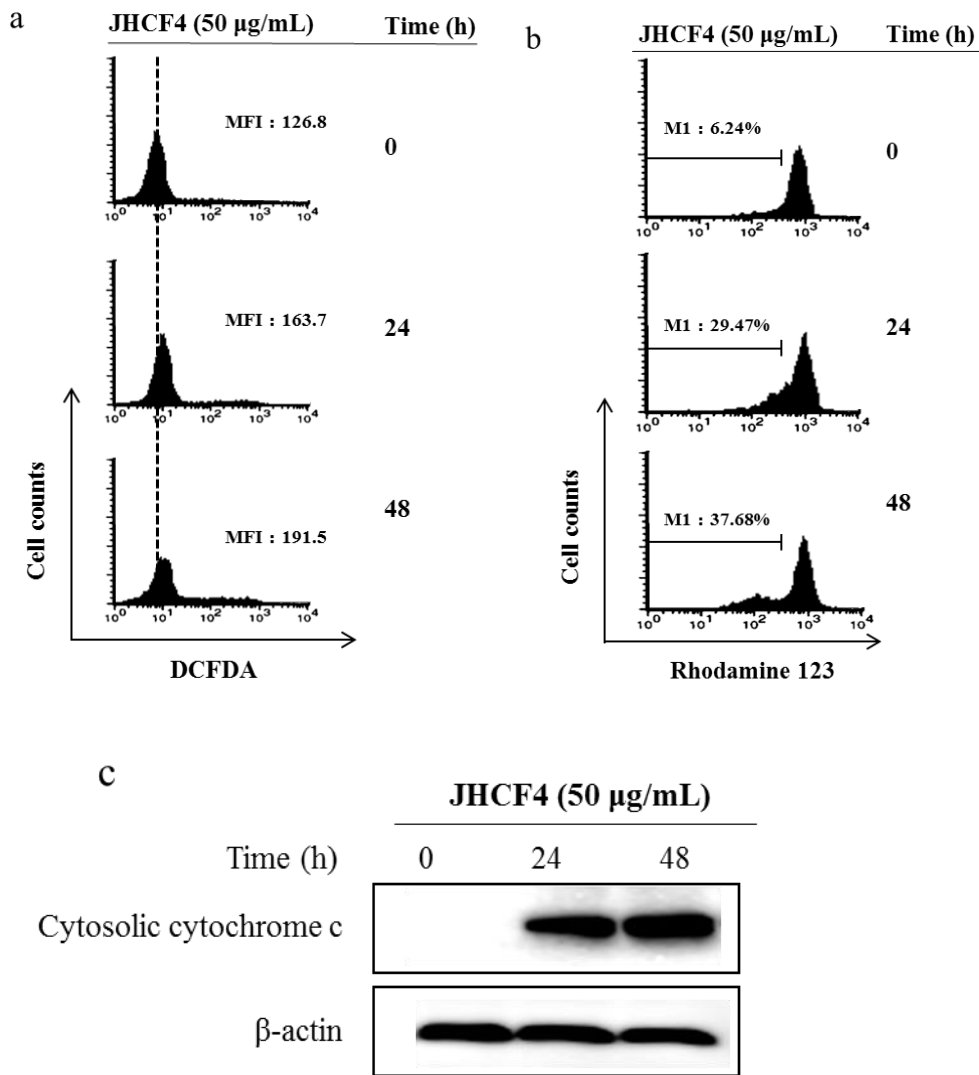


Figure 2-8 Induction of reactive oxygen species (ROS) generation, the integrity of mitochondrial membrane, and cytochrome c release by JHCF4-induced apoptosis in Hep3B cells. (a) Hep3B cells were treated with 50 $\mu\text{g/mL}$ JHCF4 for 24 and 48 h, incubated with DCFH-DA for 30 min. (b) Hep3B cells were treated with JHCF4 (50 $\mu\text{g/mL}$) for 24 and 48 h, incubated with Rhodamine 123 (200 nM) for 30 min in the dark, then analyzed by flow cytometry. Data are presented as fluorescence intensity. (c) Hep3B cells were treated with JHCF4 (50 $\mu\text{g/mL}$) for the indicated durations. All experiments were performed in triplicate, and a representative experiment is presented.

4.1.6 Apoptosis pathway regulation by JHCF4

Analysis of the intensities of western blot bands showed that increasing the concentration of JHCF4 up to 50 $\mu\text{g}/\text{mL}$ increased the expression of apoptotic and anti-apoptotic factors, as demonstrated by the increase in Bax and decrease in Bcl-xL compared to the untreated group. It also showed that increasing the concentrations of JHCF4 increased the expression of cleaved caspase-3 (Fig. 2-9a). As shown in Fig. 2-9b, JHCF4 increased cleaved caspase-3 and 9 expression, and decreased Bcl-2 expression in a time-dependent manner with various incubation periods.

The results demonstrated the significant apoptotic body formation induced by JHCF4 in Hep3B cells. During apoptosis, chromatin condenses, the cell shrinks, the membrane blebs, and finally, the cell disassembles into vesicles enclosed by membranes [138]. These results proved the hypothesis that JHCF4 mediated apoptosis in Hep3B cells, which is a process that operates through a series of signaling cascades. The suicidal factors in the Bcl-2 protein family and caspases remain dormant under inactive conditions [139]. Bcl-2 protein family members including the pro-apoptotic (Bax) and anti-apoptotic (Bcl-xL) proteins, are the main apoptotic regulators [140]. In the cellular mitochondria, disturbance of the voltage-dependent anion channel by Bax leads to the release of cytochrome c, resulting in the continuous stimulation of caspases [141]. The upregulation of Bax, coupled with the downregulation of Bcl-xL, increases the ratio of Bax/Bcl-xL, which is considered a hallmark of apoptosis [142]. Western blot analysis showed an increase in the Bax/Bcl-xL ratio, indicating apoptosis, which occurred in a concentration-dependent manner. Cytochrome c and initiator caspases contribute to activating the proenzyme form of caspases. The increased Bax/Bcl-xL ratio caused the release of cytochrome c and increased the expression of cleaved caspase-3. In the bioactivity study, JHCF4 exhibits anticancer effects via the mitochondria-mediated apoptosis pathway in cancer cells.

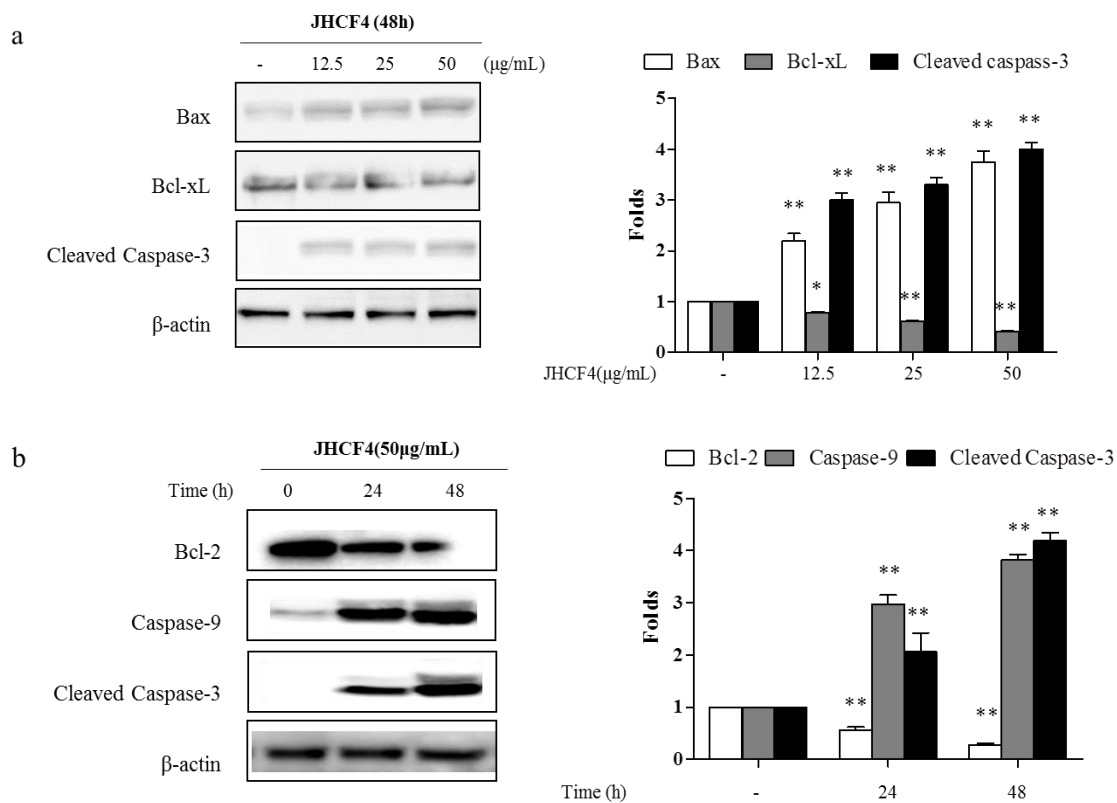


Figure 2-9 Induction of apoptosis-related proteins degradation by JHCF4. (a) Hep3B cells were treated with different concentrations of JHCF4 at 48 h. (b) Hep3B cells were treated with JHCF4 (50 $\mu\text{g/mL}$) with different incubation periods. All experiments were performed in triplicate, and each value represents the mean \pm SE. * $p < 0.05$, ** $p < 0.001$ were considered as significant compared to the control.

4.2 Antioxidant effects of JHCF4

4.2.1 Radical scavenging activities

The DPPH, alkyl, and hydroxyl radical scavenging activities are shown in Table 2-2. Among the fractions, the scavenging activities of JHCF4 had the lowest IC₅₀ values of 0.11 ± 0.01, 1.28 ± 0.02, and 0.25 ± 0.04 µg/mL, respectively.

4.2.2 Measurement of intracellular ROS levels in Vero cells

The cytotoxic and protective effects of JHCF4 against AAPH-stimulated cellular damage by MTT assay were evaluated (Fig. 2-10a). Among the fractions, no cytotoxic effects were found in Vero cells. When Vero cells were exposed to AAPH, protective effects of JHCF4 were observed (Fig. 2-10b). The cell survival rate was greater than 80% at concentrations of 37.5-150 µg/mL. The ROS levels in cells pretreated with JHCF4 were significantly lower than those of AAPH-stimulated samples, thus showing the strongest scavenging effects (Fig. 2-10c).

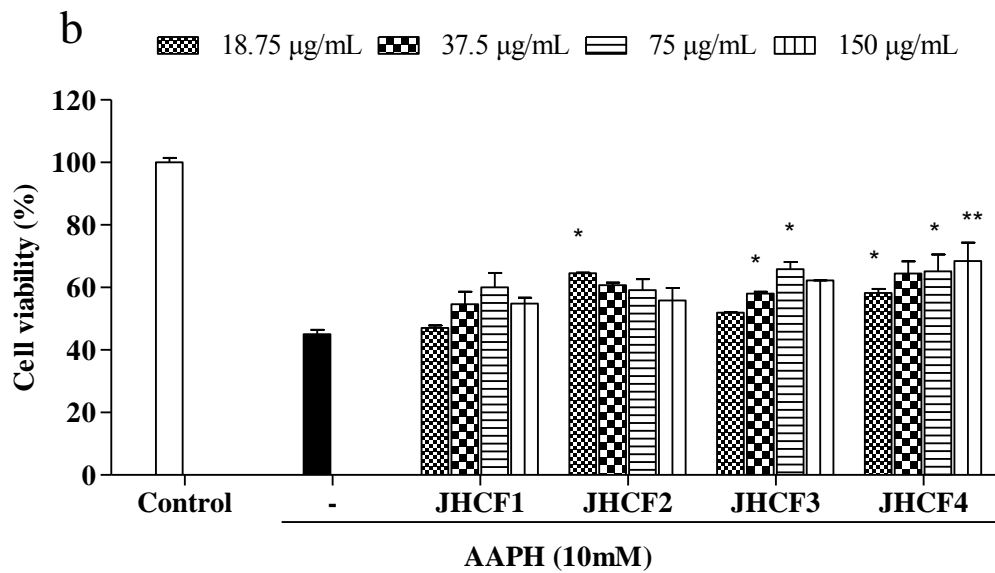
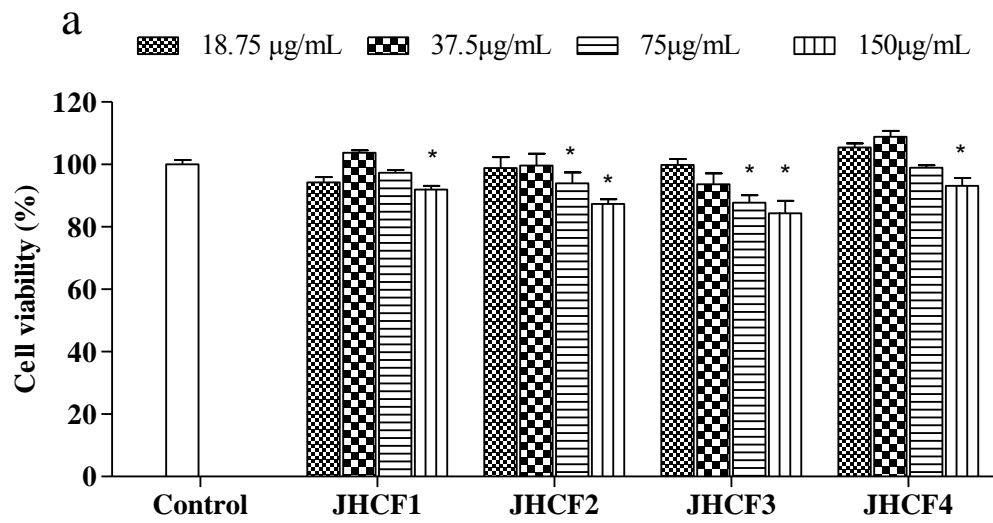
Table 2-2 Scavenging activities of crude polysaccharide (CP) and fucoidan (CF) from JH against DPPH, hydroxyl, and alkyl radical.

IC ₅₀ (mg/mL)	Crude polysaccharides(CP)	Fucoidan				
		JHCFuc	JHCF1	JHCF2	JHCF3	JHCF4
DPPH ^a	0.40±0.01	0.18±0.02	0.40±0.02	0.27±0.02	0.23±0.01	0.11±0.01
Alkyl ^b	1.47±0.03	1.67±0.02	1.65±0.04	1.47±0.01	2.65±0.02	1.28±0.03
Hydroxyl ^c	0.67±0.01	0.4±0.03	0.71±0.02	0.32±0.02	0.69±0.02	0.25±0.04

a: DPPH Radical Scavenging Activity

b: Alkyl Radical Scavenging Activity

c: Hydroxyl Radical Scavenging Activity



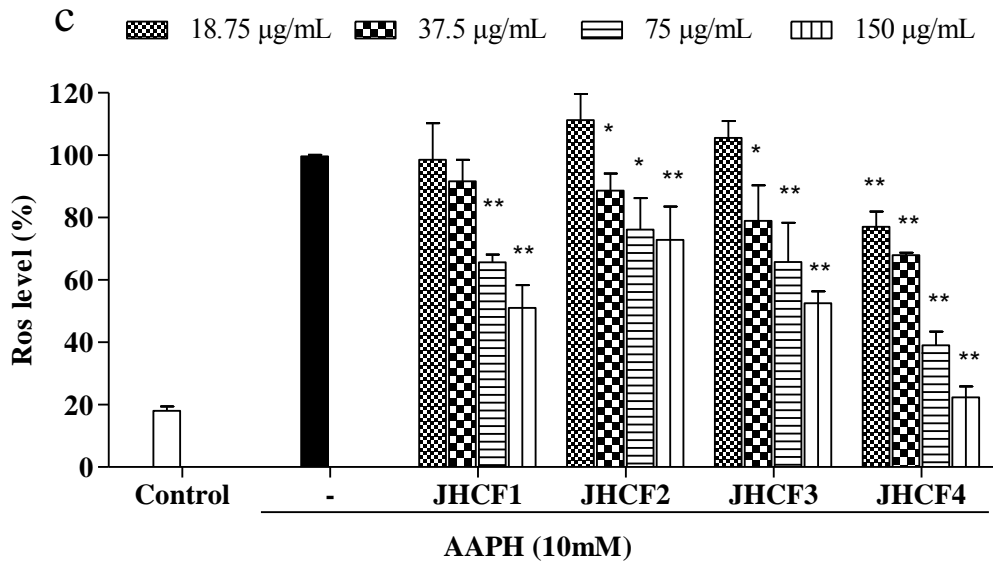


Figure 2-10 Evaluation of the four fractions for toxicity and intracellular ROS scavenging activities against AAPH-induced oxidative stress in Vero cells. (a) Toxicity assessment of the sample. (b) Protective activity of four fractions against AAPH-induced cytotoxicity. (c) Scavenging activity of four fractions on AAPH induced intracellular ROS. Results represent the percentage (%) of cell viability and intracellular ROS levels. Experiments were performed in triplicate and the data are expressed as the mean \pm SE. * $p < 0.05$, ** $p < 0.001$.

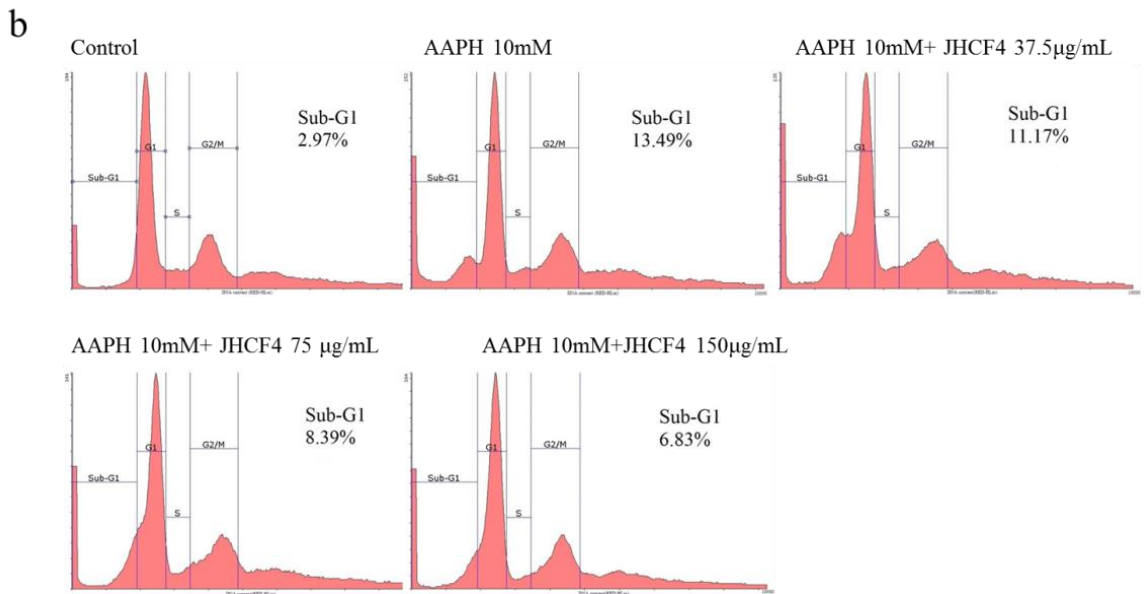
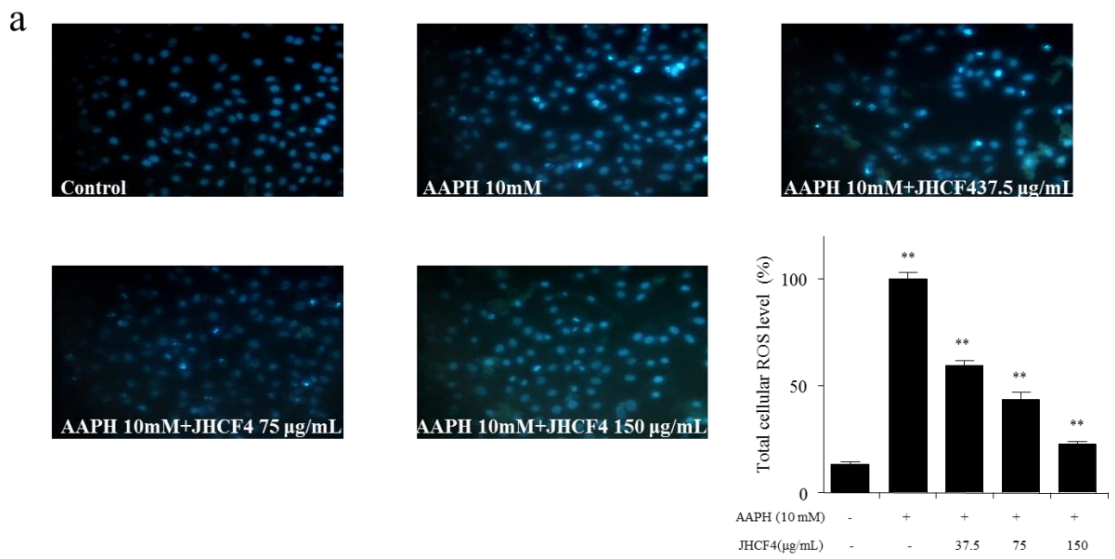
4.2.3 Apoptotic body formation of JHCF4 in Vero cells

F4 showed the highest relative antioxidant activity based on the previous results. Thus, JHCF4 was used for analysis to observe apoptotic body formation. Apoptotic body formation was easily observed in AAPH-induced cells by using fluorescence microscopy, as shown in Fig. 2-11a. However, the numbers of observed apoptotic bodies were decreased when cells were pretreated with different concentrations of JHCF4. Additionally, as the sample concentration increased, apoptotic body formation decreased. In cell flow cytometric analysis of treated Vero cells with JHCF4 and AAPH, JHCF4 showed protective effects against AAPH-induced apoptotic body formation in a concentration-dependent pattern (Fig. 2-11b).

4.2.4 Apoptosis pathway regulation by JHCF4

The intensities of western blot bands revealed that increasing concentrations of JHCF4 induced apoptotic and anti-apoptotic factors, as observed by decreased Bax and increased Bcl-xL compared to that in AAPH-treated cells (Fig. 2-11c). Moreover, increasing concentrations of JHCF4 decreased caspase-3 expression.

The results of this study explain the significant protective effect of JHCF4 in AAPH-induced Vero cells. Suicidal factors such as Bcl-2 protein family members and caspases are activated following treatment with AAPH [139]. The Bcl-2 protein family contains pro-apoptotic proteins (Bax) and anti-apoptotic proteins (Bcl-xL) as the main apoptotic regulators [140]. In cellular mitochondria, voltage-dependent anion channels are disturbed by Bax, leading to the release of cytochrome c. This pathway continuously stimulates caspases [141]. Decreased regulation of Bax and increased regulation of Bcl-xL, and particularly the ratio of Bax/Bcl-xL, showed dose-dependent protective and antioxidant effects [142]. Cytochrome c and initiator caspases contribute to activating the proenzyme form of caspases involving caspase-3 [143]. The decreased Bax/Bcl-xL ratio caused cytochrome c release and induced continuously decreased expression of caspase-3. These results showed JHCF4 antioxidant properties in Vero cells were mediated by the mitochondrial pathway.



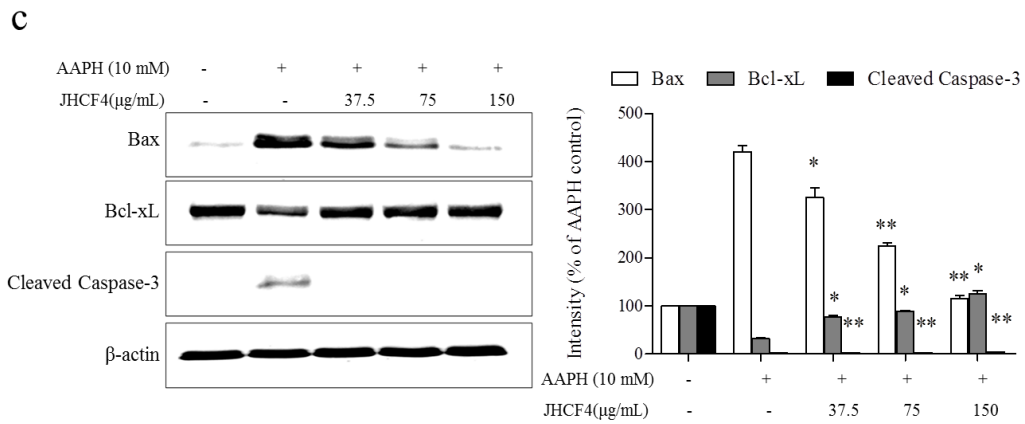


Figure 2-11 Protective effects of JHCF4 against AAPH-induced Vero cells. (a) Effect of JHCF4 on cellular ROS levels and apoptotic body formation induced by AAPH. Apoptotic body formation was observed under a fluorescence microscope after Hoechst 33342 staining. (b) Dysregulation of cell cycle progression was indicated by flow cytometric analysis of the apoptotic sub-G1 cell population in Vero cells. (c) Western blot analyses of Vero cells for measuring the expression of Bax, Bcl-xL, and caspase-3. Results are reproducible based on three independent determinations. Experiments were performed in triplicate and the data are expressed as the mean \pm SE. * $p < 0.05$, ** $p < 0.001$.

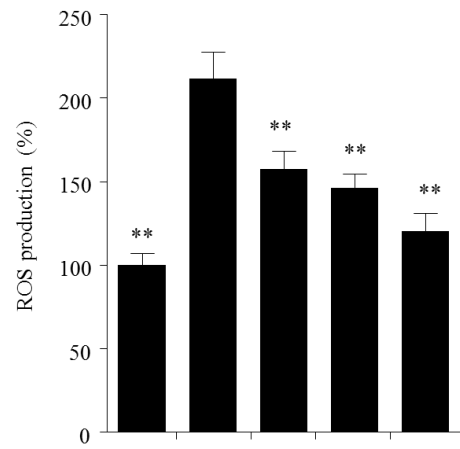
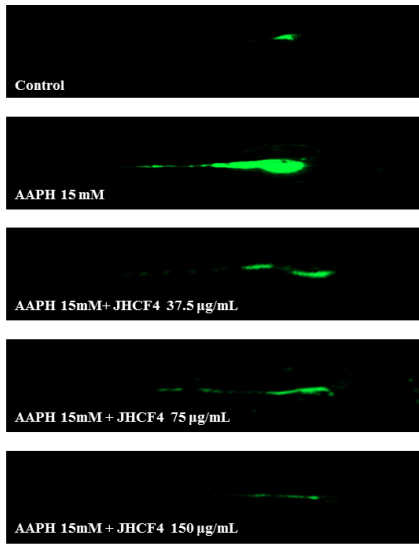
4.2.5 Toxicity of JHCF4 treatment in zebrafish embryos

Zebrafish was employed to be an animal model, because their cellular composition, signaling, and response to injury are similar to these of humans [144]. This model has many advantages such as a large clutch size, transparent embryos, low cost, and easy handling, and thus is widely used in predictive toxicology screening in pharmacological studies [145]. JHCF4 showed low toxicity compared to the control. A low viability rate was observed for AAPH-induced embryos compared to the control. The survival rates of embryos reached up to 70-80% when pretreated with JHCF4 prior to AAPH treatment.

The antioxidative effects of JHCF4 on ROS production in AAPH-induced zebrafish embryos were observed by using DCFH-DA assay. The results showed that treating embryos with JHCF4 strongly inhibited ROS production (Fig. 2-12). The fluorescence in the control group showed low intensity, whereas AAPH treatment increased fluorescence, demonstrating that ROS increased in AAPH-stimulated zebrafish embryos. Additionally, a large decrease in ROS level was observed when JHCF4 was used to pretreat AAPH-induced zebrafish embryos.

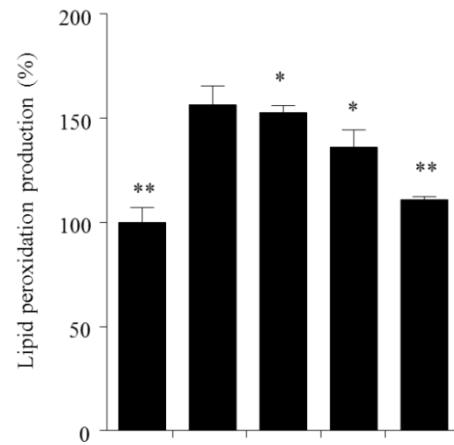
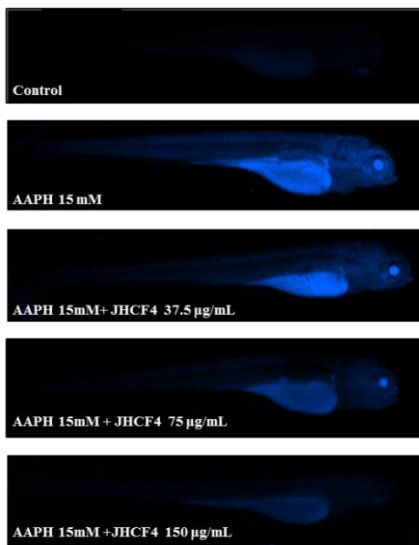
DPPP is widely used to evaluate lipid peroxidation in zebrafish. In untreated embryos, low fluorescence was detected in the embryos, while AAPH treatment resulted in higher fluorescence than in the control, indicating lipid peroxidation. However, pretreatment with JHCF4 decreased the fluorescence intensity of AAPH-induced lipid peroxidation (Fig. 2-12). These results demonstrate that JHCF4 has strong antioxidant effects.

ROS production



AAPH (15 mM)	JHCF4(µg/mL)
-	-
+	-
+	37.5
+	75
+	150

Lipid peroxidation



AAPH (15 mM)	JHCF4(µg/mL)
-	-
+	-
+	37.5
+	75
+	150

Figure 2-12 Protective effects of JHCF4 against AAPH-induced ROS production and lipid peroxidation in zebrafish embryo model. Microscopic fluorescence images of the embryos stained with DCFH-DA and DPPP in the ROS production and lipid peroxidation assay, respectively. The relative fluorescence intensities indicate the level in the stained embryos. Experiments were performed in triplicate and the data are expressed as the mean \pm SE. * $p < 0.05$, ** $p < 0.001$.

4.3 Hepato-protective effect of JHCF4 against ethanol-induced damage

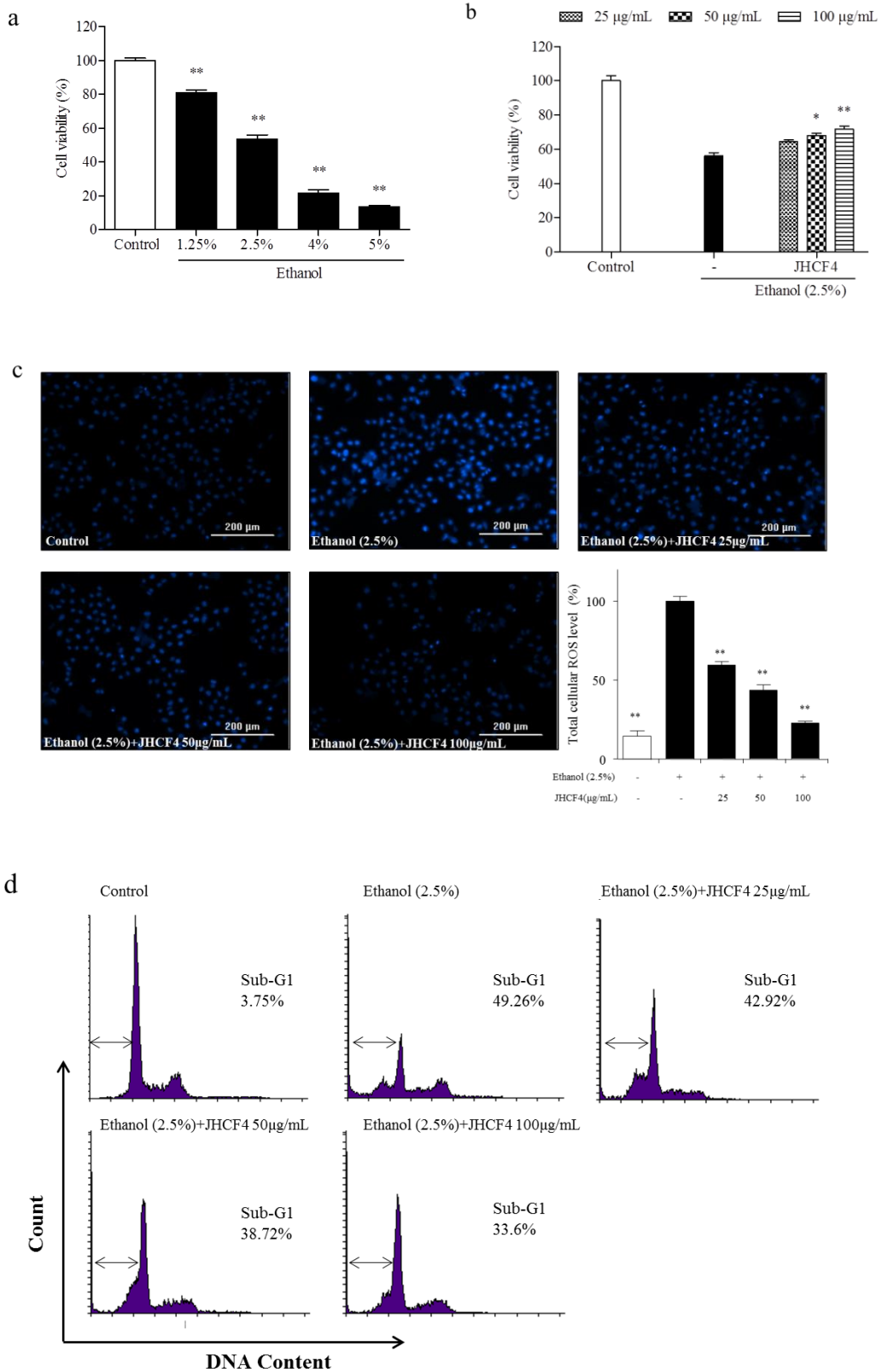
4.3.1 Protective effect against ethanol-induced damage in Chang liver cells

In order to determine the cytotoxicity of ethanol in Chang liver cells, different concentrations of ethanol were measured using an MTT assay. An ethanol concentration of 2.5% stimulated a reduction in the survival rate to 53.24%, which was confirmed by using this concentration (2.5%) for further study (Fig. 2-13a). JHCF4 showed hepato-protective effects in ethanol-treated cells in a dose-dependent manner. JHCF4 protected cells from cell death induced by ethanol and promoted cell growth (Fig. 2-13b).

Hoechst 33342, a fluorescent dye probe, was used to observe the formation of apoptotic bodies in ethanol-treated Chang liver cells. The control group (blank treatment) showed an intact nuclear morphology, while marked nuclear fragmentation, demonstrating apoptosis in cells, was easily observed in ethanol-treated cells (Fig. 2-13c). Additionally, the JHCF4 treatment was found to inhibit the formation of apoptotic bodies. This suggests that JHCF4 provides hepato-protective effect against ethanol-stimulated damage or injuries.

In addition to the morphological evaluation, cell flow cytometric analyses of JHCF4 and ethanol treatment were performed. The proportion of cells with sub-G1 DNA content in JHCF4 showed protective effects against ethanol-stimulated apoptotic body formation in a concentration-dependent manner (Fig. 2-13d). These results further confirmed the strong protective properties of JHCF4 against ethanol-induced cell death.

To further confirm the regulative ability of JHCF4 in apoptosis-associated protein in ethanol-treated Chang liver cells, Western blotting was carried out to identify apoptosis signaling proteins. Ethanol regulates apoptosis-associated factors, including Bax, Bcl-xL, and caspase-3 via the mitochondrial signal pathway in liver cells. As shown in Fig. 2-13e, exposure to ethanol markedly up-regulated the expression of Bax and caspase-3, regarded as pro-apoptotic factors, while considerably down-regulating Bcl-xL, regarded as an anti-apoptotic factor, in Chang liver cells. However, the expression in the JHCF4-treated groups was found to be decrease significantly in terms of Bax and caspase-3 expression compared to the ethanol-treated group. Additionally, the expression of Bcl-xL in the JHCF4-treated groups was considerably higher than in the ethanol-treated group. These results demonstrate that JHCF4 may have ability to inhibit apoptosis in ethanol-treated Chang liver cells.



e

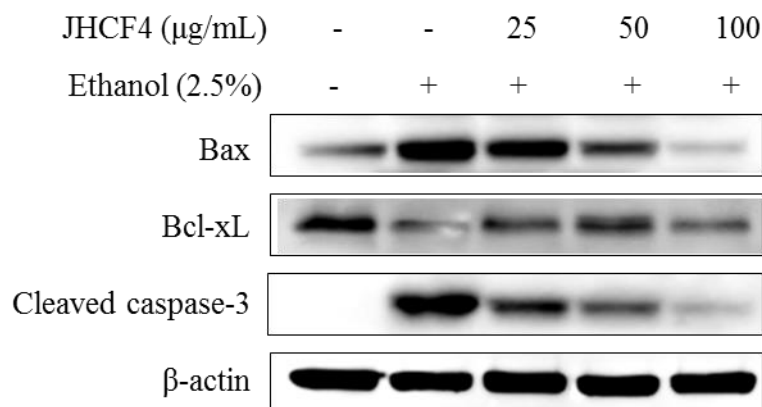


Figure 2-13 Protective effects of JHCF4 against ethanol-induced Chang liver cells. (a) Cytotoxicity of different concentrations of ethanol in Chang liver cells. (b) Protective effects of JHCF4 against ethanol-induced damage by MTT assay in Chang liver cells. (c) Protective effect of JHCF4 apoptotic body formation induced by ethanol in Chang liver cells. Apoptotic body formation was observed using a fluorescence microscope after Hoechst 33342 staining. (d) Chang liver cells were treated with or without the indicated concentrations of JHCF4 for 24 h. The percentage of apoptotic cells was subsequently analyzed by flow cytometer. (e) Western blot analyses of Chang liver cells for measuring the expression of Bax, Bcl-xL, and caspase-3. Results are reproducible based on three independent determinations. Experiments were performed in triplicate and the data are expressed as the mean \pm SE. * $p < 0.05$, ** $p < 0.001$.

4.3.2 Protective effect of JHCF4 against ethanol-treated zebrafish embryo (72 hpf)

In 72 hpf zebrafish larvae, the function of the liver was not yet well developed. Therefore, the levels of hepatic oxidative stress in the whole larvae were evaluated. Ethanol is cytotoxic in larvae and is widely used as oxidant stimulator *in vivo*.

Cell death in ethanol-induced larvae was measured using acridine orange solution staining. The results showed that ethanol induced cell death in the larvae, while treatment with JHCF4 significantly inhibited the degree of cell damage in a concentration-dependent manner in ethanol-treated larvae (Fig. 2-14a).

The antioxidative effect on ROS production in ethanol-induced larvae was measured using a DCFH-DA assay. JHCF4 treatment was found to strongly inhibit ROS production in the larvae (Fig. 2-14b). The levels of fluorescence in the untreated larvae were low, while ethanol treatment was found to increase fluorescence, indicating that ROS increased in ethanol-stimulated larvae. In addition, a gradual decrease of ROS production was found in correlation with an increasing concentration of JHCF4 in ethanol-treated larvae.

For the measurement of lipid peroxidation in larvae, similar trends were observed as those describe above (cell death and ROS production). In ethanol-treated larvae, a strong fluorescence was observed in the larvae, while JHCF4 treatment resulted in decreased intensities than in the ethanol-induced larvae, indicating the protective effects of JHCF4 in lipid peroxidation (Fig. 2-14c). These results indicate that JHCF4 inhibits hepatic oxidative stress in 72 hpf larvae.

4.3.3 Measurements of steatosis, MDA, and GSH contents and expression of p53 in ethanol-treated zebrafish embryo (128 hpf)

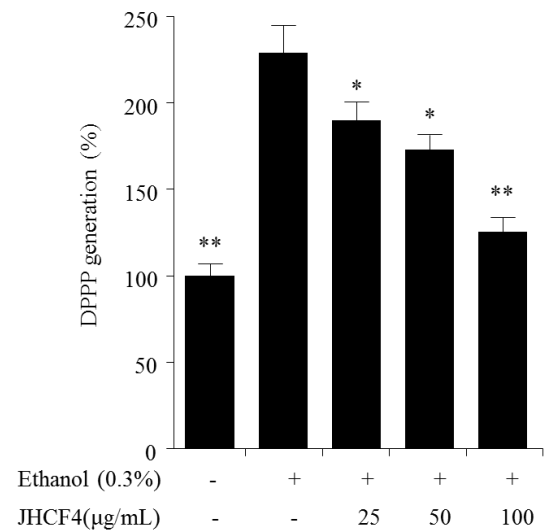
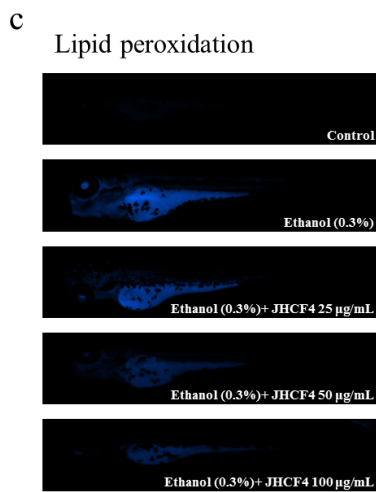
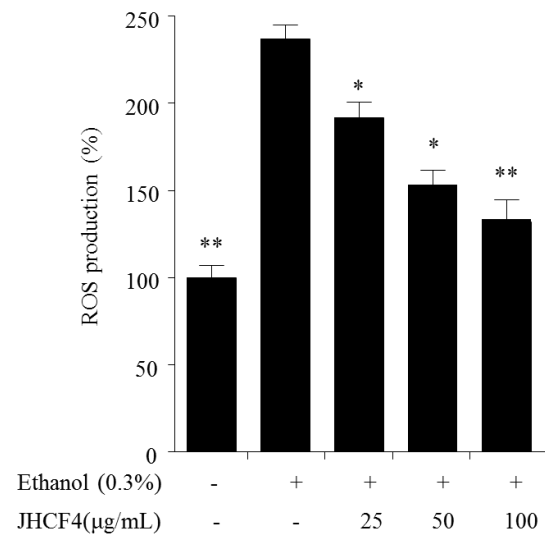
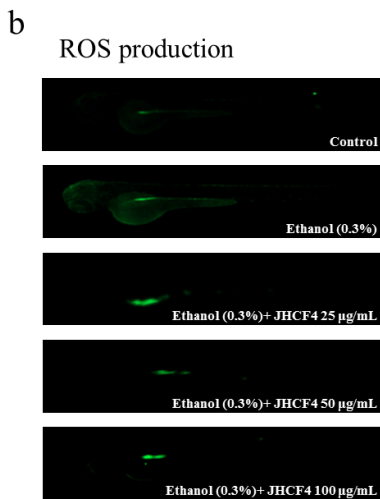
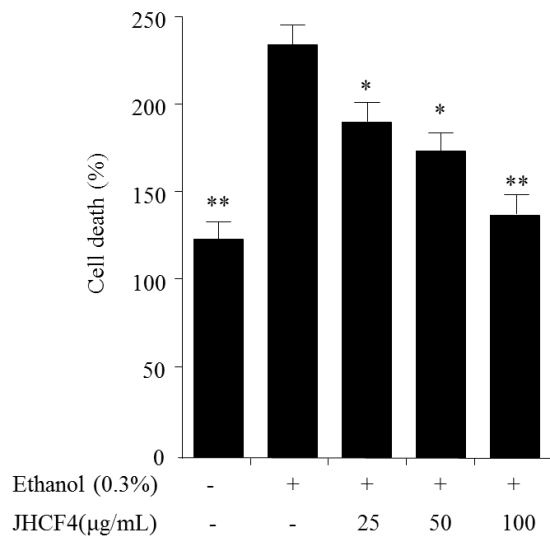
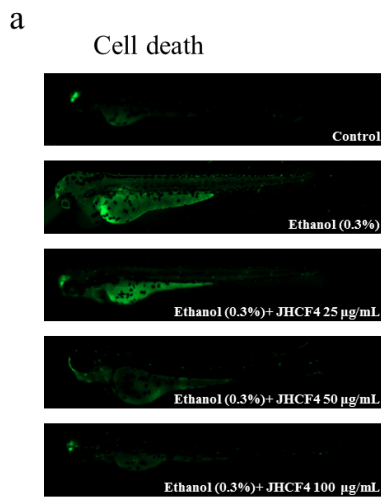
Steatosis appears as a result of an acute ethanol intake in mammals [146]. The livers obtained from 96 hpf larvae exposed to ethanol have been previously found to undergo hepatic oxidative stress in fatty liver disease models [147]. In this study, zebrafish hepatogenesis initially developed at 96 hpf. Thus, 96 hpf was selected as the exposure time for treatment with ethanol. The results of an excessive intake ethanol intake were evaluated without any internal or external factors. Considering its viability, morphology, and behavioral changes, we experimented with various ethanol exposure times (32 h, 96–128 hpf) and consistently found that the best ethanol concentration in terms of toxicity was that of 1.5%

of medium (Fig. 2-14d and 14e).

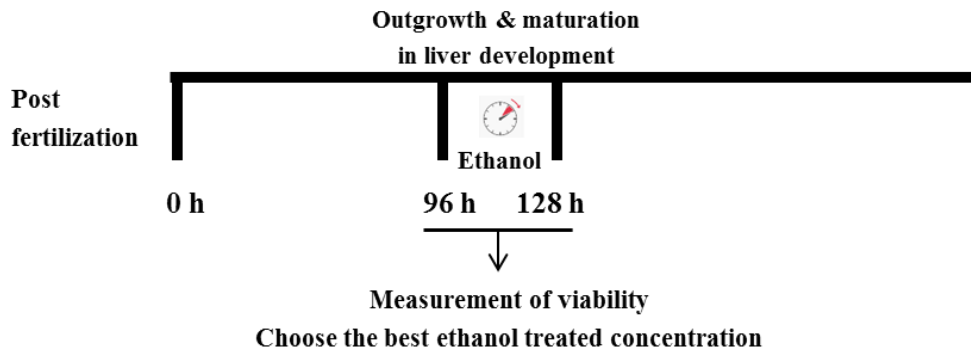
To further confirm whether JHCF4 affects steatosis in ethanol-treated 128 hpf larvae, we treated 96 hpf larvae with or without 1.5% ethanol and JHCF4 for 32 h and visualized the neutral lipids using whole-mount Oil red O staining. The untreated ethanol larvae were observed as a white color in the liver tissue, while the larvae treated with 1.5% ethanol of steatosis were observed as a red color in 128 hpf (Fig. 2-14f). With increasing concentrations of JHCF4, steatosis was found to decrease gradually, indicating that JHCF4 is capable of regulating steatosis.

The production of hepatic MDA indirectly responds to the level of lipid peroxidation. In addition, the production of GSH in JHCF4-treated liver indicates the production of antioxidants in hepatic tissues as a defensive mechanism to oxyradicals. In 128 hpf larvae, the MDA levels after ethanol treatment showed a markedly increase compared to the untreated larvae, while the levels of GSH showed a significant decrease compared to the untreated larvae. Furthermore, the production of MDA decreased in a dose-dependent manner with an increased JHCF4 concentration, while the concentration of GSH in the JHCF4-treated group increased (Fig. 2-14g and 14h).

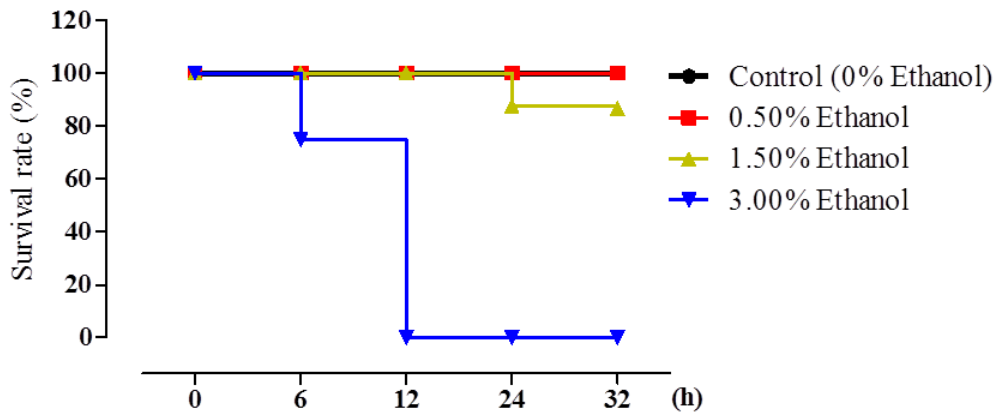
Tumor suppressor gene, p53, is expressed in response to DNA damage and is involved in the process of apoptosis [148, 149]. In the present work, ethanol stimulated DNA damage in the liver tissues of 128 hpf larvae. An increase in the expressed of p53 was observed in comparison to untreated larvae. It was also found that JHCF4 regulated the expression of p53 in ethanol-simulated larvae, suggesting that JHCF4 has protective effects against ethanol-induced damage in 128 hpf larvae (Fig. 2-14i).



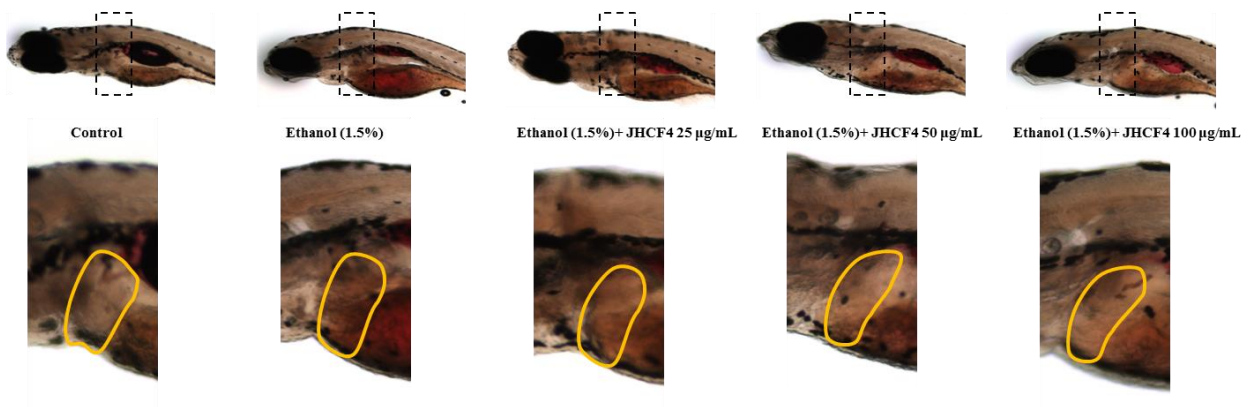
d

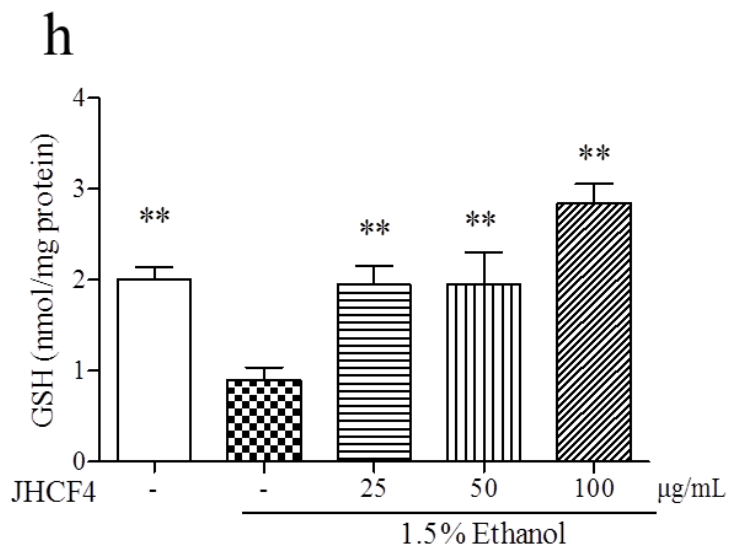
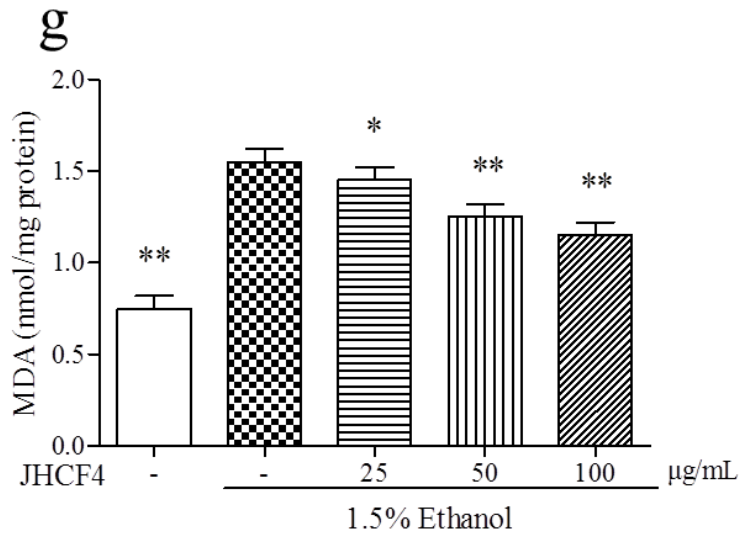
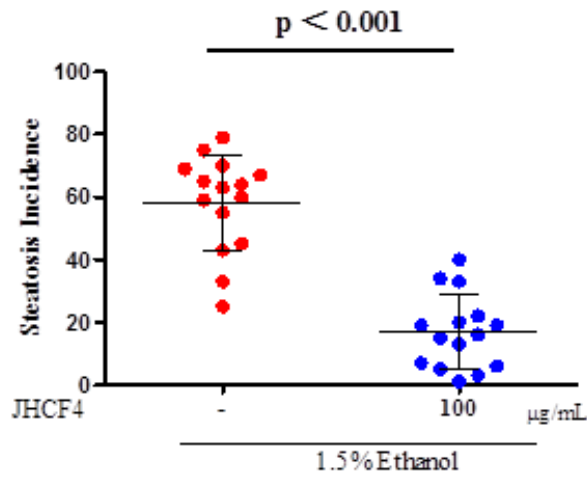


e



f Steatosis and alteration of lipid metabolism





i

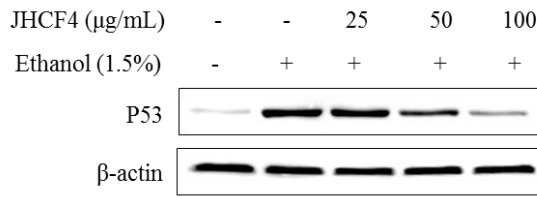


Figure 2-14 Protective effects of JHCF4 against ethanol-induced in zebrafish. (a) Cell death, (b) ROS production, and (c) Lipid peroxidation in zebrafish embryo model (72 hpf). (d) Acute ethanol exposure reduces viability of zebrafish larvae (128 hpf). Outline of the ethanol treatment protocol. Ethanol exposure began at 96 hpf and continued for up to 32 h. (e) Larvae treated with 0-3% ethanol were scored for mortality, and the average of three clutches is plotted during 32 h of exposure; error bars show the SE value. (f) Ethanol exposure results for steatosis after treatment with various concentrations of JHCF4 and alteration of lipid metabolism in zebrafish embryo model (128 hpf). Whole-mount Oil red O staining of larvae after exposure in the presence or absence of 2% ethanol for 32 h reveals steatosis; yellow dotted line denotes the liver. The percent of larvae with steatosis analyzed by Oil red O staining of 15 clutches, with an average of 20 larvae per treatment per clutch. (g) MDA and (h) total GSH contents of ethanol-induced zebrafish treated with various concentrations of JHCF4. (i) Western blot analysis of p53 in ethanol-induced zebrafish treated with various concentrations of JHCF4 for 32 h and untreated controls. Experiments were performed in triplicate and the data are expressed as the mean \pm SE. * $p < 0.05$, ** $p < 0.001$.

Recently, the use of hepato-protective therapies with low-toxicity and important economic advantages isolated from marine products have become a hot topic of discussion within the research community [150]. Brown seaweed is considered a model organism as a marine resource with hepato-protective effects. For example, previous histopathological studies have showed that extracts from *Sargassum polycystum* can have an antioxidant effect against hepatic oxidative stress in a range of toxicity levels in liver tissue [151]. The hepato-protective effects of extracts from *Ecklonia cava* have also been investigated [152]. Polysaccharides are believed to be the most active compounds in seaweed. Some studies have reported on the hepato-protective effects of polysaccharides isolated from the seaweeds *Turbinaria decurrens* [106] and *H. fusiforme* [153] in ethanol-treated rats. Previous studies have shown that fucoidan can exert an antioxidative effect in the liver of rats [154]. Another study demonstrated the anticancer effects of polysaccharides in *H. fusiforme* [155]. This anticancer effect was also investigated by our research group [156]. The molecular weight, sulfate content, and monosaccharide composition are considered the main contributory factors to the biological activity of fucoidan [28]. A moderate correlation has been previously reported between the anticancer activity and the free radical scavenging properties of fucoidan [110]. Hence, hepato-protective effects are a potential attribute of fucoidan from *H. fusiforme* and could be an interesting topic of investigation.

In the present study, these results, coupled with an increased cell growth in ethanol-treated Chang liver cells, the induction of florescence in ethanol-treated zebrafish, the down-regulation of steatosis, MDA, and GSH *in vivo*, and the regulation of signaling factors in cells and zebrafish, suggest that JHCF4 exerts a strong hepato-protective effect. The members of the Bcl-2 protein family and caspases, regarded as suicidal factors, were activated by toxic agents, such as ethanol, triggering programmed cell death [139]. The Bcl-2 protein family are frequently studied with regards to apoptotic cells; Bax and Bcl-xL are known functions in the promotion of apoptosis and anti-apoptosis, respectively [140]. In cellular mitochondria, the increased levels of Bax induce the release of cytochrome c, further stimulating the production of caspases [141]. The down-regulation of Bax and the up-regulation of Bcl-xL showed a dose-dependent protective effect [142]. Cytochrome c activates the prototype enzyme of caspases, such as caspase-3 and caspase-9 [143]. When JHCF4 was administered to ethanol-treated cells, the decreased Bax and increased Bcl-xL induced the inhibition of cytochrome c and continuously down-regulated the

expression of caspase-3. Tumor suppressor p53 regulates apoptosis and is a regulator of gene expression of the Bcl-2 protein family [157]. Following the treatment of 128 hpf larvae with ethanol, the level of p53 expression was found to be down-regulated by JHCF4 in a dose-dependent manner. These results support our hypothesis that JHCF4 has hepato-protective properties *in vitro* and *in vivo*.

4.4 Anti-inflammatory potential of HFA against FD-induced inflammatory responses

4.4.1 Compound composition and structural features of HFA

As shown in Table 2-3, the HFA is rich in carbohydrate content, whereas it has relatively low ash content because of the existence of minerals. The HFA also has low levels of polyphenols and proteins.

The FT-IR spectrum is shown in Fig. 2-15. The vibrational characteristics of the spectrum were observed at wave numbers 3625 cm^{-1} , 1680 cm^{-1} , 1420 cm^{-1} , and 1035 cm^{-1} in both commercial sodium alginate and in the unprocessed and acid-processed HFA spectra. Similar findings were observed in previous studies [158]. Relative to the polysaccharide molecular weight markers, the molecular weight distribution of HFA was in the range of 50-360 kDa (Fig. 2-16).

4.4.2 Compositional analysis of FD-stimulated keratinocytes after HFA treatment

The optimum FD concentration and exposure time was followed previous study on cell viability and inflammation [66]. After HFA treatment and FD induction for 24 h, the keratinocytes were recovered and analyzed for metal ions by ICP-OES. Relatively stable concentration of K and Na, and significant decreases in Mg, Ca, Fe, Cu, As, Sr, Ba, and Pb were observed in the blank group cells compared to the treated cells (Table 2-4). Increasing concentrations of HFA caused substantial reductions in the levels of certain elements.

Table 2-3 Chemical composition of the purified HFA.

Constituent	Composition (%)*
Carbohydrate	89.25 ±0.64
Ash	2.41 ±0.27
Polyphenol	0.96 ±0.01
Protein	0.41 ±0.02

Results are given as the means ± SE based on triplicate determinations.

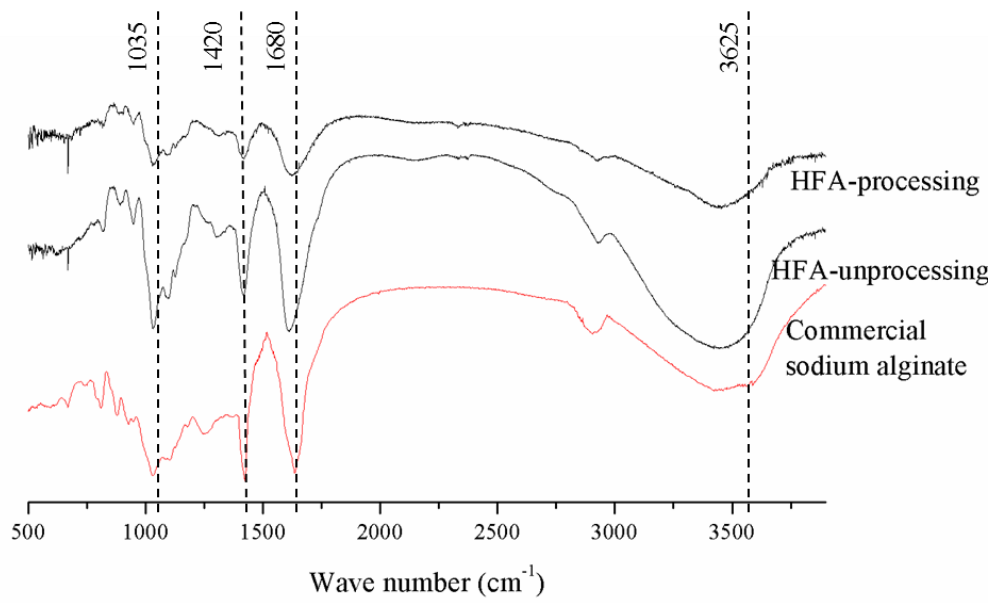


Figure 2-15 FT-IR spectroscopic analysis of structural features of HFA. HFA-processing: alginic acid isolated from 1% citric acid washed Hijiki; HFA-unprocessing: alginic acid isolated from original Hijiki.

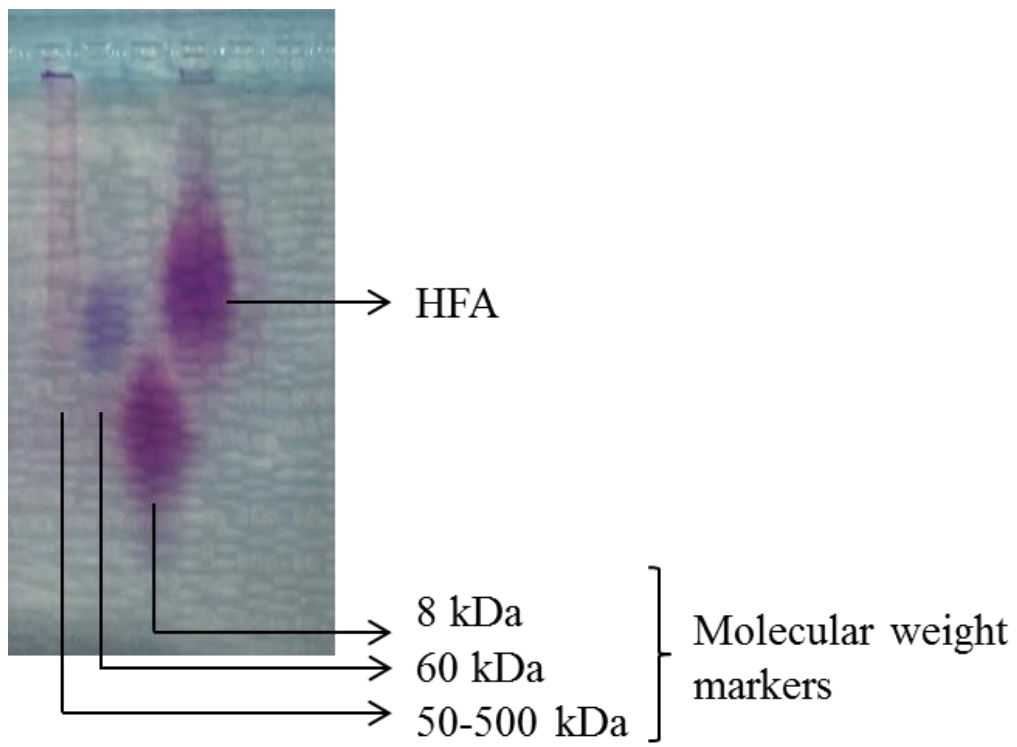


Figure 2-16 Approximate molecular weight distribution of HFA.

Table 2-4 Elemental metal composition of keratinocytes.

Element (ppm)	Blank	FD (125µg/mL)	FD+HFA (25µg/mL)	FD+HFA (50µg/mL)	FD+HFA (100µg/mL)
K	454±32	451±32	456±24	435±26	424±38
Ca	149±15*	435±21	345±26	159±38	62±25**
Na	612±9	609±29	623±22	657±34	665±25
Mg	115±9	165±23	132±21	65±14	38±10**
Sr	5±6**	149±19	94±12*	44±18*	18±20**
Fe	49±9**	258±35	165±11	140±25*	94±33**
Al	N.D.	79±14	75±4	62±8	51±14
As	N.D.	39±16	42±18	31±11	19±6
Mn	N.D.	65±6	45±15	32±14	11±9
Pb	N.D.*	368±15	217±38	111±15*	39±25**
Cu	N.D.	32±15	32±7	11±10	1±3
Cr	N.D.	32±11	25±15	12±24	N.D.
Ba	N.D.	101±11	78±28	14±12	N.D.

Results are given as the means ± SE based on triplicate determinations. For a specific element, * p < 0.05 and ** p < 0.01 were considered significant compared to the FD treated group. (N.D. stands for “not detected”).

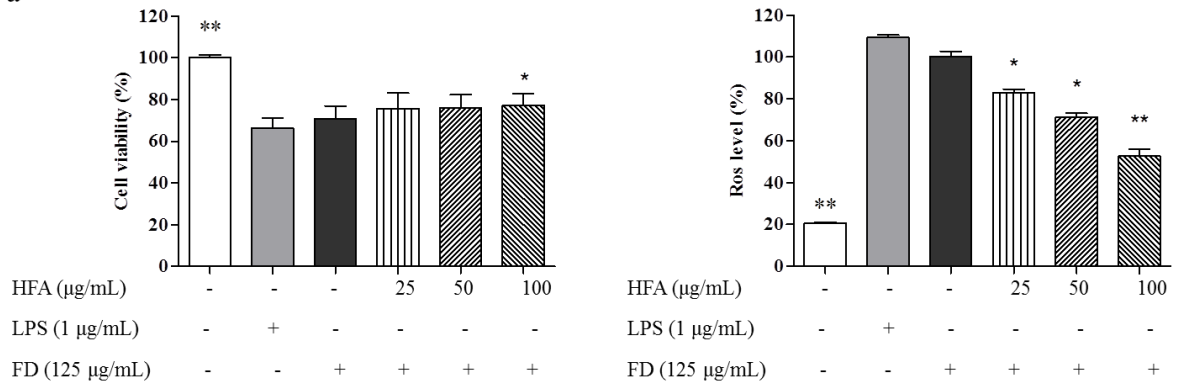
4.4.3 Ability of HFA to reduce FD-induced inflammatory responses in keratinocytes

The effect of the inflammatory mediators and anti-inflammatory cytokines induced by HFA on FD-stimulated keratinocyte damage was evaluated by MTT and DCFH-DA assays. As the positive control, lipopolysaccharide (LPS) treatment increased the intracellular ROS levels and decreased cell viability in HaCaT keratinocytes. Protective effects of HFA were observed in HaCaT keratinocytes exposed to FD (Fig. 2-17a). In cell viability assay, we found these data in each group showed high SE value because FD contains high amount heavy metal. Heavy metals influence the results of cell viability when UV measurement was performed. iNOS and NO production are absent in keratinocytes. Compared to the LPS and FD group, the levels of COX-2 and inflammatory mediators including IL-1 β , IL-6, PGE₂, and tumor necrosis factor- α (TNF- α) were decreased markedly in the untreated group in a dose-dependent manner (Fig. 2-17b and 17c). HFA treatment substantially reversed the FD-stimulated inflammatory responses in HaCaT keratinocytes.

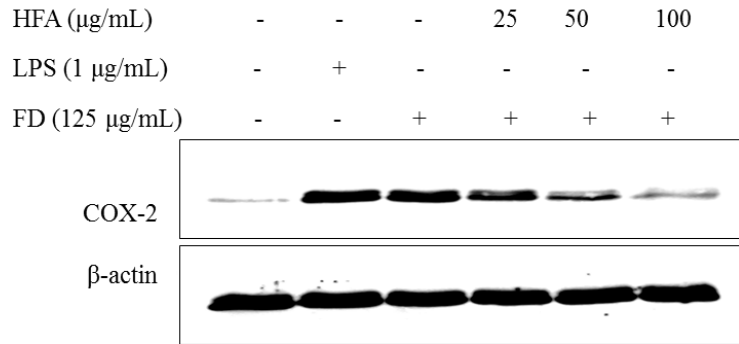
4.4.4 Protective effect of HFA against FD-induced apoptotic body formation in keratinocytes

After MTT assay for measurement of cell viability, DCFH-DA assay and Hoechst 33342 staining were carried out for further confirm the protective effect of HFA against FD-induced keratinocytes. In Fig. 2-17d and 2-17e, apoptotic body formations were observably found in FD-induced cells by using fluorescence microscopy. However, the numbers of observed apoptotic bodies were decreased when cells were pretreated with different concentrations of HFA. Additionally, as the sample concentration increased, apoptotic body formation decreased.

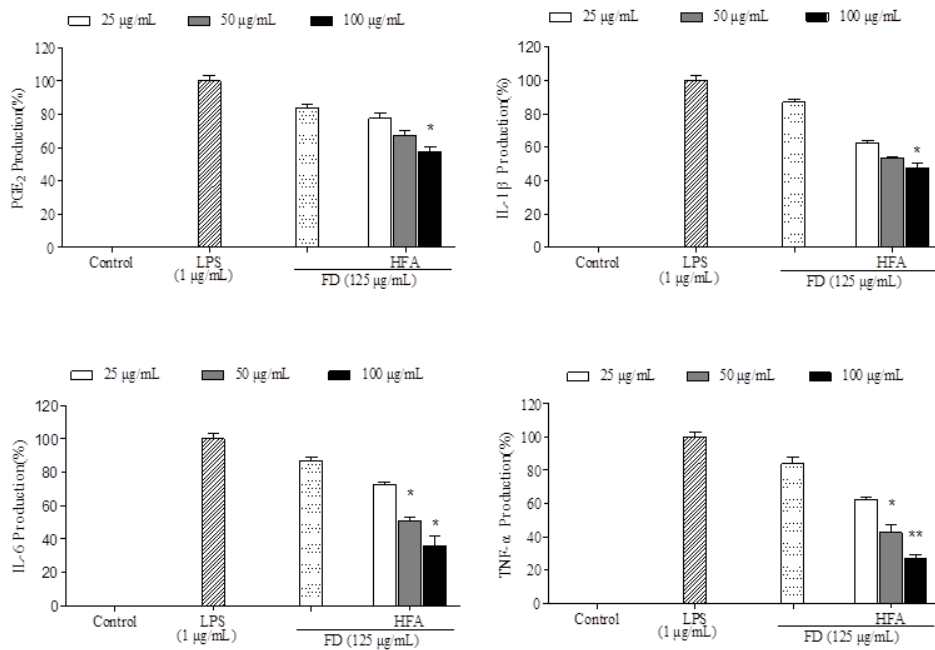
a



b



c



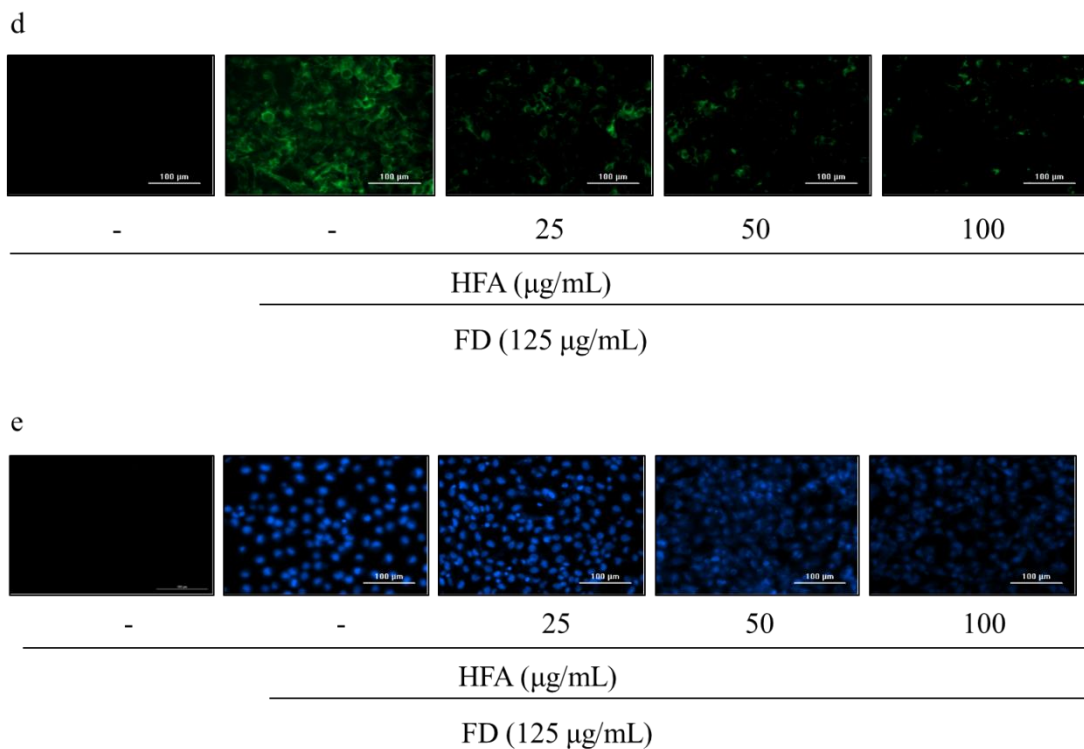
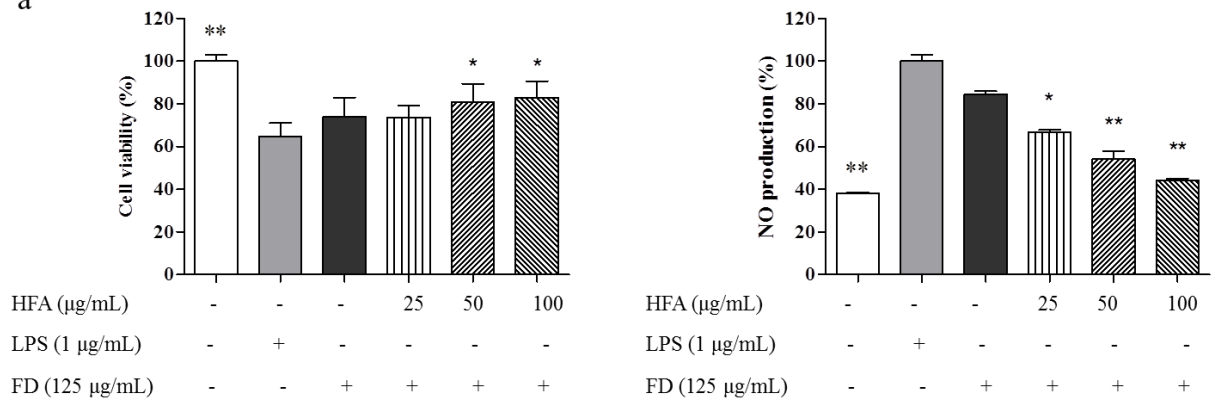


Figure 2-17 Efficacy of HFA against inflammation induced by FD in HaCaT keratinocytes. (a) Analyses of HaCaT cell viability and intracellular ROS levels; (b) Western blot analyses of COX-2 expressions; and (c) ELISA of prostaglandin E₂ (PGE₂) and pro-inflammatory cytokines (IL-1 β , IL-6, and TNF- α). Pre-seeded cells (1×10^5 cells/mL) were treated with different HFA concentrations after 24 h and stimulated with FD after 30 min. Cells were harvested after 24 h to measure inflammatory mediators (COX-2 and PGE₂) and pro-inflammatory cytokines (IL-1 β , IL-6, and TNF- α). Apoptotic body formation was observed under a fluorescence microscope after (d) DCFH-DA treatment and (e) Hoechst 33342 staining. Graphical representations are means \pm SE based on three replications. * $p < 0.05$ and ** $p < 0.01$ indicate that the values of sample treated groups were significantly different from those for the FD-treated group.

4.4.5 Anti-inflammatory effect of HFA in FD-induced RAW 264.7 macrophages

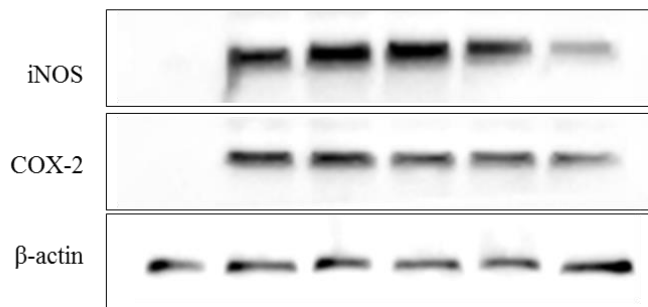
As shown in Fig. 2-18a, NO production was increased in FD- and LPS-stimulated macrophages. Among these, NO production by LPS induction was higher than that by FD induction. In the HFA treated FD-induced macrophages, NO production decreased and cell viability increased in a dose-dependent manner. Key inflammatory regulators such as iNOS and COX-2 regulate the production of NO and PGE₂ indirectly. Western blot analysis indicated that FD-stimulation significantly increased iNOS and COX-2 expression, whereas treatment with HFA resulted in a marked dose-dependent decrease in their intensities as shown in Fig. 2-18b. Consistent with these observations, the FD-induced group showed slightly lower expression of TNF- α and PGE₂ compared with that in the LPS-induced cells (Fig. 2-18c). In fact, the protein level of IL-1 β and IL-6 upon FD stimulation was significantly decreased compared to the blank treatment. The observations of the present study are in good agreement with those of previous studies [131].

a



b

HFA (μg/mL)	-	-	-	25	50	100
LPS (1 μg/mL)	-	+	-	-	-	-
FD (125 μg/mL)	-	-	+	+	+	+



C

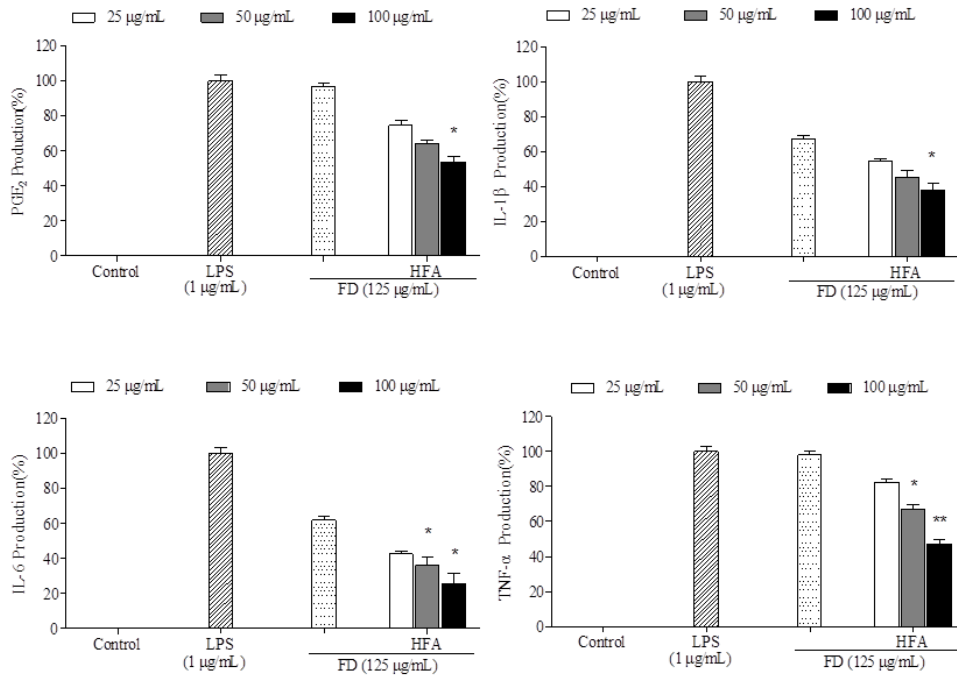
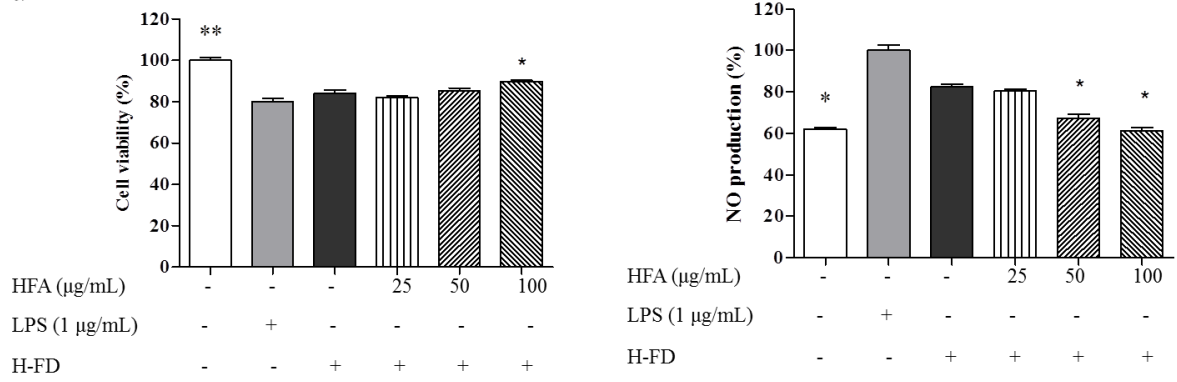


Figure 2-18 Efficacy of HFA against inflammation induced by FD in RAW 264.7 macrophages. (a) Analyses of RAW cell viability and intracellular ROS levels; (b) Western blot analyses of iNOS and COX-2 expressions; and (c) ELISA of PGE₂ and pro-inflammatory cytokines (IL-1β, IL-6, and TNF-α). Pre-seeded cells (1×10^5 cells/mL) were treated with different HFA concentrations after 24 h and stimulated with FD after 30 min. Cells were harvested after 24 h to measure inflammatory mediators (COX-2 and PGE₂) and pro-inflammatory cytokines (IL-1β, IL-6, and TNF-α). Graphical representations are means \pm SE based on three replications. * $p < 0.05$ and ** $p < 0.01$ indicate that the values of sample treated groups were significantly different from those for the FD-treated group.

4.4.6 Inflammatory responses in macrophages induced with culture medium harvested from FD-induced HFA treatment keratinocytes

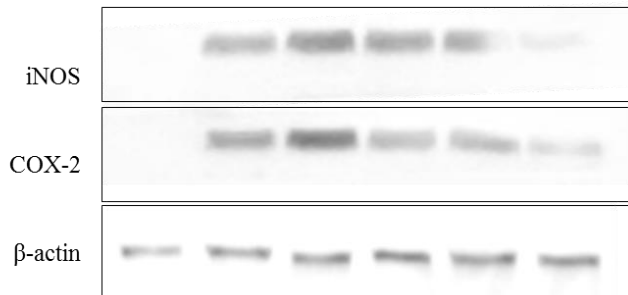
The relationship between keratinocytes and macrophages in transferring the inflammatory potential was investigated. Cell viability, NO production, levels of iNOS, COX-2, PGE₂, and pro-inflammatory cytokines, including IL-6, IL-1 β , and TNF- α were analyzed in H-FD-induced macrophages. HFA treatment showed a protective effect and effectively decreased the inflammatory responses in a dose-dependent manner (Fig. 2-19a). Accordingly, with an increase in the HFA concentrations, the intensities of iNOS and COX-2 were decreased (Fig. 2-19b). Moreover, the levels of pro-inflammatory mediators were reduced by HFA. In Fig. 2-19c, the H-FD triggered an increase of all inflammatory mediators and pro-inflammatory cytokines in the macrophages compared to the blank. Interestingly, the NO production upon indirect stimulation by FD (Fig. 2-19a) was higher than that upon direct stimulation in macrophages (Fig. 2-18a). In fact, interleukins such as IL-1 β and IL-6, produced in keratinocytes have been proven to simulate inflammatory responses in macrophages [159]. Hence, FD-induced HaCaT keratinocytes contribute inflammatory mediators and pro-inflammatory cytokines that might trigger inflammatory responses in macrophages.

a



b

HFA (μg/mL)	-	-	-	25	50	100
LPS (1 μg/mL)	-	+	-	-	-	-
H-FD	-	-	+	+	+	+



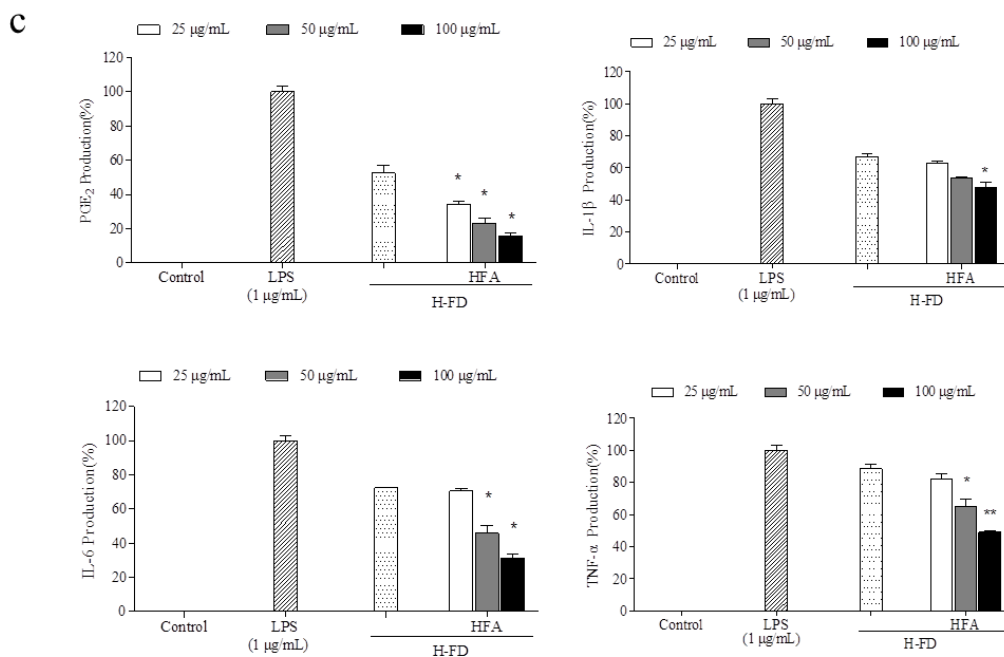


Figure 2-19 Inflammatory stimulation of the RAW 264.7 macrophages by the culture medium of FD-induced HaCaT cells and the anti-inflammatory effects of HFA. (a) NO production and cytotoxicity, (b) Analysis of iNOS and COX-2 levels, and (c) inflammatory mediators, including tumor necrosis factor α (TNF- α), interleukin (IL)-1 β , IL-6, and PGE₂. The HaCaT cells were pre-seeded in culture plates (1×10^5 cells/mL), incubated for 24 h, and treated with different concentrations of HFA. After 1 h, the cells were treated with FD (125 μ g/mL) and 24 h later, the culture medium were treated to each pre-seeded RAW 264.7 macrophages culture well plates in real time. The evaluations were made after a 24 h. Experiments were carried out in triplicate, and the results are represented as means \pm SE. * $p < 0.05$ and ** $p < 0.01$ indicate that the values of sample treated groups were significantly different from those for the FD-treated group. H-FD: The cultured medium of FD-stimulated in keratinocytes.

4.4.7 The anti-inflammatory effects of HFA in the FD-induced zebrafish embryo model

As shown in Fig. 2-20, a low viability rate and high ROS and NO production were observed in FD-induced embryos compared to the blank. However, the cell death rate of embryos was decreased by 80% when pretreated with HFA prior to FD treatment. HFA treatment markedly attenuated the ROS and NO levels in the larvae against FD-induced cell death. Additionally, treatment with HFA strongly inhibited the inflammatory responses of FD in a dose-dependent manner in the zebrafish embryo model.

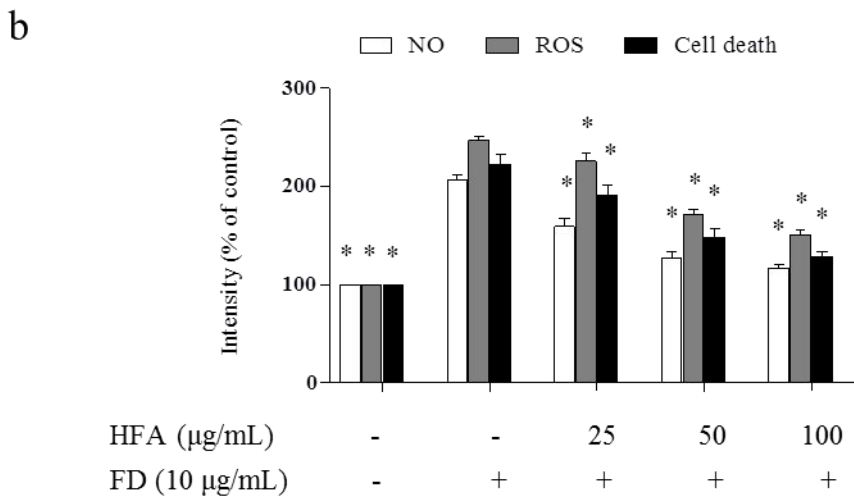
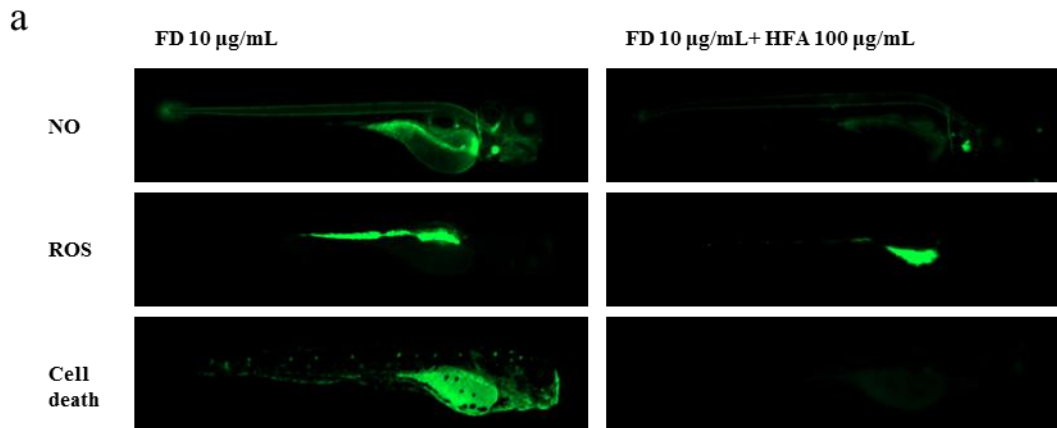


Figure 2-20 Inflammatory stimulation of zebrafish larvae by FD and anti-inflammatory effects of HFA. The anti-inflammatory properties were evaluated by measuring NO and ROS production, and cell death in the zebrafish embryo model. Experiments were carried out in triplicate, and the results are represented as means \pm SE. * $p < 0.05$ indicate that the values of sample treated groups were significantly different from those for the FD-treated group.

Generally, there are two main factors contributing to air pollution, anthropogenic activities and natural events. Anthropogenic activities that release emissions to the atmosphere include industrial expansion [160], coal or plant burning [161], vehicle consumption [162], and mineral particles [163]. Most of the air contaminated in natural events is characterized by visible changes such as hazy weather and sand storms from the Gobi desert [164]. FD particles, especially PM 2.5 (Particulate matter less than 2.5 μm in size), cause severe damage to the respiratory system and blood [165], and are the main contributors of air pollution in East Asia [166]. Although FD has become a serious problem in most developing countries, only a few studies describe their chemical composition and mobility trends. Some study have investigated the ambient ultra-fine particles during the fine dust season in Gwangju, Korea and Stuttgart, Germany [167, 168]. Accordingly, the polluted air has been analyzed to contain particles composed of Ca^{2+} , Mg^{2+} , K^+ , Na^+ , Cl^- , NO_x , SO_2 , SO_4^{2-} , NO_3^- , and NH_4^+ ions from 2011 to 2013 in China [169]. Another study investigated the markers OC2, EC1, and $\text{NO}_3^-/\text{SO}_4^{2-}$ ratio in PM 2.5 emissions in Xi'an in the wintertime of 2006, 2008, and 2010 [170]. The composition of the dust (Mg, Al, Ca, V, Cr, Mn, Fe, Co, Ni, Zn, As, Se, Cd, Sb, Pb) was measured by inductively coupled plasma-mass spectrometry [171]. An interesting study describes the pathway of FD-induced inflammation and oxidative stress in macrophages [172]. The evidence supports that dust particles can activate IL-1 β , IL-16, NF- κ B, and COX-2 expression in human myeloid leukemia cells indicating strong inflammatory responses [173]. Although many studies have examined the adverse effects of FD on single organ systems, this work investigated the transfer inflammatory response between skin cells and macrophages.

The keratinocyte model is widely used in dermatological studies to investigate results from the outside layers of the skin. They play a vital role in maintaining the stratum corneum barrier, thereby protecting the inner layers of skin cells. Keratinocytes induced by FD undergo apoptosis that likely manifests as skin irritation and damage [174], which further produces secondary mediators that upregulating the expression of IL-1 β and IL-6, resulting in an inflammatory response in HaCaT cells [175]. Macrophages play an essential role in regulating inflammation via phagocytosis, antigen presentation, and via the production of various growth factors and cytokines [176]. Activation of macrophages is an important strategy to manage external invasion and it is also stimulated by cytokines such as interferon γ , IL-1 β , and TNF- α , or by certain bacterial extracellular components such as LPS, and

certain chemicals [177].

Based on the results of this study, FD induced inflammatory responses in keratinocytes. Further, the stimulator is probably a pro-inflammatory cytokine that induces keratinocytes and transfers the inflammatory responses to macrophages. Previous studies have demonstrated the anti-inflammatory and protective effects of marine bioactive components against FD-induced inflammation. *Sargassum horneri* (Turner) C. Agardh extract has been proposed as a potential treatment in FD-induced inflammatory and oxidative stress via the p38 MAPK pathway and Nrf2/HO-1 expression [178]. Moreover, alginic acid from *Sargassum horneri* was shown to be effective against FD-induced inflammation in keratinocytes and RAW 264.7 macrophages [66]. The result of the animal experiment in this study indicated the ability of FD to induce inflammatory responses in zebrafish embryos. However, these responses could be markedly countered by HFA treatment at a concentration of 100 µg/mL.

5 Conclusion

JHCF4 was selected as the most active fraction among four fractions from AS-lower Hijiki. The chemical analysis confirmed the presence of high sulfate in JHCF4. It is found that JHCF4 showed antitumor activities on six tumor cell lines. Additionally, JHCF4 has strong peroxy radical scavenging activity via ESR and intracellular ROS scavenging activity in AAPH-induced Vero cells *in vitro* and exhibited strong hepato-protective activity via promoting cell growth in ethanol-induced Chang liver cells *in vitro* and reduced ethanol-induced damage in different hours old zebrafish models *in vivo*. Therefore, JHCF4 could be a natural nutrition in AS-lower Hijiki and expand application in market.

Part III. Anti-inflammatory potential of the fucoxanthin-rich fraction from *Hizikia fusiforme* against fine dust-induced inflammatory responses *in vitro* and in a zebrafish model

1 Abstract

Air pollution caused by fine dust (FD) particles has become a serious threat as it causes disorders of the skin and immune system. This part aims at evaluating the anti-inflammatory potential of the fucoxanthin-rich fraction (FxRF) of *Hizikia fusiforme* extract in FD-mediated inflammatory responses. The anti-inflammatory effect of the FxRF against FD-induced inflammation was also investigated. The composition of the FxRF was analyzed by high-performance liquid chromatography (HPLC) and rapid resolution liquid chromatography mass spectrometry (RRLC-MS), and fucoxanthin (Fx) and other pigments including cis-fucoxanthin, β -carotene, chlorophyll a, and phaeophytin a were identified. In cell assay, the medium of FD-induced HaCaT cells (H-FD) to activate macrophages to increase NO, iNOS, PGE₂, and pro-inflammatory cytokines was observed. FxRF treatment markedly attenuated the inflammatory responses including COX-2, PGE₂, interleukin (IL)-1 β , and IL-6 in FD-induced HaCaT keratinocytes, indicating its effectiveness in suppressing inflammatory responses. Further, FxRF was significantly decreased the expression of NO, iNOS, PGE₂, and tumor necrosis factor- α (TNF- α) in FD-induced and (H-FD)-induced RAW 264.7 macrophages. Our results also showed FxRF decreased NO, cell death, and reactive oxygen species (ROS) production in FD-induced zebrafish embryos indicates anti-inflammatory effect of FxRF. These results explain the potential anti-inflammatory effect of FxRF against FD-induced inflammation both *in vitro* and *in vivo*.

2 Introduction

Fine dust (FD) particles are the main contributors to air contamination, inducing harmful effects on organisms in developing countries nowadays [90]. FD mainly comes from unlimited industrial emissions and seasonal natural dust emissions [179, 180]. In the last four decades, China has experienced a dramatic economic rise, but at the cost of breaking its ecological balance [181]. The increasing usages of coal-burning power plants, oil consumption of vehicles, and a series of agricultural activities go along with the occurrence of haze or smog episodes [92]. A new study was performed in Beijing, the capital of China, that small size of FD could be transported towards the fetus and indicates a high risk induced by air pollution from infant [182]. In the other Asian countries, FD is often present with potentially toxic metals in aerosols at higher concentrations than it naturally occurs [93, 94]. FD particles poses a high risk to health, including lung cancer, chronic respiratory and heart diseases, weakening of the immune system, and reduction in lung function [95]. These particles are proven to be adversely effected in respiratory complications and induced allergic reactions or responses [96, 97]. Some studies have described the potential toxicological mechanism [98] and gene expression [99] linking FD and skin in human epidermal keratinocytes. Skin being the largest organ in the human body, it is most easily influenced by ambient stimulators, inducing infectious diseases in face, neck, and arms [183]. Evidence shows that harmful chemicals could disrupt the growth and differentiation patterns in human tissues. These reactions, starting from the skin to the inner tissue, might trigger inflammatory responses and immune suppressions [100]. Hence, an evaluation of anti-inflammatory agents induced by FD becomes necessary.

Fucoxanthin (Fx) is one of the carotenoids easily found in brown macroalgae, such as *Phaeodactylum tricornutum*, *Laminaria japonica*, *Eisenia bicyclis*, *Undaria pinnatifida*, and *Sargassum siliquastrum* [184-186]. These seaweeds serve as traditional foods in Asian countries. Fx has been used in a wide range of applications because of its antioxidant, anticancer, anti-inflammatory, and anti-UV effects [184, 187-189]. However, as a functional food ingredient, it is still expensive for people living in low-income countries. Its low concentration range with 0.02 to 0.58% of fresh weight restricts its commercial application [190]. The extract of a fucoxanthin-rich fraction (FxRF) is abundant and feasible, which contains Fx and other similar bioactive pigments. Previous studies have shown that FxRF improved the antioxidant and anti-obesity capacities were observed [191]. A other previous study was

highlighted that a fucoxanthin-rich extraction from seaweed decrease body fat was available [192]. In the assay of gene expression, FxRF regulated lipid metabolism in rats with a high-fat diet were also investigated [193]. Therefore, FxRF has a strong potential in bioactivity fields.

An FxRF of Hijiki showed its higher DPPH radical scavenging activity compared to that of *Undaria pinnatifida* and *Sargassum fulvellum* [194]. However, little information on the protective effect of FxRF on FD-induced inflammation from Hijiki is available. Zebrafish is used as a model for determination of *in vivo* anti-inflammation activity because its genes are more than 90% similar to those in humans [195]. Therefore, FxRF was isolated from Hijiki and its anti-inflammatory effect against FD-induced inflammation was evaluated both *in vitro* and *in vivo*.

3 Materials and methods

3.1 Preparation of FxRF

The *H. fusiforme* powder (500 g) was extracted with distilled water (DW) containing 80% methanol and filtered. The extracted solution was dried using an evaporator under vacuum, then dissolved in DW and partitioned with chloroform. The chloroform extract (5.4g) was performed and separated by silica column chromatography with initially elution of CHCl_3 -MeOH mixture (100:0, 90:10, 80:20, 70:30, 60:40, and 50:50) to afford separated fractions; the six active fractions were marked from 0M to 50M. According to the following chemical analysis, 0M showed the highest contents of Fx (18.46%) than those of other five fractions, therefore it was considered as FxRF (Fig. 3-1a).

3.2 Chemical analysis of FxRF

In order to determine FxRF, HPLC was used for quantified and rapid resolution liquid chromatography mass spectrometry (RRLC-MS) was used for identified compounds. The structure of Fx was compared with commercial Fx standard (NO.16337, Sigma-Aldrich) with previous report [196]. A 10 μL of sample was injected into the Agilent 1220 Infinity LC system equipped with a binary pump. The column was used in proshell 120 EC-C18 (150 \times 4.6 mm, 4 μm) in Agilent Technologies Inc., Santa Clara, CA, USA. The mobile phases used in the isocratic elution comprising of eluent (A) containing 0.1% formic acid DW, and eluent (B) consisting of 95% methanol. The flow rate was 0.3 mL/min and UV detection was observed at 445 nm. The Fx was eluted at retention time of 9.899 min (Fig. 3-1b). The standard curve and retention times were calibrated using Fx standard at six continuously increasing

concentrations. The automated integration software (Agilent ChemStation software, Waldbronn, Germany) was performed to acquire peaks area (mAU*s). The contents of Fx were expressed as milligram Fx per gram dry weight biomass as those in the previous report [197].

A RRLC-MS system was equipped with a quadrupole-time-of-flight mass spectrometer (Agilent Technologies Inc.) with an electrospray ionization source in positive ion mode. The samples were injected and separated using an Agilent Eclipse Plus C₁₈ column (2.1 mm × 150 mm, 3.5 μm) at 30°C. The flow rate was 0.3 mL/min, and the volume of injection was 5 μL. The mobile phases and isocratic elute mode were followed that of HPLC analysis. The MS conditions were set as: nebulizer of 30 psig, capillary voltage of 2,800 V, cone voltage of 35 V, fragmentation voltage of 120 V, drying gas temperature of 350 °C, drying gas (N₂) flow rate of 8 L/min, atomization gas pressure of 2.41×10^5 Pa, and a mass-scanning range of m/z 100-2000. Data analysis was performed using Agilent MassHunter (B.03.01).

3.3 Cell culture

RAW 264.7 macrophages and HaCaT keratinocytes cells were obtained from the Korean Cell Line Bank (KCLB, Seoul, Korea). DMEM, FBS, and PS were obtained from Thermo Fisher Scientific, Waltham, MA, USA.

3.4 Nuclear staining and ROS measurement

The protective properties of FxRF after FD-induced on nuclear morphology changed in keratinocytes was identified followed the protocol of Hoechst 33342/PI nuclear staining and DCFH-DA assay. Keratinocytes were seeded at a density of (1×10^5 cells/mL) in 24-well culture plates and added to various concentrations FxRF after incubation of 24 h. Then 25 μL of Hoechst 33342 (stock 1 mg/mL)/PI (5 μg/mL) staining were treated to cells for nuclear staining, 25 μL of DCFH-DA (5 μg/mL) were treated to cells for ROS detection. After 24 h incubation, cells were stained in 10 min in the dark and imaged using a fluorescence microscope coupled with CoolSNAP-Pro color digital camera (Meyer Instruments, Inc., Houston, TX, USA).

3.5 Evaluation of inflammatory responses

RAW 264.7 macrophages and HaCaT keratinocytes were separately pre-seeded in different 24-well plates and incubated for 24 h. The different concentrations of FxRF were then treated to each well. After 1 h, fresh medium containing 25 μL of FD (125 μg/mL) was substituted in the cells. The cells were washed

with fresh medium after 30-min incubation. The cells were continuously incubated for 24 h, and then harvested and analyzed the inflammatory-related mediators and cytokines. In HaCaT keratinocytes, cell viability, intracellular ROS production, and inflammatory-related mediators and cytokines were evaluated by MTT assay, DCFH-DA assay, and commercial kit [130]. The MTT assay is recognized as a colorimetric assay, heavy metals strongly influence the value of cell viability. To avoid the influence of heavy metals in cell viability, we developed a method to remove the remaining heavy metals. The DMSO solution containing formazan was centrifuged ($10,000 \times g$ for 10 min) and the supernatant was measured under 540 nm. Cytokine kits were purchased from Thermo Fisher Scientific (Waltham, MA, USA), R&D Systems (Minneapolis, MN, USA), Becton Dickinson & Co. (Franklin Lakes, NJ, USA), and Invitrogen (Carlsbad, CA, USA). The analysis method was followed by the manufacturer's guidelines. In macrophages, the treatment concentration of FD, cell viability, NO production, the inflammatory-related mediators and cytokines were evaluated followed the previous protocols [131].

The keratinocytes were seeded at a density of (1×10^5 cells/mL) in 24-well culture plates. After 24 h incubation, the different concentrations of FxRF were treated to cells for 1 h incubation. After 1 h, fresh medium containing 25 μ L of FD (125 μ g/mL) was substituted in the cells. The cells were washed with fresh medium after 30-min incubation. The cells were continuously incubated for 24 h. The medium of keratinocytes cells were harvested and directly treated with the pre-seeded macrophages. Following the 24 h incubation, the macrophages cells were harvested and analyzed for the inflammatory-related mediators and cytokines.

3.6 Western blot analysis

In order to further determine the anti-inflammatory effects against FD-induced damage, Western blotting was performed to evaluate inflammatory-related mediators. RAW 264.7 macrophages and HaCaT keratinocytes were separately seeded at a density of 2×10^5 cells/mL in single culture plates for 24 h incubation and treatment of FxRF and FD (or H-FD) as the described above. After 30-min incubation, the cells were rinsed by fresh DMEM and harvested after 24 h. The cell lysates were obtained by homogenizing with lysis buffer and centrifuging to remove pellet. The cell lysates then were determined total protein content using a BCA protein kit (Thermo Fisher Scientific, MA, USA). A totally 50 μ g of proteins from lysates were separated by 12% polyacrylamide depending on molecular weight by using

electrophoresis. The proteins in gels were transferred onto nitrocellulose membranes. The membranes were blocked in 5% nonfat milk and incubated with primary antibodies and secondary antibodies (Santa Cruz Biotechnology, Dallas, TX, USA). The blots were treated by the chemiluminescent substrate (Cyanagen Srl, Bologna, Italy) and the fluorescence images were carried out a FUSION SOLO Vilber Lourmat system (FUSION, Paris, France) [120]. Image J software was carried out for calculating the intensity of bands.

3.7 Zebrafish embryo experiments

Adult zebrafish were purchased from pet shop in Jeju city, South Korea. Embryos were collected by natural spawning with light/dark cycle in 28.5 °C. According to previous protocol [131], FD treated concentration at 10 µg/mL in each well was selected. The experiments of FD-induced ROS, NO production, and cell death in embryos were evaluated. Briefly, the embryos were randomly divided into 12-well plates and treated with different concentrations FxRF followed by FD treatment. Following incubation for 72 h, DAF-FM DA, DCFH-DA and acridine orange were used as fluorescent dyes to identify NO productions, ROS levels, and cell death of hatched larvae, respectively. The spectrofluorometer (Perkin–Elmer LS-5B, Austria) was carried out to calculate the fluorescence intensity of embryos and Image J software was performed to calculate the intensities of embryos.

3.8 Statistical analysis

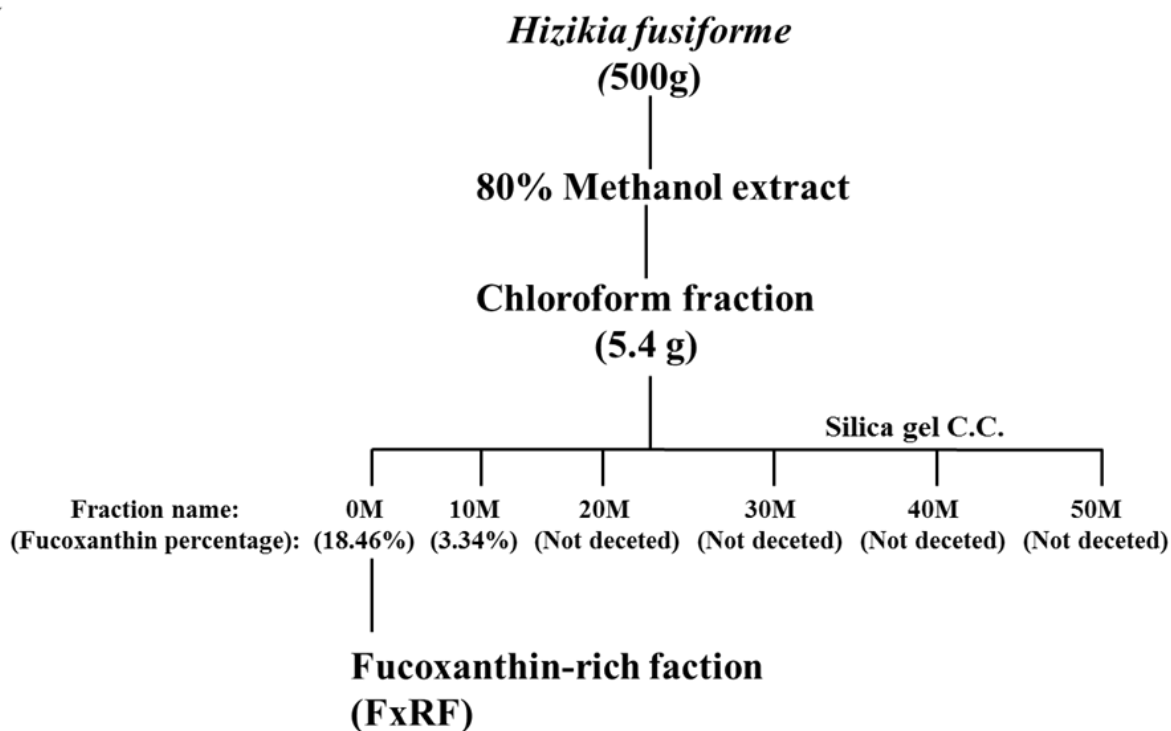
All assays were made in three independent experiments. Values were expressed as the mean ± SE. One-way ANOVA was used to analyze the mean values in GraphPad prism 5 software. Student's t-test (*p < 0.05 and **p < 0.01) was used to analyze the means of the parameters of significant differences.

4 Results and Discussion

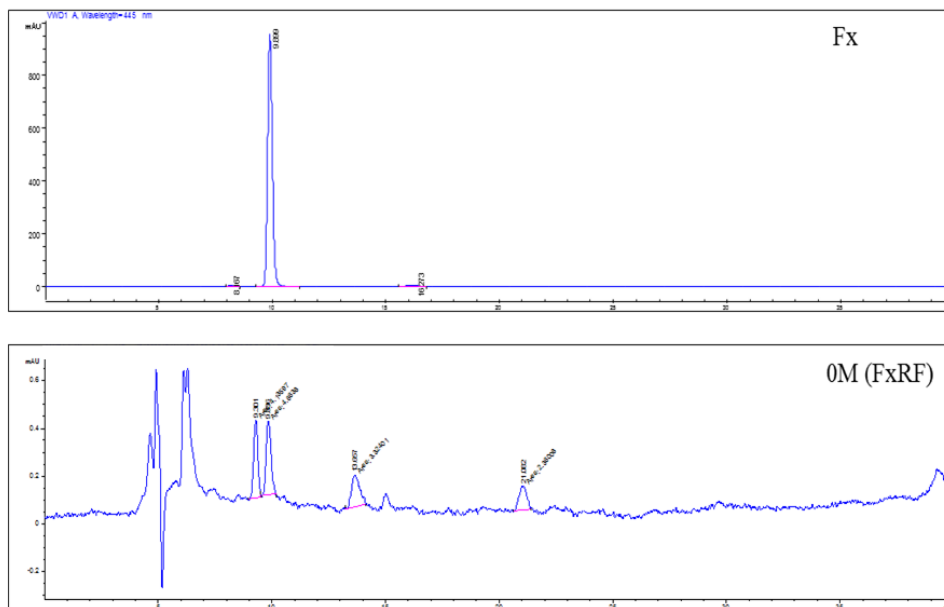
4.1 HPLC and RRLC-MS analysis of FxRF

HPLC analysis of six active fractions (0M, 10M, 20M, 30M, 40M, and 50M) from Hijiki was carried out. As shown in Fig. 3-1b, 0M contains the highest concentration of 18.46 % fresh weight of Fx among the six fractions. Subsequently, RRLC-MS was carried out for the identified Fx. The $[M+H]^+$ ion (m/z 659.3) and the adduct $[M+Na]^+$ ion (m/z 681.9) were identified based on the fragment pattern in Fig. 3-1c. The daughter ions of Fx at m/z 581.4 and 641.4 were generated by the loss of H_2O (18 Da) and H_2O+CH_3COOH (78 Da), respectively. Thus, with ion m/z 581.4 and 641.4 peaks, we considered the mass spectrum to be that of Fx. In addition, other pigments phaeophytin a, chlorophyll a, and β -carotene were deduced and identified by determination of molecular weight and fragments. The identified compounds match well with the previously reported compounds [198, 199].

a



b



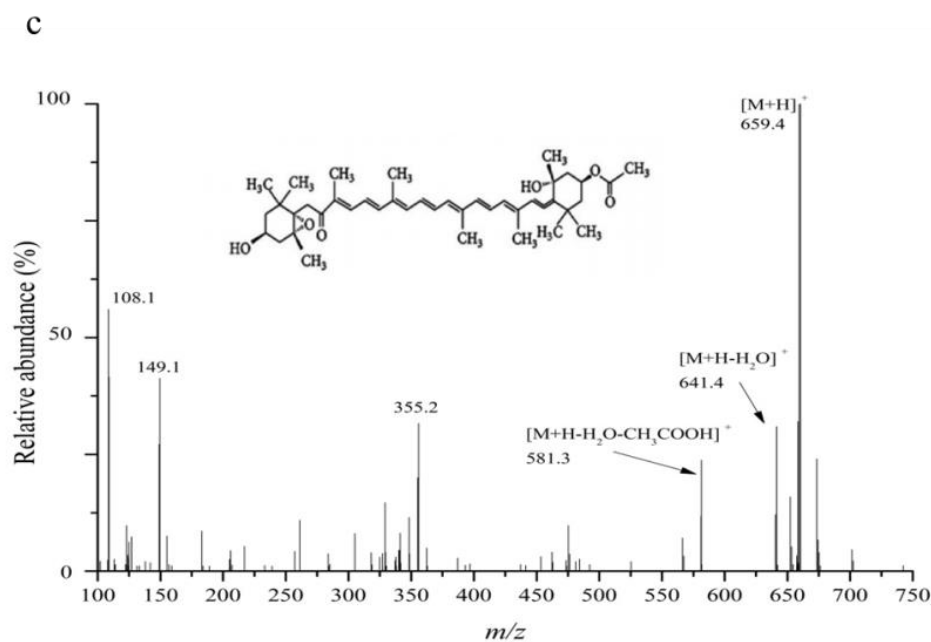


Figure 3-1 Chemical information of fucoxanthin-rich fraction (FxRF) from *Hizikia fusiforme*. (a)

Extraction and isolation scheme for FxRF, 0M: The separated active fraction from elution of CHCl₃-MeOH mixture (100:0); 10M: The separated active fraction from elution of CHCl₃-MeOH mixture (90:10); 20M: The separated active fraction from elution of CHCl₃-MeOH mixture (80:20); 30M: The separated active fraction from elution of CHCl₃-MeOH mixture (70:30); 40M: The separated active fraction from elution of CHCl₃-MeOH mixture (60:40); 50M: The separated active fraction from elution of CHCl₃-MeOH mixture (50:50). (b) The HPLC chromatographs of Fx standard and FxRF. The mobile phases used in the isocratic elution consisted of eluent: 0.1% formic acid water and 95% methanol. The flow rate was 0.3 mL/min and UV detection was observed at 445 nm. (c) The mass spectrum of fucoxanthin from FxRF.

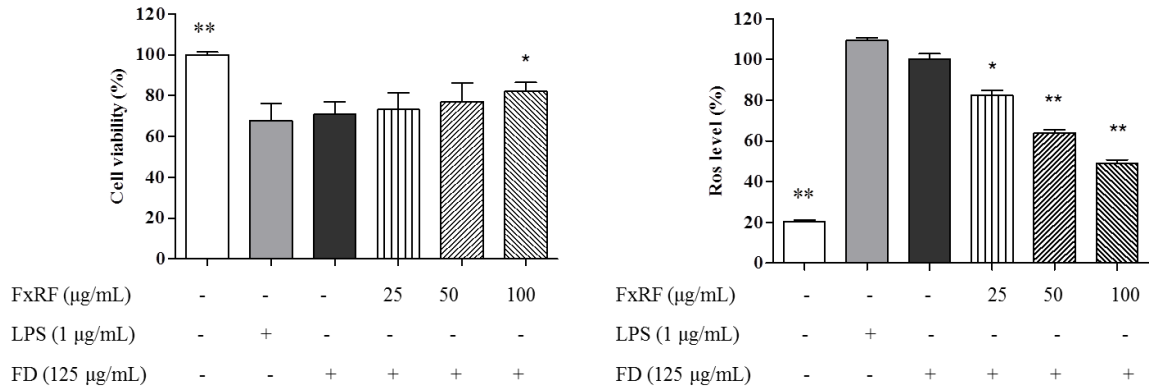
4.2 Measurement of FxRF against FD-induced inflammatory responses in keratinocytes

The expression of inflammatory-related mediators and cytokines of FxRF against FD-stimulated keratinocytes damage by MTT and DCFH-DA assay was evaluated. As a positive control, LPS treatment increased the ROS production and the cell death rate of HaCaT keratinocytes. The protective effects of FxRF on FD-induced HaCaT keratinocytes (Fig. 3-2a) were observed. It is hard to determine the expression of iNOS and NO production in the keratinocytes. In cell viability assay, we found these data in each group showed high SE value because FD contains high amount heavy metal. Heavy metals were strongly influenced the results in cell viability in UV measurement. Thus, we measured cell survive rate before centrifuging. The levels of COX-2 and phosphorylation of p-p38 MAPK, P-Erk1/2, and P-JNK decreased significantly in the untreated group in a dose-dependent manner compared to those of the LPS and FD groups (Fig. 3-2b, 2c). FD treatment also increased the levels of PGE₂ and pro-inflammatory cytokines, including interleukin (IL)-6, interleukin (IL)-1 β , and tumor necrosis factor- α (TNF- α) (Fig. 3-2d). FxRF treatment substantially reversed the FD-stimulated inflammatory responses in HaCaT keratinocytes and inflammatory mediators including IL-1 β , IL-6, PGE₂, and TNF- α .

4.3. Protective effect of FxRF against FD-induced apoptotic body formation in keratinocytes

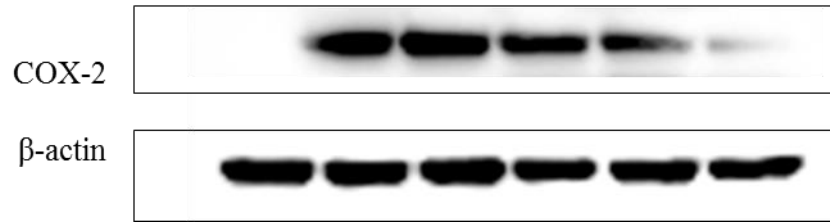
After MTT assay for measurement of cell viability, DCFH-DA assay and Hoechst 33342 and PI staining were carried out for further confirm the protective effect of FxRF against FD-induced keratinocytes. In Fig. 3-2e and 3-2f, apoptotic body formations were observably found in FD-induced cells by using fluorescence microscopy. However, the numbers of observed apoptotic bodies were decreased when cells were pretreated with FxRF. Additionally, as the sample concentration increased, apoptotic body formation decreased.

a



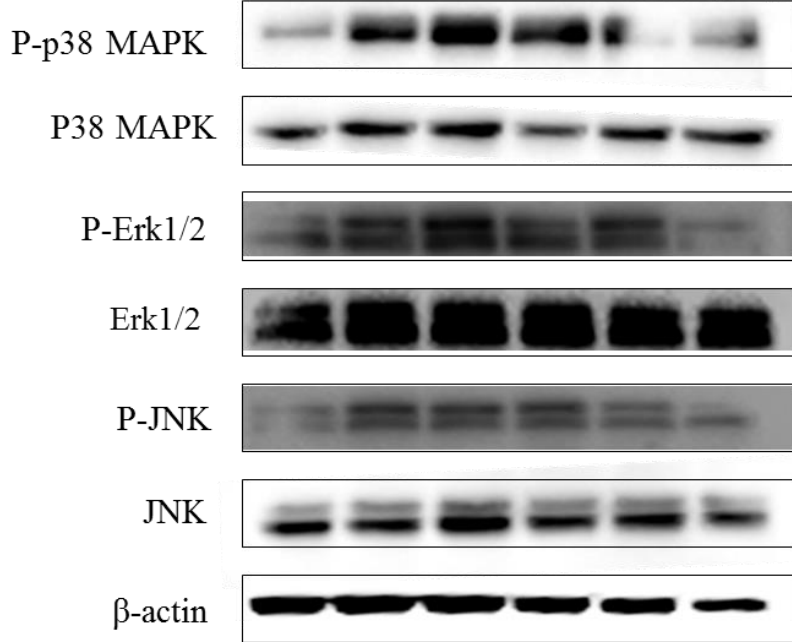
b

FxRF (μg/mL)	-	-	-	25	50	100
LPS (1 μg/mL)	-	+	-	-	-	-
FD (125 μg/mL)	-	-	+	+	+	+

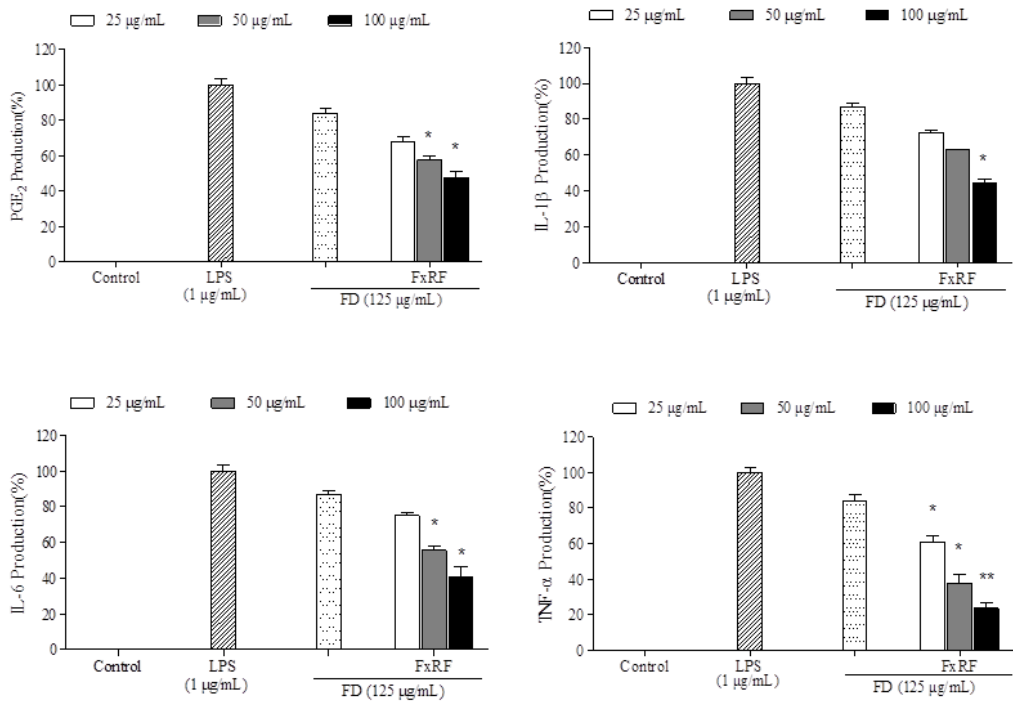


c

FxRF ($\mu\text{g/mL}$)	-	-	-	25	50	100
LPS ($1 \mu\text{g/mL}$)	-	+	-	-	-	-
FD ($125 \mu\text{g/mL}$)	-	-	+	+	+	+



d



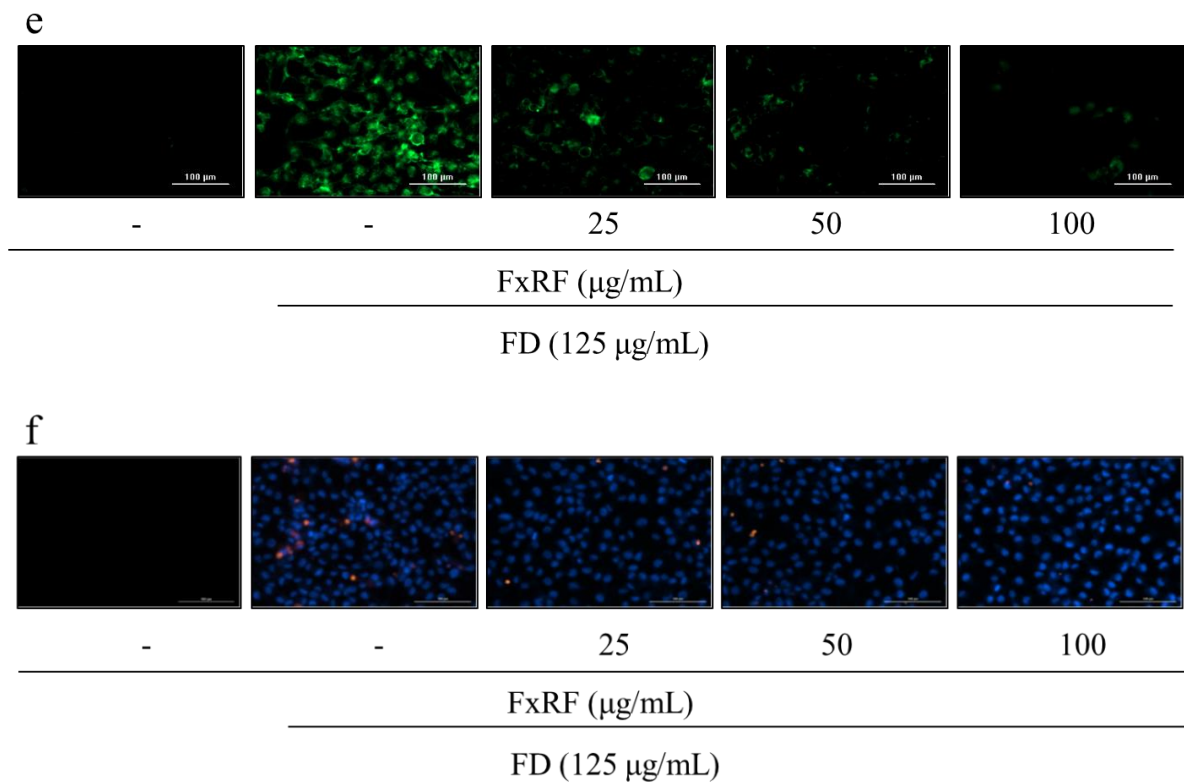
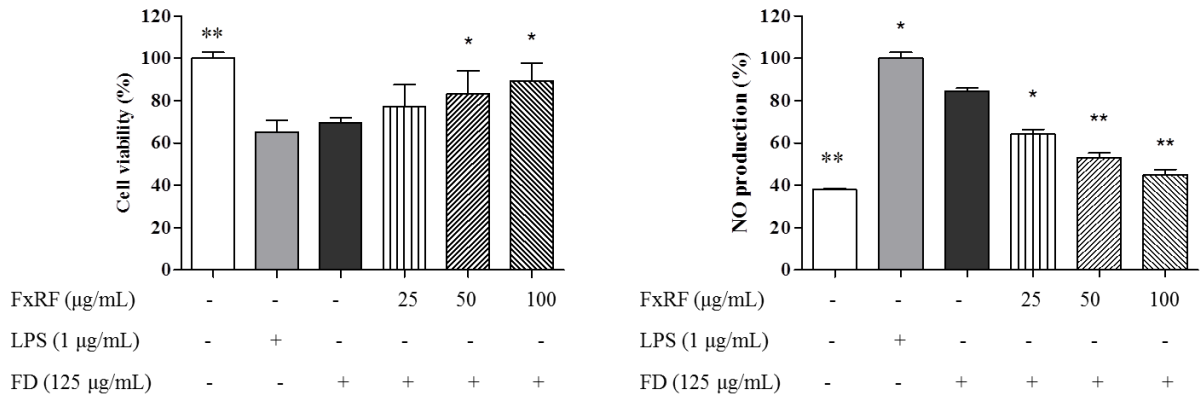


Figure 3-2 Efficacy of FxRF against inflammation induced by FD in HaCaT keratinocytes. (a) Analyses of HaCaT cell viability and intracellular ROS levels; (b) Western blot analyses of COX-2 expressions; (c) Levels of key molecular mediators in the MAPK pathways; and (d) ELISA of PGE₂ and pro-inflammatory cytokines (IL-1 β , IL-6, and TNF- α). Pre-seeded cells (1×10^5 cells/mL) were treated with different FxRF concentrations after 24 h and stimulated with FD after 30 min. Cells were harvested after 24 h to measure inflammatory mediators (COX-2 and PGE₂) and pro-inflammatory cytokines (IL-1 β , IL-6, and TNF- α). Apoptotic body formation was observed under a fluorescence microscope after (e) DCFH-DA treatment and (f) Hoechst 33342 and PI staining. Graphical representations are means \pm SE based on three replications. * $p < 0.05$ and ** $p < 0.01$ indicate that the values of sample treated groups were significantly different from those for the FD-treated group.

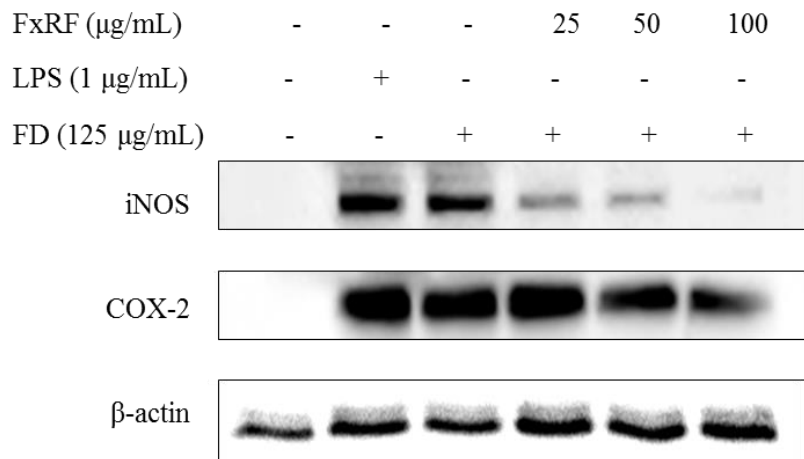
4.4 Measurement of FxRF against FD-induced inflammatory responses in RAW 264.7 macrophages

As shown in Fig. 3-3a, the NO productions were increased in FD- and LPS-stimulated macrophages. Among them, the production of LPS-induced NO was higher than that of FD-induced NO. In FxRF treatment, the NO production decreased and the viability increased in FD-induced macrophages significantly and dose-dependently. The key inflammatory regulators such as iNOS and COX-2 regulate the level of NO and PGE₂ indirectly. Western blot analysis indicated that FD-stimulation significantly increased iNOS and COX-2 expressions; however, treatment with FxRF dose-dependently down-regulated their intensities in Fig. 3-3b. Consistent with these observations, the FD-induced group slightly downregulated the expressions of IL-1 β and IL-6 compared to the LPS-induced group (Fig. 3-3c). In fact, the protein level of TNF- α and PGE₂ upon FD stimulation caused a marked decrease compared to the control value. All results are in agreement with a previous study [131].

a



b



C

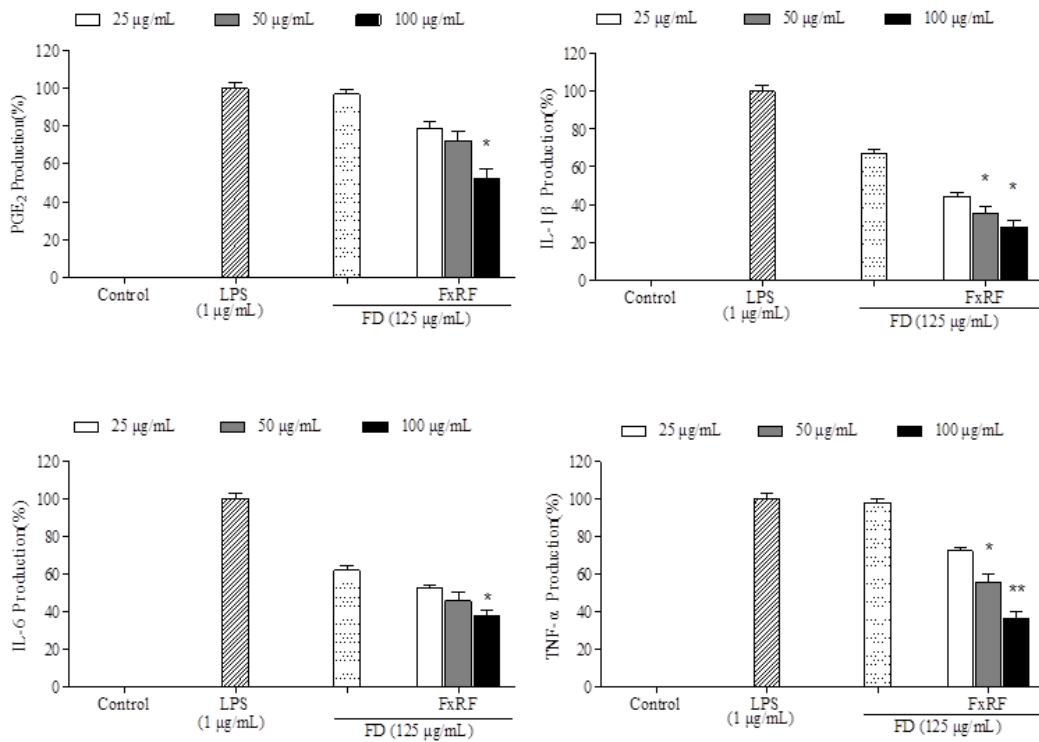
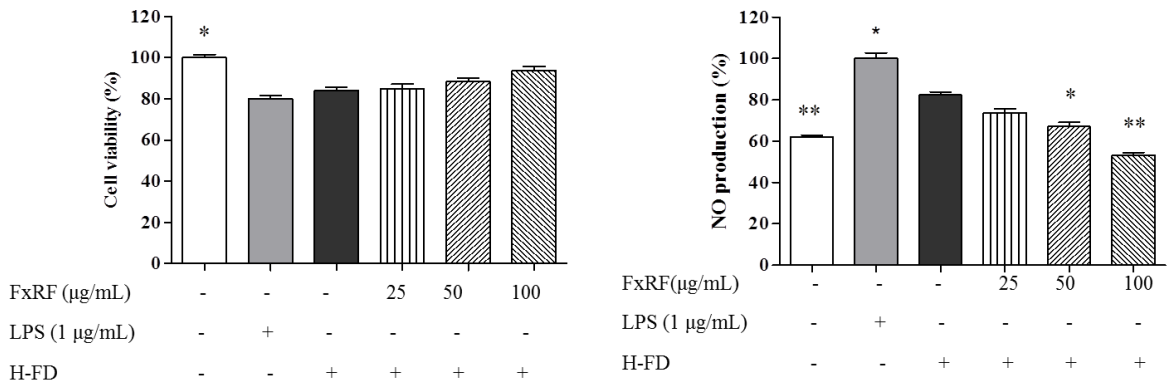


Figure 3-3 Efficacy of FxRF against inflammation induced by FD in RAW 264.7 macrophages. (a) Analyses of RAW cell viability and intracellular ROS levels; (b) Western blot analyses of iNOS and COX-2 expressions; and (c) ELISA of PGE₂ and pro-inflammatory cytokines (IL-1β, IL-6, and TNF-α). Pre-seeded cells (1×10^5 cells/mL) were treated with different FxRF concentrations after 24 h and stimulated with FD after 30 min. Cells were harvested after 24 h to measure inflammatory mediators (COX-2 and PGE₂) and pro-inflammatory cytokines (IL-1β, IL-6, and TNF-α). Graphical representations are means \pm SE based on three replications. * $p < 0.05$ and ** $p < 0.01$ indicate that the values of sample treated groups were significantly different from those for the FD-treated group.

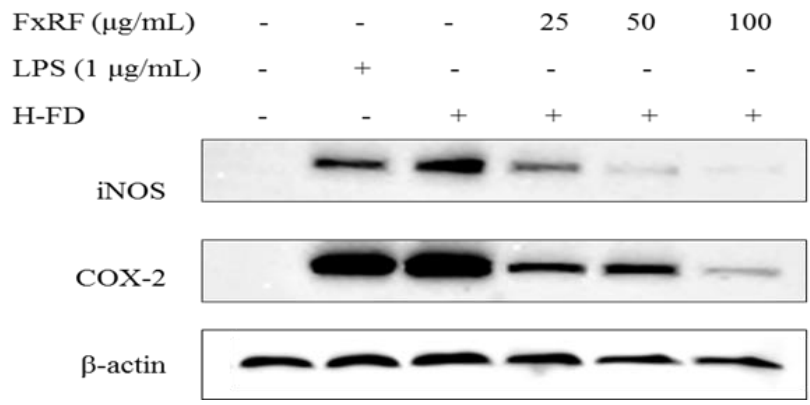
4.5 Inflammatory responses in RAW 264.7 macrophages induced with a culture medium collected from FD-induced FxRF treatment keratinocytes

The stimulate factors from keratinocytes transferred to macrophages, induces the potential inflammatory response was investigated. The H-FD was transferred to macrophages culture plates and analyzed for inflammatory mediator levels after 24 h incubation. Cell viability, NO production, levels of iNOS, COX-2, PGE₂, and pro-inflammatory cytokines, including IL-6, IL-1 β , and TNF- α in macrophages were analyzed. FxRF treatment showed a dose-dependently protective effect and markedly inhibited the inflammatory responses (Fig. 3-4a). Accordingly, with the increase in FxRF concentrations, the expressions of iNOS and COX-2 were decreased (Fig. 3-4b). Further, FxRF reduced the expressions of pro-inflammatory mediators were observed. As depicted in Fig. 3-4c, the H-FD group triggers an increase in inflammatory-related mediators and cytokines in macrophages compared to the blank group. According to a previous report [159], the interleukin family including IL-1 β and IL-6, produced in keratinocytes, has been proven to stimulate inflammatory responses in macrophages. Hence, FxRF treatment might contribute to reduce inflammatory responses in macrophages.

a



b



C

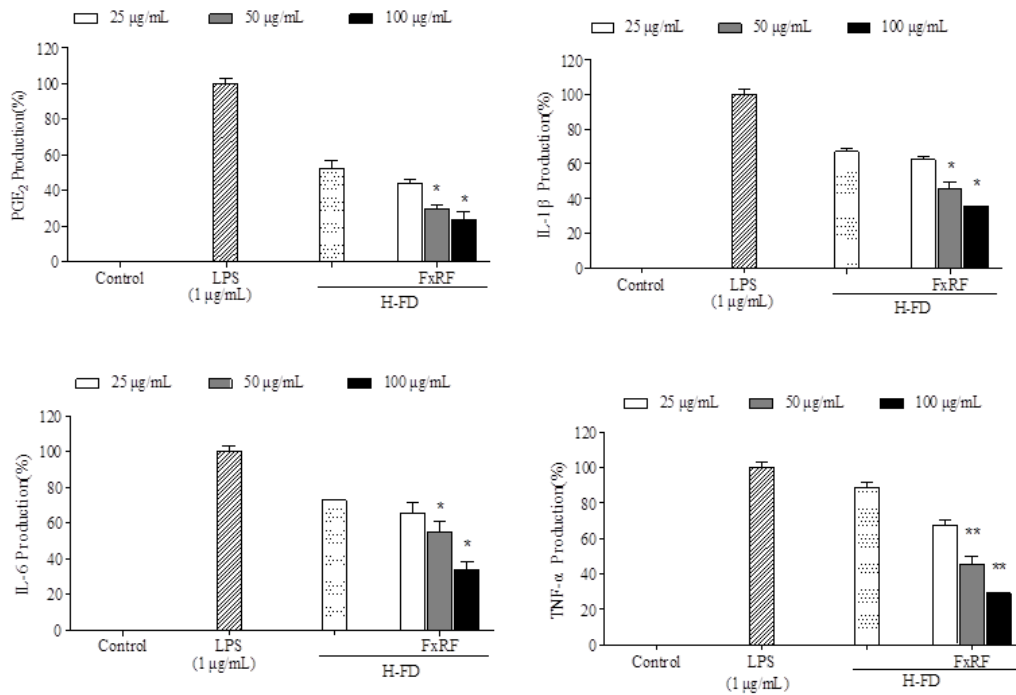
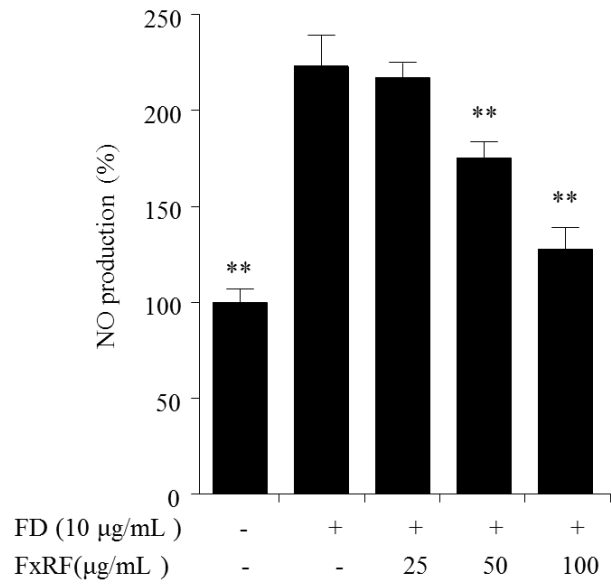
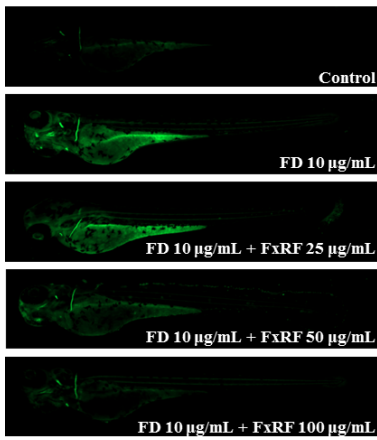


Figure 3-4 Inflammatory stimulation of the RAW 264.7 macrophages by the culture medium of FD-induced HaCaT cells and the anti-inflammatory effects of FxRF. (a) NO production and cytotoxicity, and (b) Analysis of iNOS and COX-2 levels and (c) Inflammatory mediators, including tumor necrosis factor α (TNF- α), interleukin (IL)-1 β , IL-6, and PGE₂. The HaCaT cells were pre-seeded in culture plates (1×10^5 cells/mL), incubated for 24 h, and treated with different concentrations of FxRF. After 1 h, the cells were treated with FD (125 μ g/mL) and 24 h later, the culture medium were treated to each pre-seeded RAW 264.7 macrophages culture well plates in real time. The evaluations were made after a 24 h. Experiments were carried out in triplicate, and the results are represented as means \pm SE. * $p < 0.05$ and ** $p < 0.01$ indicate that the values of sample treated groups were significantly different from those for the FD-treated group. H-FD: The cultured medium of FD-stimulated in keratinocytes.

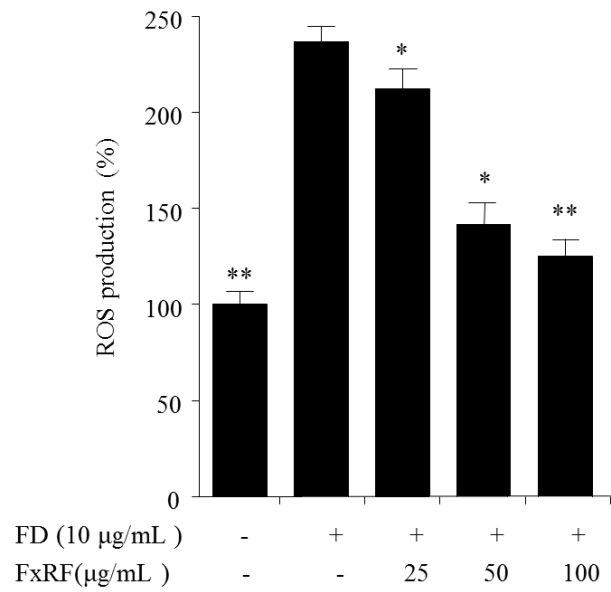
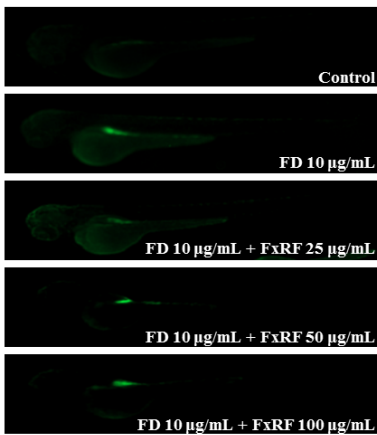
4.6 The anti-inflammatory effects of FxRF on the FD-induced zebrafish embryo model

As shown in Fig. 3-5, a low viability rate and high ROS and NO productions were observed for FD-induced embryos compared to the blank. However, the cell death rate of embryos was decreased by 90% when they were pretreated with FxRF prior to the FD treatment. The FxRF treatment markedly decreased ROS and NO production in the embryo against FD-induced cell death. Upon cell death, an interesting observation was found that the FD-treated larvae cerebrum exhibits a visible fluorescence intensity spot, indicating that FD may have the ability to damage the larvae head tissue. Additionally, the observations showed that treating embryos with FxRF is dose-dependently inhibited by the inflammatory responses of FD in the zebrafish embryo model. Our results demonstrated that the ability of FxRF was markedly reduced FD-induced inflammatory responses in zebrafish embryos.

NO production



ROS production



Cell death

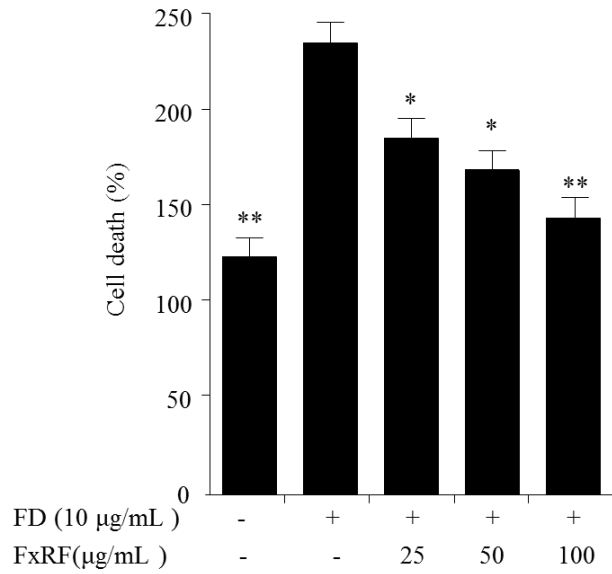
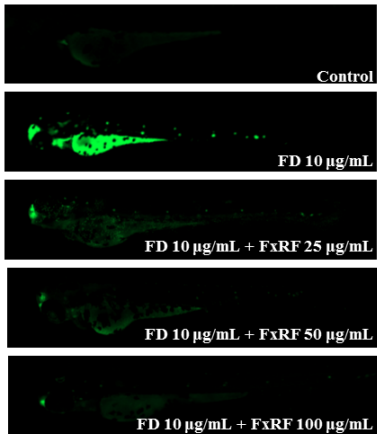


Figure 3-5 Inflammatory stimulation of zebrafish larvae by FD and anti-inflammatory effects of FxRF. The anti-inflammatory properties were evaluated by measuring NO and ROS production, and cell death in the zebrafish embryo model. Experiments were carried out in triplicate, and the results are represented as means \pm SE. Values are significantly different from the positive control (FD treated group) at * $p < 0.05$ and ** $p < 0.001$.

FD has become a serious public health concern in most countries, and several studies have described their chemical composition and detrimental physiological effects. Among FD particles, particulate matter less than 2.5 μm in size, known as PM 2.5, cause severe damage to the respiratory and circulatory systems [165], in addition to causing air pollution [166]. FD induces apoptosis of keratinocytes, which form the outside layer of the skin [174], and this leads to the production of secondary immune mediators such as IL-1 β and IL-6 by the surviving keratinocytes, resulting in the induction of an inflammatory response [175]. As a strategy to manage the external invasion, activation of macrophages is stimulated by cytokines, such as interferon γ , IL-1 β , and TNF- α , or by foreign agents [177]. FD induced inflammatory responses in keratinocytes. Furthermore, the stimulator is probably the pro-inflammatory cytokine, which induced keratinocytes and transferred the inflammatory responses to macrophages. Previous studies support the evidence that the anti-inflammatory effect of DPHC isolated from *Ishige okamurae* elicited by FD in keratinocytes and macrophages was investigated [131]. Moreover, the alginic acid from *Sargassum horneri* proved to be useful against FD-induced inflammation in keratinocytes and RAW 264.7 macrophages [66].

Carotenoids are the major pigments in seaweeds and have strong bioactivities [200]. In this study, FxRF was found to contain a mixture of five pigments, namely, Fx, cis-fucoanthin, β -carotene, chlorophyll a, and phaeophytin a. The results were in accordance with the chemical profile of other brown seaweeds [201]. Previous studies have reported the antioxidant capacity of β -carotene [202], as well as the anti-inflammatory action of chlorophyll a via the NF- κ B signaling pathway [203]. Moreover, Fx has been shown to reduce the levels of NO, PGE₂, IL-6, IL-1 β , and TNF- α via suppression of MAPK phosphorylation in RAW 264.7 cells [204]. Hence, the anti-inflammatory effect of FxRF on stimulated macrophages is promising. FD treatment reduced the viability of macrophages to approximately 60%, whereas FxRF treatment showed cytoprotective effects against FD-induced inflammatory responses.

The MAPK signaling pathway, one of the most studied pathways, is most mediated by extracellular stimulators, including pro-inflammatory cytokines and antigen receptors [204]. In this study, the inflammatory responses in FD-induced keratinocytes were determined by measuring the levels of COX-2, PGE₂, IL-1 β , IL-6, TNF- α , and intracellular ROS and quantifying cell viability. Comparison of LPS- and FD-induced inflammations revealed that the levels of p-p38 MAPK, P-Erk1/2, and P-JNK decreased in

the latter group and the decrease was FD concentration dependent. This result indicated the significant anti-inflammatory effect of FxRF against FD induced inflammatory responses.

5 Conclusion

The present study demonstrates that FxRF of *H. fusiforme* extract exerts strong anti-inflammatory effects by attenuating FD-induced oxidative stress and inflammation in keratinocytes and macrophages. Collectively, our findings suggest that *H. fusiforme* is a promising anti-inflammatory agent and an appropriate functional food ingredient.

**Part IV. Isolation of saringosterol acetate from
Hizikia fusiforme and its bioactivities**

1 Abstract

In this part, saringosterol acetate (SA) isolated from Hijiki, was investigated for its anticancer effect against MCF-7 tumor cell line, and inhibitory effect of SA on adipogenesis in 3T3-L1 adipocyte cells. SA was isolated from hexane fraction by centrifugal partition chromatography, and its structure was identified by thin layer chromatography, mass spectroscopic, and nuclear magnetic resonance spectroscopy analysis.

In the anticancer effective assay, SA attenuated the survival rate of the MCF-7 cell line with IC_{50} value of $63.16 \pm 3.6 \mu\text{g/mL}$. SA showed a strongly inhibited effect in cell viability to MCF-7 cells. Staining with Hoechst 33342 indicated that SA treatment mediated apoptotic body formation. SA down-regulated Bcl-xL, while up-regulating both Bax protein in a dose-dependent manner. Base on the results, we deduced that SA induces apoptosis via the mitochondria-mediated pathway on MCF-7 cell lines.

In the anti-obesity effective assay, SA attenuated the differentiation and reduced lipid accumulation and triglycerides contents in 3T3-L1 adipocytes. At the period of adipocyte differentiation, SA suppressed fat accumulation and decreased expression of adipogenesis signal factors. In SA treated adipocytes cells, it dose-dependently down-regulated intensities of fatty acid synthase, while up-regulated intensities of phosphorylated AMPK. These finding suggest that SA potentially to be an anti-obesity drug to improve metabolic disorders. This is the first report on the anti-obesity effect of SA from Hijiki.

2 Introduction

In the United States, over 1.7 million new cancer cases are projected to happen in 2019. Among cancers, there are still huge gaps for prevention. Especially for the poorest places, cancer prevention is recognized an effective strategies against cancer [205]. The aging and unhealthy behaviors increased the financial burden in low-income countries, and promote the cancer risk to these people [206]. Thus, an easily and cheaper method to prevent cancer becomes necessary.

Nowadays, obesity become a worldwide epidemic, is regarded as accumulation of fat resulting to metabolic disorder [207]. The terms “Fat taxes” introduced by a research literature, which means the US government potential taxing on unhealthy foods to improve people’s health [208]. A ten years survey in the cost of obesity-related diseases for elder in US was performed, indicating a heavy financial burden for government [209]. For obese young people in Western countries, over weight occurs the high risk of acute and chronic diseases such as morphological changes, diabetes and hypertension [210]. An interesting investigation was observed in California; the more residence time in America results in more higher obesity risk to Korean Americans [211]. It was deduced that Westernized dietary pattern could result to the various degree of body mass [212]. Compare to America or Europe, dietary habits of Korea with high in fruits and vegetables such as Hijiki salad, which decrease the risk of overweight than those of American or European [213]. Recent literatures have been showed that adipocyte differentiation plays a key role in development of anti-obesity resources [214]. In adipocytes, regulation of fat accumulation are associated with the adipogenic-related factors, such as enhancer binding protein family (C/EBP), sterol regulatory element-binding protein (SREBP), and peroxisome proliferator activated receptor- γ (PPAR γ) [215].

Sterols are recognized as essential compounds in seaweeds [216]. Previous studies observed that phytosterols exhibit potentially preventive cancer properties [217], and sterol fraction from seaweed *Porphyra dentate* showed anticancer effects as well [218]. Nowadays, saringosterol was isolated from *Sargassum fusiforme* and recognized as a selective LXR β agonist [219]. Saringosterol and saringosterol acetate (SA) have the same main chemical structure. Due to its interesting structure, we are fascinated the bioactivities of SA. Two decades ago, SA was first isolated from seaweed *Sargassum asperifolium* [220]. Previous published reports showed that SA has anticancer effects on A549 cancer cells [221]. However,

anticancer activities of SA still needs deeply explorations and wide its application in cancer therapy. In this work, SA isolated and identified from hexane extraction of *H. fusiformis*, and discovered its anticancer effects on MCF-7 cancer cells.

Sterol was also found its ability to regulate SREBPs signal proteins. The function of SREBPs are proved to associated with cholesterol homeostasis [222] and lipogenesis in adipocyte development [223]. A recent study observed that the anti-obesity activity of saringosterol from *sargassum muticum* in 3T3-L1 adipocyte cells [224]. Therefore, coupling with the Korean diet habit, Korean average body mass, and the various functions of sterol from Hijiki, SA may play an important role in anti-obesity property. Especially, as the best of our knowledge, no report has yet been study on the anti-obesity effects of SA in adipocytes. In this part of work, the second objective is evaluating the suppressed effects of SA against adipogenesis in adipocytes.

3 Materials and Methods

3.1 Preparation and identification of saringosterol acetate (SA)

3.1.1 Preparation of hexane extracts from Hijiki

Hijiki (100 g) was cleaned with tap water, lyophilized, and immediately extracted three times in 70% ethanol for 24 h at 40°C. The mixed solutions were evaporated in vacuum at 37°C, and separated into water and hexane layers. The hexane fraction was concentrated by evaporation under vacuum at 37°C until centrifugal partition chromatography (CPC) separation.

3.1.2 Isolation and identification of SA

The CPC assay was performed as the previous protocol [225]. The phases solvent systems were mixed at the ratio of hexane:ethylacetate:methanol:water = 5:5:7:1. The upper layer was used as the mobile phase, and the lower layer was considered as the stationary phase. Each fraction of CPC was collected imaged by thin-layer chromatography (TLC) analysis. The mobile phase was mixed at the ratio as chloroform:methanol =20:1. The identified method of SA was followed by previous study [221].

3.2 Anticancer effect of SA against on MCF-7 cancer cells

3.2.1 Cell culture

MCF-7 (human breast cancer) and Vero kidney cell lines were purchased from the American Type Culture Collection (Manassas, VA, United States). DMEM, FBS, and P/S were purchased from Gibco Inc.,

(Grand Island, NY, USA). MTT was purchased from Sigma-Aldrich (Missouri, USA). Vero kidney and MCF-7 cells were maintained in RPMI and DMEM containing 10% FBS and 1% P/S, respectively. Cells were cultured at 37°C with a 5% CO₂ atmosphere.

3.2.2 Measurement of cell viability

The growth rate was measured by MTT assay [116]. The cancer cells (1×10^5 cells/mL) were seeded in 96-well culture plates for 24 h, and treated in the presence or absence of indicated concentrations of SA. The cells untreated with SA were considered as control. Following incubation for 24 h, cells were treated in 50 μ L phosphate-buffered saline (PBS) containing MTT (2 mg/mL). Cells were incubated for 3 h in the dark, and then a 200 μ L of DMSO was replaced excess medium in each well. The optical density of cells was measured at 540 nm.

3.2.3 Apoptotic and necrotic body formation

Cells (1×10^5 cells/mL) were seeded in 24-well culture plates and treated in the presence or absence of indicated concentrations (12.5, 25, 50 μ g/mL) of SA. The cells untreated with SA were considered as control. Following incubation for 24 h, cells were resuspended in 25 μ L of PBS containing Hoechst 33342 (1 mg/mL). Each well was washed twice with PBS after 10 min staining in the dark. Cells were observed under a fluorescence microscope equipped with CoolSNAP-Pro color digital camera (Meyer Instruments, Inc., Houston, TX, USA) [226].

3.2.4 Apoptosis analysis by flow cytometry

Apoptotic cells were measured by a high-end performance flow cytometer (Becton Dickinson, San Jose, CA, USA) following Annexin V-FITC apoptosis detection kit (Merck KGaA, Darmstadt, Germany) guidance. Briefly, cells (1×10^5 cells/mL) were treated with SA at the indicated concentrations (12.5, 25, 50 μ g/mL) for 24 h. Cells were harvested and washed by PBS, and continuously subsequently maintained in by binding buffer. Following a 15-min staining (Annexin V-FITC and PI solutions) in the dark, cells were measured by flow cytometry.

3.2.5 Western blot analysis

Cells (2×10^5 cells/mL) were pre-seeded in culture plates. The sample treatment was performed as described in “3.2.2”. After 24 h exposure, cells were harvested, subsequently homogenized in lysis buffer, and clarified by centrifugation (12,000 $\times g$ for 20 min). The supernatants containing proteins were

measured using a BCA protein kit (Thermo Fisher Scientific, MA, USA). A totally 30 µg of protein, mixed with lysis buffer were separated using a polyacrylamide gel. The protein bands were transferred onto nitrocellulose membranes, blocked in 5% blocking buffer, and incubated for 2 h. The membranes were then incubated with primary and secondary antibodies by step. Signals were developed using a chemiluminescent substrate (Cyanagen Srl, Bologna, Italy), and fluorescence imaging was performed using a FUSION SOLO Vilber Lourmat system (FUSION, Paris, France) [227].

3.3 Anti-obesity effect of SA against adipogenesis in adipocytes

3.3.1 Cell culture and adipocyte differentiation

Mouse 3T3-L1 adipocytes cells were purchased from the American Type Culture Collection (Manassas, VA, USA). The cells were maintained in DMEM containing 1% P/S and 10% bovine calf serum (Gibco Inc., Grand Island, NY, USA) at 37°C with 5% CO₂ atmosphere. MDI differentiation medium is composition to 1% P/S, 10% FBS, 0.5 mM IBMX, 0.25 µM dexamethasone, and 5 µg/mL insulin of DMEM. After two days seeding, MDI medium containing 10% FBS was treated for induction of cell differentiation. Following two days cell differentiation, the medium was substituted with fresh medium containing 1 µg/mL insulin and 10% FBS. After four days differentiation, cells were rinsed to medium containing 10% FBS. At six days differentiation, cells were repeated the same processed method as four day's treatment. The cells were treated with various concentrations of SA for every two days (0, 2, 4, 6 days). The MTT assay was performed to cell viabilities of different periods of 3T3-L1 adipocytes in each 2 days.

3.3.2 Measurement of lipid accumulation

Following eight days differentiation, cells were washed by PBS, then fixed with PBS containing 4% formaldehyde for 30 min, and subsequently washed with PBS and 70% ethanol. The isopropanol solution containing 5% Oil Red O was introduced to cells for 60 min incubation, and the dye retained cells were rinsed by 100% isopropanol. Stained lipid droplets were observed with a microscope same as the described above and measured at wavelength of 510 nm.

3.3.3 Measurement of triglyceride contents

Following eight days differentiation and SA treatment in cells, triglyceride contents were measuring using commercial triglyceride assay kit followed guidance (Zen-Bio, Research Triangle Park, NC, USA)

with wavelength at 540 nm.

3.3.4 Western blot analysis.

3T3-L1 adipocytes cells were harvested and lysed on ice for 1 h in lysis buffer. The lysates were centrifuged at 14,000 *g* for 20 min at 4°C to obtain the supernatant. The measurement of protein contents of lysates, separation by polyacrylamide gel, transformation onto membranes, and imagination of bands were performed as described in “3.2.5”.

3.4 Statistical analysis

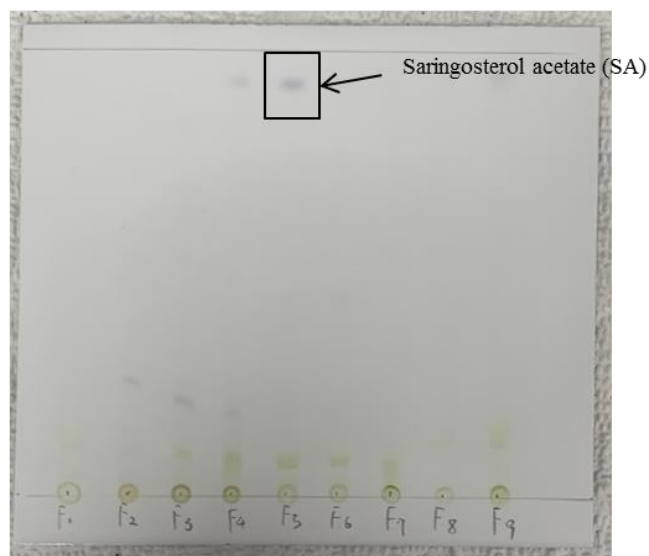
All assays were made in three independent experiments. Values were expressed as the mean \pm SE. One-way ANOVA was used to analyze the mean values in GraphPad prism 5 software. Student’s t-test (* $p < 0.05$ and ** $p < 0.01$) was used to analyze the means of the parameters of significant differences.

4 Results and Discussion

4.1 Isolation and identification SA from Hijiki

SA was isolated from the partition consisting of ethanol and hexane in Hijiki. The compounds in hexane fraction were separated by CPC; the structure of SA was identified and confirmed by comparing to the TLC and mass spectrum (Fig. 4-1). These results were same to previous published reports [221].

a



Mobile phase: chloroform: methanol =20:1

b

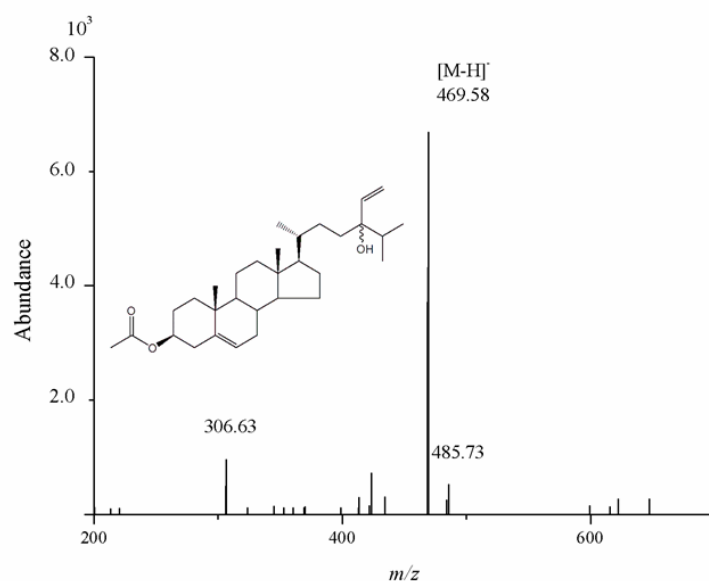


Figure 4-1 Preparation of SA of *H. fusiformis*. (a) TLC of SA collected from hexane extract of *H. fusiformis* by CPC, SA indicated by black line, and (b) Structure and ESI-MS data of isolated SA. CPC producer: Stationary phase: upper organic phase; mobile phase: lower aqueous phase; flow rate: 2 mL/min; rotation speed: 1000 rpm; sample: 500 mg dissolved in 6 mL mixture of lower phase and upper phase (1:1, v/v) of the solvent system.

4.2 Anticancer effect of SA against on MCF-7 cancer cells

4.2.1 Cytotoxicity of SA

Fig. 4-2 shows the effect of SA in cell viability of Vero kidney normal cell and MCF-7 cell lines. It is observed that the survival rate of the tested cancer cell line was decrease dose-dependently with the increasing concentrations of SA treatment. Importantly, the survival rate in SA treated Vero cell line higher 80% compared with untreated cells was found, indicates low cytotoxic effects of SA on the normal cells. The MCF-7 cell line with IC_{50} values of $63.16 \pm 3.6 \mu\text{g/mL}$. Based on these initial results, MCF-7 cells were selected to further investigate the anticancer effect of SA.

4.2.2 Apoptosis morphology of SA on MCF-7 cancer cells

The increasing apoptotic body formations were observed in a dose-dependent manner with the increasing concentrations of SA treated in cells, indicating apoptotic effects of SA (Fig. 4-3a). After a 24 h-incubation, early apoptotic body formations were observed in cells treated with the low concentration ($12.5 \mu\text{g/mL}$) of SA. It is showed that several cells were in late apoptotic and necrotic stages. As the concentration of SA increased, the intensities and the numbers of white spots in cells were increased, indicating the numbers of late apoptotic bodies and necrotic cells markedly increased. In the high concentration SA treatment ($50 \mu\text{g/mL}$), the densities of cells were lower than those of untreated group.

In the flow cytometric assay, MCF-7 cells were treated with the indicated concentrations of SA to evaluate their apoptotic effects. The percentages of early apoptosis in the gate of Q4 and late apoptosis cells in the gate of Q2 were markedly increased with increased concentrations of SA. These results go along with the data of cell death. The percentages of apoptosis in cells demonstrate dose-dependently up-regulation of apoptotic body formation (Fig. 4-3b).

4.2.3 Apoptosis pathway regulated by SA

To further elucidate the involvement of the apoptosis pathway initiated by SA on MCF-7 cancer cells, we examined expression of several signal factors. The treatment with SA ($50 \mu\text{g/mL}$) caused the expression of apoptosis-associated factors fluctuation significantly. In cellular, Bax is regarded as apoptotic factor, whereas, Bcl-xL is regarded as anti-apoptotic factor. Compared to the untreated group, it is observed that the expression of signal proteins was dose-dependent: Bax and increased, while the Bcl-xL decreased (Fig. 4-4).

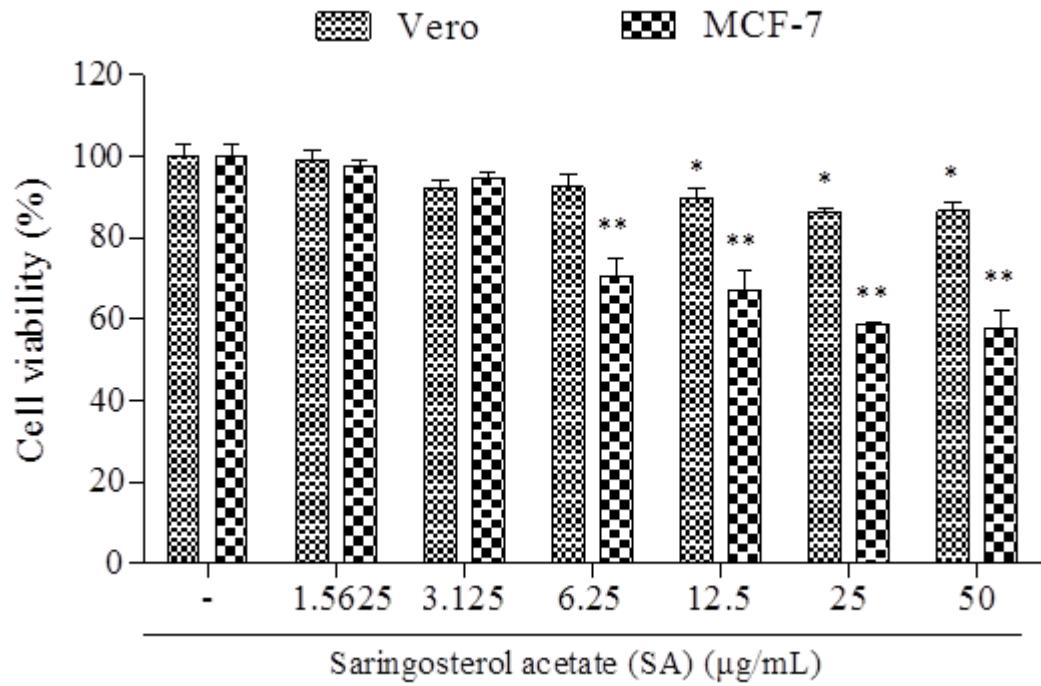
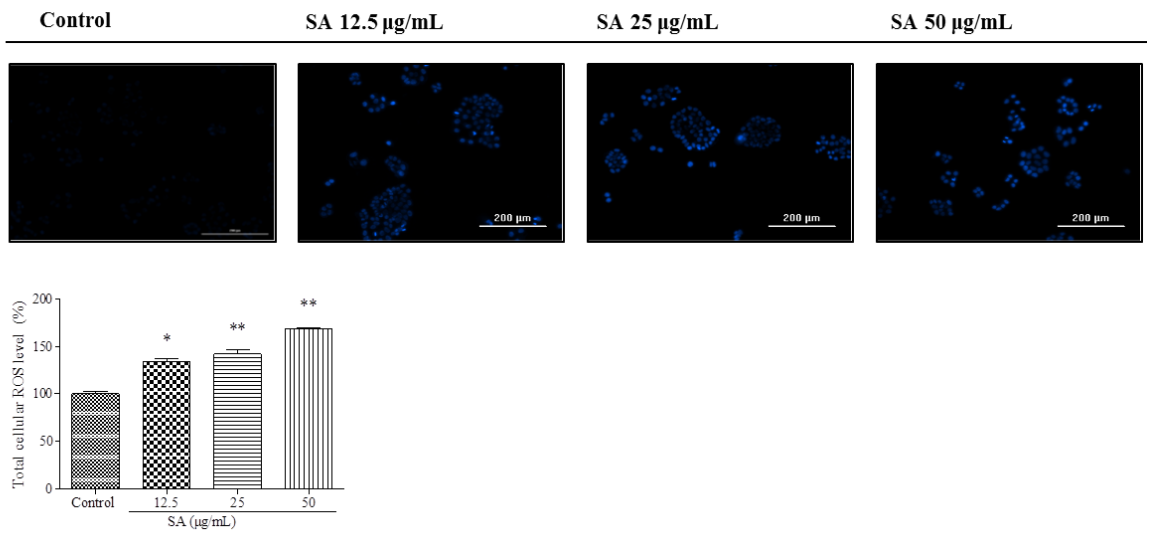


Figure 4-2 Cytotoxicity of SA on MCF-7 cancer cells and Vero kidney normal cells. Cells were treated to indicate concentrations of SA and measured by MTT assay. Experiments were performed in triplicate and the data are expressed as the mean \pm SE. * $p < 0.05$, ** $p < 0.001$.

a



b

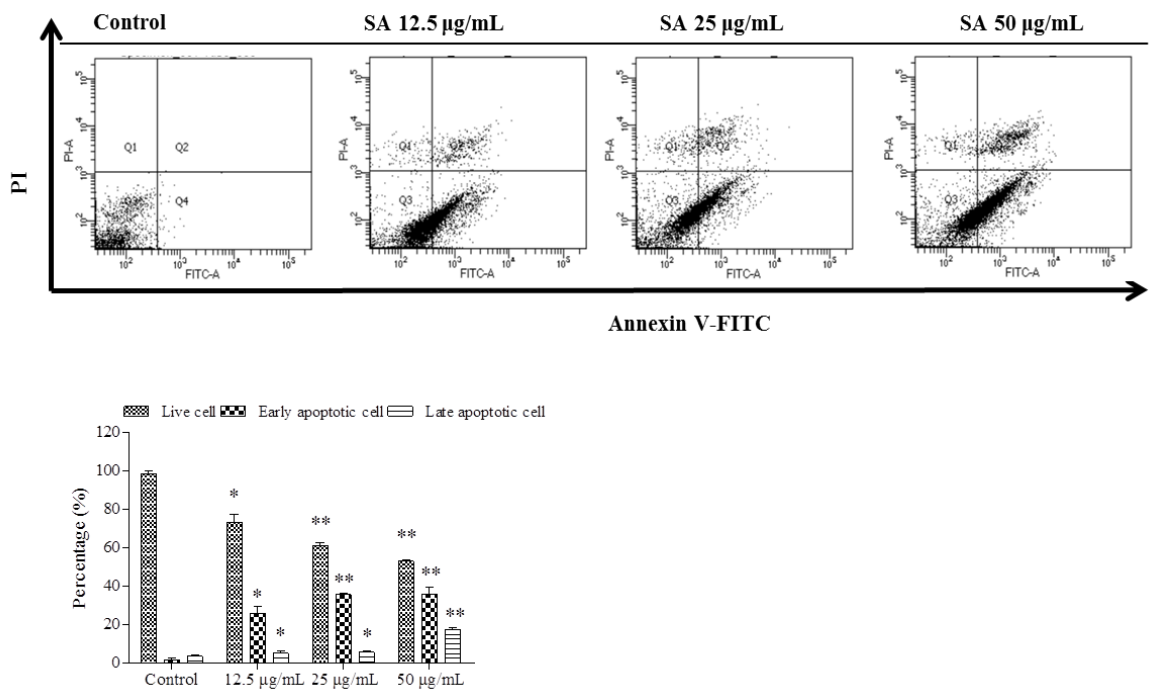


Figure 4-3 Apoptosis effects of SA. (a) Effect of SA on the induction of apoptotic bodies, and (b) Flow cytometry analysis of SA on the nuclear morphology in cancer cells. Cells were stained with PI and Annexin V-FITC. Experiments were performed in triplicate and the data are expressed as the mean \pm SE.

* $p < 0.05$, ** $p < 0.001$.

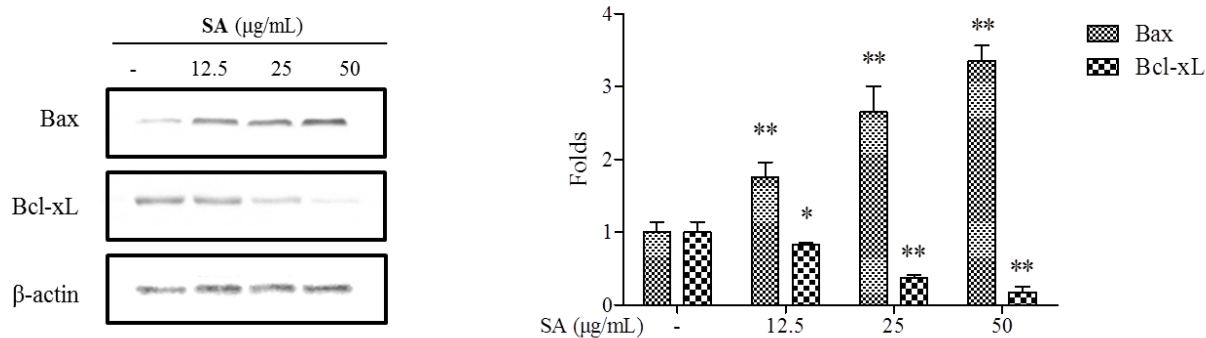


Figure 4-4 Apoptosis effects of SA on apoptosis-proteins on MCF-7 cancer cells. Cells were treated with SA at the indicated concentration for 24 h. Experiments were performed in triplicate and the data are expressed as the mean \pm SE. * $p < 0.05$, ** $p < 0.001$.

Hijiki is the rich produced brown seaweeds and it has been used as folk medical food in Korea, Japan, and China [37]. A recent study reported that the hexane fraction of Hijiki was found high sterol content [228]. Further, sterols are used as anticancer agents and have widely medical applications [229, 230]. It is well known that hexane fraction tends to contains sterol, which are believed to exist anticancer bioactive compounds [231]. In this work, a deeply and widely investigation of anticancer activity of SA was evaluated on MCF-7 cancer cells. Our results showed that SA has strong anticancer properties against MCF-7 cancer cells. Moreover, it is observed that SA plays a key role in regulatory apoptotic body formation. During the period of apoptosis, chromatin condenses, the cell shrinks, membrane blebbing occurs, and cells can fragment into membrane-bound vesicles [138, 232]. These observations demonstrated that the anticancer properties of SA to cancer cells are based on regulation of the expression of cell death-related factors. These regulatory factors, such as the Bcl-2 protein family, stay dormant under inactive conditions in cells [139]. In the Bcl-2 protein family, Bax regarded as pro-apoptotic, while Bcl-xL is regarded as anti-apoptotic proteins. These are two of the most frequently studied apoptotic regulators in cells [140]. The mitochondrion is a cellular double-membrane-bound organelle and regulates homeostasis balance [233]. In mitochondria, Bax acts as an apoptotic factor by disrupting voltage-dependent anion channels, simulating the release of cytochrome c, which leads to caspase activation and programmed death [141]. The up-regulation of Bax as well as the down-regulation of Bcl-xL indicates the occurrence of apoptosis in cells [142]. In this study, we found that SA increased the expression of Bax and decreased expression of Bcl-xL in Western blotting analysis. We raised a hypothesis that the anticancer activity of SA via the mitochondria-mediated apoptosis pathway on MCF-7 cancer cells. Therefore, the anticancer mechanism of SA was found and its application in anticancer therapies becomes more widely.

4.3 Anti-obesity effect of SA against adipogenesis in adipocytes

4.3.1 SA suppresses adipocyte differentiation

In this work, the cell viability and the inhibit effects of SA on adipogenesis in 3T3-L1 cells were evaluated. It was observed that low cytotoxicity of SA in different concentrations after 2days, 4 days, 6 days, and 8 days differentiation treatment, which was found to higher than 80% compared to the untreated cells (Fig. 4-5a). Oil Red O staining was carried out to measure lipid accumulation in cells. Our observations demonstrated that SA dose-dependently suppressed adipocyte differentiation and markedly decreased lipid accumulation (Fig. 4-5b and 5c). Further, triglyceride production was indicated a significantly decrease in SA treated groups compared to the untreated cells (Fig. 4-5d). These results showed that reduction of the accumulation of fat and triglyceride in SA treated adipocytes was found.

4.3.2 SA regulates adipogenesis-related factors in adipocytes

According to published reports, C/EBP α , SREBP-1c, PPAR γ , and adiponectin are signal proteins to regulation of fat accumulation in adipocytes [234]. Hence, it is important to determine the expressions of these signal factors in adipocytes. Our results indicated that SA significantly down-regulated expressions of C/EBP α , SREBP-1c, PPAR γ , and adiponectin dose-dependently in adipocytes (Fig. 4-6a). These factors are regarded as key adipogenic transcriptional factors. Moreover, SA decreased the expressions of adipogenesis-related factors such as fatty acid synthase (FAS), leptin, fatty acid binding protein (FABP4), and perilipin (Fig. 4-6b). The observations showed that SA suppressed accumulation in fat by reduced adipogenesis-related factors in adipocytes.

4.3.3 SA regulates AMPK and ACC factors in adipocytes

AMPK activation inhibits on adipogenesis [235], and inhibits synthesizes of fatty acid and triglyceride by activating acetyl-CoA carboxylase (ACC) in adipocytes [236]. Therefore, it is necessary to measure the levels of AMPK and ACC. Our results showed that SA increase levels of AMPK and ACC compared to the untreated cells (Fig. 4-7a and 7b). It is suggested that SA decreases the triglyceride synthesis pathway and inhibits accumulation in fat.

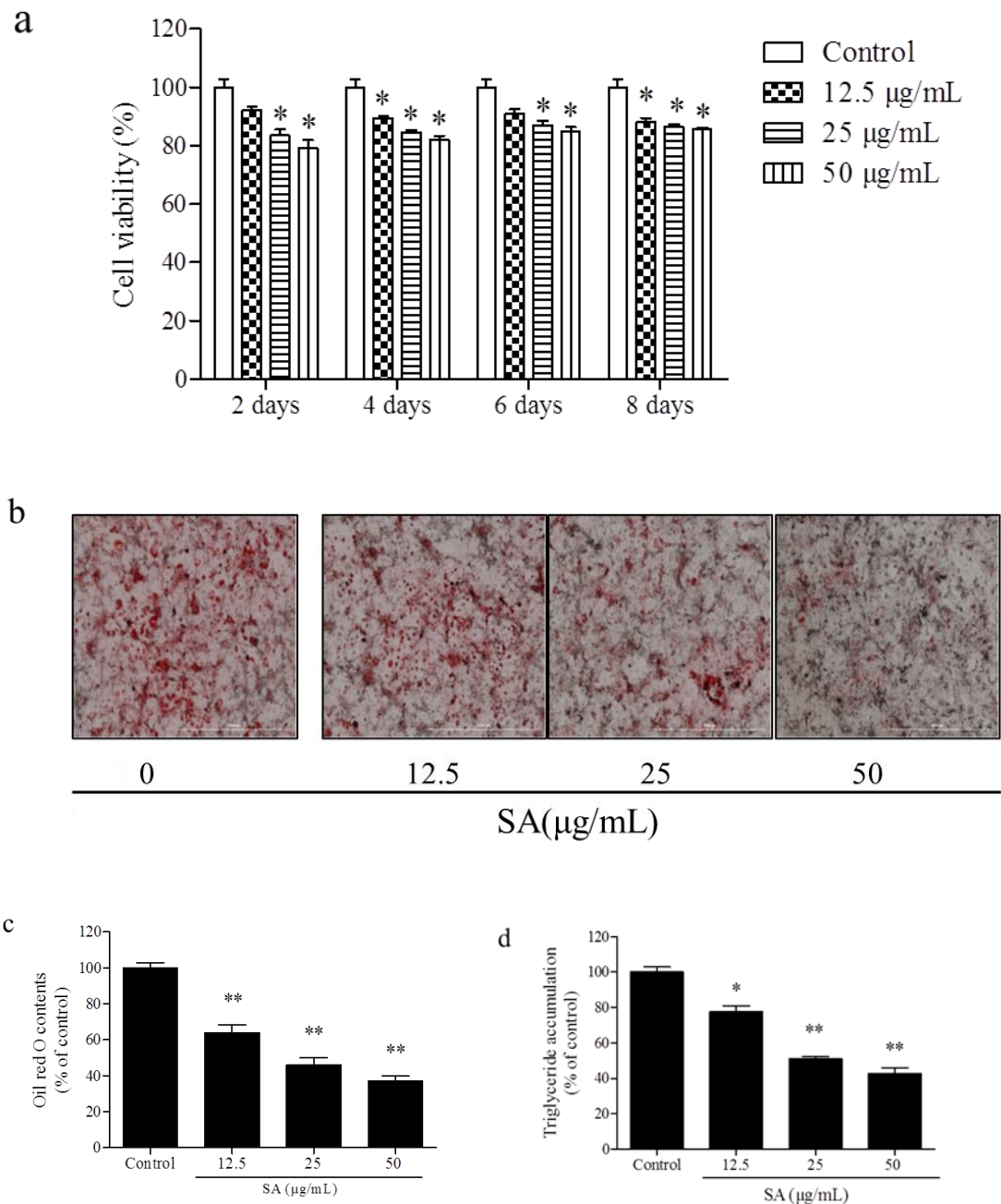


Figure 4-5 Anti-obesity effect of SA in 3T3-L1 adipocytes. (a) Cytotoxicity of SA on cell viability of 3T3-L1 adipocytes for 2 days, 4 days, 6 days, and 8 days differentiation, and (b) SA inhibits intracellular lipid accumulation in 3T3-L1 adipocytes. (c) Lipid accumulation was determined by Oil Red O staining, and (d) triglyceride levels. Experiments were performed in triplicate and the data are expressed as the mean \pm SE. * $p < 0.05$, ** $p < 0.001$.

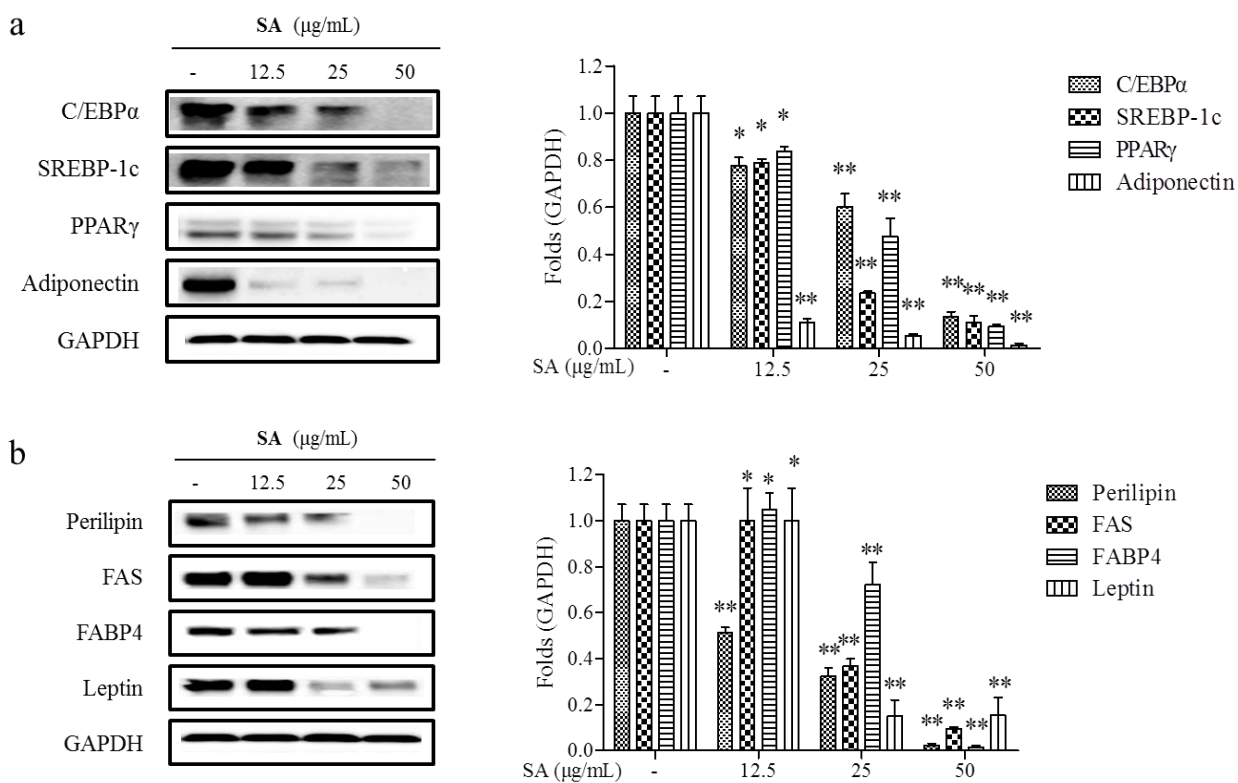


Figure 4-6 Anti-obesity effect of SA on signal factors in 3T3-L1 adipocytes. (a) Effect of SA treatment on adipogenic-related protein levels in 3T3-L1 adipocytes. (b) Effect of SA on phosphorylation of adipogenic-specific proteins in 3T3-L1 adipocytes. Experiments were performed in triplicate and the data are expressed as the mean \pm SE. * $p < 0.05$, ** $p < 0.001$.

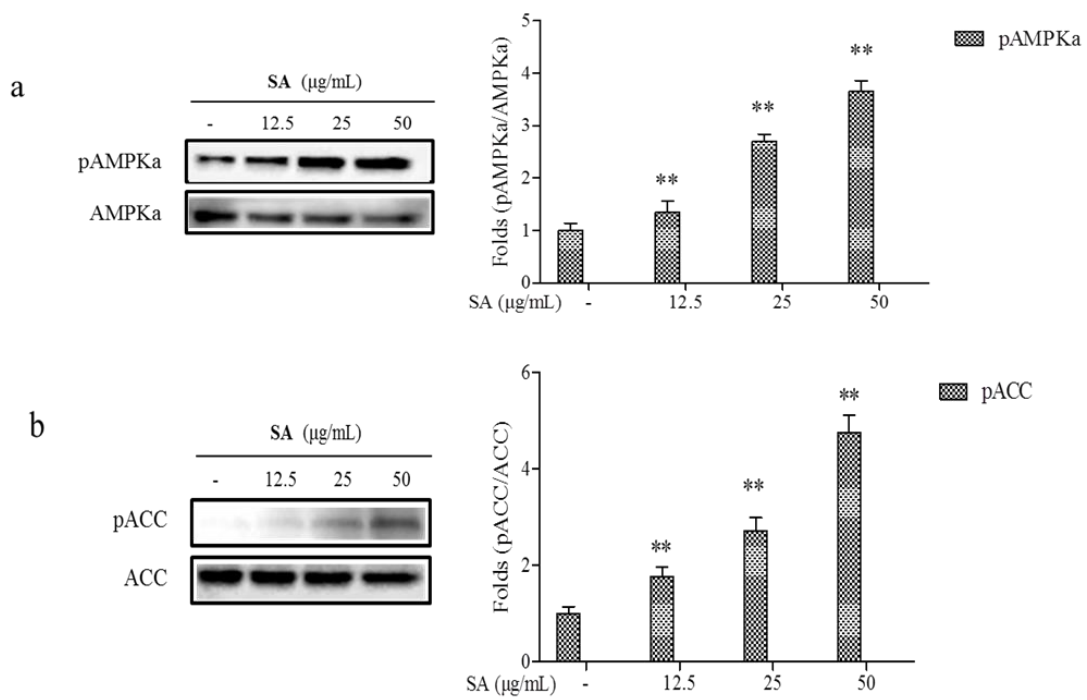


Figure 4-7 SA suppresses activation of p-AMPK α in 3T3-L1 pre-adipocytes. Experiments were performed in triplicate and the data are expressed as the mean \pm SE. * $p < 0.05$, ** $p < 0.001$.

Obesity is recognized as a metabolic disorder for overweight in human body [237]. Overweight dramatically increases the risk in health conditions such as gallbladder disease and diabetes [238]. Scientists concluded that there are two types of adipose tissue in mammals: white fat and brown fat. White fat contains a single lipid droplet and brown fat contains numerous smaller droplets [239]. White fat plays a key role in maintains energy in human and associated with adipocytes cells. Overweight consumers with junk food daily, have to face a series risk of diseases such as hypertension and cardiovascular disease [240]. 3T3-L1 adipocytes cells are widely used for anti-obesity assay *in vitro* [241]. In this work, we focused on an effective compound, SA, and its suppressed effect against adipogenesis in adipocytes. According to these results, SA could markedly decrease lipid accumulation and triglyceride contents, and dose-dependently regulate adipogenesis-related proteins in adipocytes.

Fat accumulation is activated by the lipogenesis-related factors in adipocytes. FAS, FABP4, leptin, and perilipin are regarded as important transport signal proteins for lipogenesis in cell [234]. FABP4 is a lipid transport factor, which promotes glucose metabolism and mediates fatty acid in lipogenesis pathway. Further, it is found that FABP4 could synergistically decrease PPAR γ and adipogenesis [242], whereas increase leptin content in adipocytes [243]. Perilipin is an important and promising factor for fat mobilization [244]. Phosphorylated FAS is activated by perilipin, then continuously decreased fatty acid synthase in adipocytes [245]. Adipocytes have the ability to produce circulating hormone like leptin. The level of leptin in cellular is strongly depends on the size and level of adipocytes [246]. A previous article has highlighted the function of lipogenesis-specific proteins in adipocytes such as promoting lipid convey, uptake, and metabolism [247]. Our results showed that SA could inhibit fat accumulation mediator in C/EBP α , SREBP-1c, PPAR γ , adiponectin, FAS, FABP4, leptin, and perilipin in adipocytes. In AMPK pathway, it could operate the functions of glucose metabolism, fatty acid oxidation and insulin sensitivity in mammals. Importantly, AMPK could inhibit ACC protein, and then suppress the lipid synthesis. The activated AMPK has been proved to suppressed the fat accumulation in adipocytes [248]. These results in present work also demonstrated that SA triggers the activation of AMPK, suppressing adipogenesis, whereas, inhibits the accumulation in fat by down-regulating adipogenesis-related factors and up-regulating phosphorylated AMPK expressions. This part finds evidence that SA exhibit potential anti-obesity activity in adipocyte cells.

5 Conclusion

In this work, we showed the anti-proliferative and anti-obesity effects of SA from Hijiki. This research expanded our understanding of the biological properties of SA, and yielded promising results. The study lays a foundation for further research into additional active compounds extracted from Hijiki.

REFERENCE

- [1] F. Wang, Y. Li, Y.-J. Zhang, Y. Zhou, S. Li, H.-B. Li, Natural products for the prevention and treatment of hangover and alcohol use disorder, *Molecules* 21(1) (2016) 64.
- [2] R. Goonesekere, Y. Guo, Unmanned Underwater Drone Design for Ocean Exploration, ASME 2018 International Mechanical Engineering Congress and Exposition, American Society of Mechanical Engineers Digital Collection, 2018.
- [3] C. Mora, D.P. Tittensor, S. Adl, A.G. Simpson, B. Worm, How many species are there on Earth and in the ocean?, *PLoS biology* 9(8) (2011) e1001127.
- [4] F. Guérard, N. Decourcelle, C. Sabourin, C. Floch-Laizet, L. Le Grel, P. Le Floc'H, F. Gourlay, R. Le Delezir, P. Jaouen, P. Bourseau, Recent developments of marine ingredients for food and nutraceutical applications: a review, *Journal des sciences Halieutique et Aquatique* 2 (2010) 21-27.
- [5] K.M. Drew, Life histories in the algae with special reference to the Chlorophyta, Phaeophyta and Rhodophyta, *Biological Reviews* 30(4) (1955) 343-387.
- [6] Y.-J. Hsieh, S.-J. Jiang, Application of HPLC-ICP-MS and HPLC-ESI-MS procedures for arsenic speciation in seaweeds, *Journal of agricultural and food chemistry* 60(9) (2012) 2083-2089.
- [7] S. Kobayashi, K. Murakami, S. Sasaki, H. Okubo, N. Hirota, A. Notsu, M. Fukui, C. Date, Comparison of relative validity of food group intakes estimated by comprehensive and brief-type self-administered diet history questionnaires against 16 d dietary records in Japanese adults, *Public health nutrition* 14(7) (2011) 1200-1211.
- [8] Y. Liu, Z. Wang, J. Zhang, *Dietary Chinese Herbs*, Springer 2015.
- [9] Y. Li, X. Fu, D. Duan, J. Xu, X. Gao, Comparison study of bioactive substances and nutritional components of brown algae *Sargassum fusiforme* strains with different vesicle shapes, *Journal of Applied Phycology* (2018) 1-13.
- [10] Y. Okai, K. Higashi - Okai, S. Ishizaka, U. Yamashita, Enhancing effect of polysaccharides from an edible brown alga, *Hijikia fusiforme* (hijiki), on release of tumor necrosis factor - α from macrophages of endotoxin - nonresponder C3H/HeJ mice, (1997).
- [11] Y. Okai, K. Higashi - Okai, S. Ishizaka, K. Ohtani, I. Matsui - Yuasa, U. Yamashita, Possible immunomodulating activities in an extract of edible brown alga, *Hijikia fusiforme* (Hijiki), *Journal of the Science of Food and Agriculture* 76(1) (1998) 56-62.
- [12] Y. Okai, K. Higashi - Okai, Identification of antimutagenic activities in the extract of an edible brown alga, *Hijikia fusiforme* (Hijiki) by umu gene expression system in *Salmonella typhimurium* (TA 1535/pSK 1002), *Journal of the Science of Food and Agriculture* 66(1) (1994) 103-109.

- [13] P. Rup érez, Mineral content of edible marine seaweeds, *Food chemistry* 79(1) (2002) 23-26.
- [14] F. Joint, W.E.C.o.F. Additives, W.H. Organization, Evaluation of certain food additives and contaminants: thirty-third report of the Joint FAO, (1989).
- [15] K. Jomova, Z. Jenisova, M. Feszterova, S. Baros, J. Liska, D. Hudecova, C. Rhodes, M. Valko, Arsenic: toxicity, oxidative stress and human disease, *Journal of Applied Toxicology* 31(2) (2011) 95-107.
- [16] X.r. Zhang, R. Cornelis, J. De Kimpe, L. Mees, V. Vanderbiesen, A. De Cubber, R. Vanholder, Accumulation of arsenic species in serum of patients with chronic renal disease, *Clinical chemistry* 42(8) (1996) 1231-1237.
- [17] K.i. Hanaoka, K. Yosida, M. Tamano, T. Kuroiwa, T. Kaise, S. Maeda, Arsenic in the prepared edible brown alga hijiki, *Hizikia fusiforme*, *Applied organometallic chemistry* 15(6) (2001) 561-565.
- [18] D. Kuehnelt, K.J. Irgolic, W. Goessler, Comparison of three methods for the extraction of arsenic compounds from the NRCC standard reference material DORM - 2 and the brown alga *Hizikia fusiforme*, *Applied Organometallic Chemistry* 15(6) (2001) 445-456.
- [19] S. Ichikawa, M. Kamoshida, K.i. Hanaoka, M. Hamano, T. Maitani, T. Kaise, Decrease of arsenic in edible brown algae *Hizikia fusiforme* by the cooking process, *Applied Organometallic Chemistry* 20(9) (2006) 585-590.
- [20] Y. Sugawa-Katayama, M. Katayama, Y. Arikawa, Y. Yamamoto, R. Sawada, Y. Nakano, Diminution of the arsenic level in *Hizikia fusiforme* (Harvey) Setchell, through pre-cooking treatment, *Trace Nutrients Research* 22 (2005) 107-109.
- [21] K. Draget, G.S. Bræk, O. Smidsrød, Alginic acid gels: the effect of alginate chemical composition and molecular weight, *Carbohydrate Polymers* 25(1) (1994) 31-38.
- [22] B. Li, F. Lu, X. Wei, R. Zhao, Fucoidan: structure and bioactivity, *Molecules* 13(8) (2008) 1671-1695.
- [23] J. Wang, Q. Zhang, Z. Zhang, H. Song, P. Li, Potential antioxidant and anticoagulant capacity of low molecular weight fucoidan fractions extracted from *Laminaria japonica*, *International journal of biological macromolecules* 46(1) (2010) 6-12.
- [24] N.M. Ponce, C.A. Pujol, E.B. Damonte, M.L. Flores, C.A. Stortz, Fucoidans from the brown seaweed *Adenocystis utricularis*: extraction methods, antiviral activity and structural studies, *Carbohydrate Research* 338(2) (2003) 153-165.
- [25] J.-Y. Kwak, Fucoidan as a marine anticancer agent in preclinical development, *Marine drugs* 12(2) (2014) 851-870.
- [26] H.Y. Park, M.H. Han, C. Park, C.-Y. Jin, G.-Y. Kim, I.-W. Choi, N.D. Kim, T.-J. Nam, T.K. Kwon, Y.H. Choi, Anti-inflammatory effects of fucoidan through inhibition of NF- κ B, MAPK and Akt activation

in lipopolysaccharide-induced BV2 microglia cells, *Food and chemical toxicology* 49(8) (2011) 1745-1752.

[27] A. Cumashi, N.A. Ushakova, M.E. Preobrazhenskaya, A. D'incecco, A. Piccoli, L. Totani, N. Tinari, G.E. Morozevich, A.E. Berman, M.I. Bilan, A comparative study of the anti-inflammatory, anticoagulant, antiangiogenic, and antiadhesive activities of nine different fucoidans from brown seaweeds, *Glycobiology* 17(5) (2007) 541-552.

[28] A.V. Skriptsova, N.M. Shevchenko, D.V. Tarbeeva, T.N. Zvyagintseva, Comparative study of polysaccharides from reproductive and sterile tissues of five brown seaweeds, *Marine biotechnology* 14(3) (2012) 304-311.

[29] M. Honya, H. Mori, M. Anzai, Y. Araki, K. Nisizawa, Monthly changes in the content of fucans, their constituent sugars and sulphate in cultured *Laminaria japonica*, Sixteenth International Seaweed Symposium, Springer, 1999, pp. 411-416.

[30] L.-E. Rioux, S.L. Turgeon, M. Beaulieu, Characterization of polysaccharides extracted from brown seaweeds, *Carbohydrate polymers* 69(3) (2007) 530-537.

[31] T.N. Zvyagintseva, N.M. Shevchenko, A.O. Chizhov, T.N. Krupnova, E.V. Sundukova, V.V. Isakov, Water-soluble polysaccharides of some far-eastern brown seaweeds. Distribution, structure, and their dependence on the developmental conditions, *Journal of Experimental Marine Biology and Ecology* 294(1) (2003) 1-13.

[32] G. Bryan, The absorption of zinc and other metals by the brown seaweed *Laminaria digitata*, *Journal of the Marine Biological Association of the United Kingdom* 49(1) (1969) 225-243.

[33] D. Aderhold, C. Williams, R. Edyvean, The removal of heavy-metal ions by seaweeds and their derivatives, *Bioresource Technology* 58(1) (1996) 1-6.

[34] S.E. Bailey, T.J. Olin, R.M. Bricka, D.D. Adrian, A review of potentially low-cost sorbents for heavy metals, *Water research* 33(11) (1999) 2469-2479.

[35] K. Vijayaraghavan, T.T. Teo, R. Balasubramanian, U.M. Joshi, Application of *Sargassum* biomass to remove heavy metal ions from synthetic multi-metal solutions and urban storm water runoff, *Journal of Hazardous Materials* 164(2-3) (2009) 1019-1023.

[36] J. He, J.P. Chen, A comprehensive review on biosorption of heavy metals by algal biomass: materials, performances, chemistry, and modeling simulation tools, *Bioresource technology* 160 (2014) 67-78.

[37] Y.-L. Dai, Y.-F. Jiang, H.G. Lee, Y.-J. Jeon, M.-C. Kang, Characterization and screening of anti-tumor activity of fucoidan from acid-processed hijiki (*Hizikia fusiforme*), *International journal of biological macromolecules* 139 (2019) 170-180.

[38] S. Pinteus, J. Silva, C. Alves, A. Horta, N. Fino, A.I. Rodrigues, S. Mendes, R. Pedrosa,

Cytoprotective effect of seaweeds with high antioxidant activity from the Peniche coast (Portugal), *Food chemistry* 218 (2017) 591-599.

[39] J.-H. Oh, J. Kim, Y. Lee, Anti-inflammatory and anti-diabetic effects of brown seaweeds in high-fat diet-induced obese mice, *Nutrition research and practice* 10(1) (2016) 42-48.

[40] H. Kesteloot, J.V. Joossens, Relationship of dietary sodium, potassium, calcium, and magnesium with blood pressure. *Belgian Interuniversity Research on Nutrition and Health, Hypertension* 12(6) (1988) 594-599.

[41] F.A. Tylavsky, L.A. Spence, L. Harkness, The importance of calcium, potassium, and acid-base homeostasis in bone health and osteoporosis prevention, *The Journal of nutrition* 138(1) (2008) 164S-165S.

[42] M. Jaishankar, T. Tseten, N. Anbalagan, B.B. Mathew, K.N. Beeregowda, Toxicity, mechanism and health effects of some heavy metals, *Interdisciplinary toxicology* 7(2) (2014) 60-72.

[43] M. Bouga, E. Combet, Emergence of seaweed and seaweed-containing foods in the UK: focus on labeling, iodine content, toxicity and nutrition, *Foods* 4(2) (2015) 240-253.

[44] B.K. Mandal, K.T. Suzuki, Arsenic round the world: a review, *Talanta* 58(1) (2002) 201-235.

[45] M. Rose, J. Lewis, N. Langford, M. Baxter, S. Origgi, M. Barber, H. MacBain, K. Thomas, Arsenic in seaweed—forms, concentration and dietary exposure, *Food and Chemical Toxicology* 45(7) (2007) 1263-1267.

[46] C.-H. Chou, C. Harper, *Toxicological profile for arsenic*, (2007).

[47] R.N. Ratnaïke, Acute and chronic arsenic toxicity, *Postgraduate medical journal* 79(933) (2003) 391-396.

[48] W.-H. Choi, S.-R. Lee, J.-Y. Park, Cement based solidification/stabilization of arsenic-contaminated mine tailings, *Waste management* 29(5) (2009) 1766-1771.

[49] W.H. Organization, *Arsenic in drinking-water: background document for development of WHO guidelines for drinking-water quality*, World Health Organization, 2003.

[50] C. Steinmaus, K. Carrigan, D. Kalman, R. Atallah, Y. Yuan, A.H. Smith, Dietary intake and arsenic methylation in a US population, *Environmental health perspectives* 113(9) (2005) 1153-1159.

[51] Z. Ning, D.T. Lobdell, R.K. Kwok, Z. Liu, S. Zhang, C. Ma, M. Riediker, J.L. Mumford, Residential exposure to drinking water arsenic in Inner Mongolia, China, *Toxicology and applied pharmacology* 222(3) (2007) 351-356.

[52] S.V. Flanagan, R.B. Johnston, Y. Zheng, Arsenic in tube well water in Bangladesh: health and economic impacts and implications for arsenic mitigation, *Bulletin of the World Health Organization* 90

(2012) 839-846.

[53] S. Mabeau, J. Fleurence, Seaweed in food products: biochemical and nutritional aspects, Trends in Food Science & Technology 4(4) (1993) 103-107.

[54] A.N.Z.F. Authority, The 19th Australian total diet survey, Australia & New Zealand: ANZFA (2001).

[55] C. Almela, M.J. Clemente, D. Vázquez, R. Montoro, Total arsenic, inorganic arsenic, lead and cadmium contents in edible seaweed sold in Spain, Food and Chemical Toxicology 44(11) (2006) 1901-1908.

[56] Food Additives Code in Ministry of Food and Drug Safety Korea(#2019-63, 2019.7.25.).
<https://www.mfds.go.kr>

[57] K. Yokoi, A. Konomi, Toxicity of so-called edible hijiki seaweed (*Sargassum fusiforme*) containing inorganic arsenic, Regulatory Toxicology and Pharmacology 63(2) (2012) 291-297.

[58] T. Wondimu, A. Ueno, I. Kanamaru, Y. Yamaguchi, R. McCrindle, K.-I. Hanaoka, Temperature-dependent extraction of trace elements in edible brown alga hijiki, *Hizikia fusiforme*, Food chemistry 104(2) (2007) 542-550.

[59] Y. Nakamura, T. Narukawa, J. Yoshinaga, Cancer risk to Japanese population from the consumption of inorganic arsenic in cooked hijiki, Journal of agricultural and food chemistry 56(7) (2008) 2536-2540.

[60] E.F. Brandon, P.J. Janssen, L. de Wit-Bos, Arsenic: bioaccessibility from seaweed and rice, dietary exposure calculations and risk assessment, Food Additives & Contaminants: Part A 31(12) (2014) 1993-2003.

[61] 片山眞之, 片山洋子, Effect of Temperature on the Diminution of Retained Arsenic in Dried Hijiki, *Sargassum fusiforme* (Harvey) Setchell, by Water-Soaking', Journal of Home Economics of Japan 58(2) (2007) 75-80.

[62] T. Zheng, C.C. Liu, J.Y. Yang, Q.G. Liu, J.L. Li, Hijiki Seaweed (*Hizikia fusiformis*): Nutritional value, safety concern and arsenic removal method, Advanced Materials Research, Trans Tech Publ, 2013, pp. 1247-1252.

[63] Zhang Jinling. (2013). Study on Detection of Arsenic and Removal of Inorganic Arsenic in *Sargassum Fusiforme*(Harv.)羊栖菜中砷的检测及去除无机砷方法的研究. (Doctoral dissertation)

[64] G.-y. Park, D.-e. Kang, M. Davaatseren, C. Shin, G.-J. Kang, M.-S. Chung, Reduction of total, organic, and inorganic arsenic content in *Hizikia fusiforme* (Hijiki), Food science and biotechnology 28(2) (2019) 615-622.

[65] I.S. Fernando, K.A. Sanjeewa, K.W. Samarakoon, W.W. Lee, H.-S. Kim, N. Kang, P. Ranasinghe, H.-S. Lee, Y.-J. Jeon, A fucoidan fraction purified from *Chnoospora minima*; a potential inhibitor of LPS-induced inflammatory responses, International journal of biological macromolecules 104 (2017)

1185-1193.

[66] I.S. Fernando, T.U. Jayawardena, K.A. Sanjeeva, L. Wang, Y.-J. Jeon, W.W. Lee, Anti-inflammatory potential of alginic acid from *Sargassum horneri* against urban aerosol-induced inflammatory responses in keratinocytes and macrophages, *Ecotoxicology and environmental safety* 160 (2018) 24-31.

[67] P. Hu, R. Xue, Z. Li, M. Chen, Z. Sun, J. Jiang, C. Huang, Structural investigation and immunological activity of a heteropolysaccharide from *Sargassum fusiforme*, *Carbohydrate research* 390 (2014) 28-32.

[68] T. Bitter, A modified uronic acid carbazole reaction, *Anal. Biochem.* 4 (1962) 330-334.

[69] K. Dodgson, R. Price, A note on the determination of the ester sulphate content of sulphated polysaccharides, *Biochemical Journal* 84(1) (1962) 106.

[70] L. Zhang, T. Zhang, *Method and Technology of Biological Experiment*, High Education Press, Beijing (1997).

[71] X. Yang, Y. Zhao, Q. Wang, H. WANG, Q. MEI, Analysis of the monosaccharide components in *Angelica* polysaccharides by high performance liquid chromatography, *Analytical sciences* 21(10) (2005) 1177-1180.

[72] E. Gómez-Ordóñez, P. Rupérez, FTIR-ATR spectroscopy as a tool for polysaccharide identification in edible brown and red seaweeds, *Food Hydrocolloids* 25(6) (2011) 1514-1520.

[73] J. Kang, Y.G. Lee, D.U. Jeong, J.S. Lee, Y.H. Choi, Y.K. Shin, Effect of abalone farming on sediment geochemistry in the shallow sea near Wando, South Korea, *Ocean Science Journal* 50(4) (2015) 669-682.

[74] S.-K. Kim, *Marine Pharmacognosy: Trends and Applications*, CRC press 2012.

[75] M.-K. Park, M. Choi, L. Kim, S.-D. Choi, An improved rapid analytical method for the arsenic speciation analysis of marine environmental samples using high-performance liquid chromatography/inductively coupled plasma mass spectrometry, *Environmental monitoring and assessment* 191(8) (2019) 525.

[76] FAO, *The State of World Fisheries and Aquaculture 2018 - Meeting the sustainable development goals*, FAO Rome, Italy, 2018.

[77] D.J. Grignon, Prostate cancer reporting and staging: needle biopsy and radical prostatectomy specimens, *Modern Pathology* 31(S1) (2018) S96.

[78] R.A. Smith, K.S. Andrews, D. Brooks, S.A. Fedewa, D. Manassaram - Baptiste, D. Saslow, O.W. Brawley, R.C. Wender, Cancer screening in the United States, 2018: A review of current American Cancer Society guidelines and current issues in cancer screening, *CA: A Cancer Journal for Clinicians* 68(4) (2018) 297-316.

- [79] B.N. Ames, L.S. Gold, W.C. Willett, The causes and prevention of cancer, *Proceedings of the National Academy of Sciences* 92(12) (1995) 5258-5265.
- [80] S.W. Fesik, Promoting apoptosis as a strategy for cancer drug discovery, *Nature Reviews Cancer* 5(11) (2005) 876.
- [81] H. Lum, K.A. Roebuck, Oxidant stress and endothelial cell dysfunction, *American Journal of Physiology-Cell Physiology* 280(4) (2001) C719-C741.
- [82] C. Dunnill, T. Patton, J. Brennan, J. Barrett, M. Dryden, J. Cooke, D. Leaper, N.T. Georgopoulos, Reactive oxygen species (ROS) and wound healing: the functional role of ROS and emerging ROS - modulating technologies for augmentation of the healing process, *International wound journal* 14(1) (2017) 89-96.
- [83] D.W. Crabb, G.Y. Im, G. Szabo, J.L. Mellinger, M.R. Lucey, *Diagnosis and Treatment of Alcohol - Related Liver Diseases: 2019 Practice Guidance from the American Association for the Study of Liver Diseases*, *Hepatology* (2019).
- [84] M.A. Schuckit, Alcohol-use disorders, *The Lancet* 373(9662) (2009) 492-501.
- [85] S.C. Larsson, N. Orsini, A. Wolk, Alcohol consumption and risk of heart failure: a dose - response meta - analysis of prospective studies, *European journal of heart failure* 17(4) (2015) 367-373.
- [86] S.C. Larsson, N. Drca, A. Wolk, Alcohol consumption and risk of atrial fibrillation: a prospective study and dose-response meta-analysis, *Journal of the American College of Cardiology* 64(3) (2014) 281-289.
- [87] Y. Yang, D.-C. Liu, Q.-M. Wang, Q.-Q. Long, S. Zhao, Z. Zhang, Y. Ma, Z.-M. Wang, L.-L. Chen, L.-S. Wang, Alcohol consumption and risk of coronary artery disease: A dose-response meta-analysis of prospective studies, *Nutrition* 32(6) (2016) 637-644.
- [88] C. Zhang, Y.-Y. Qin, Q. Chen, H. Jiang, X.-Z. Chen, C.-L. Xu, P.-J. Mao, J. He, Y.-H. Zhou, Alcohol intake and risk of stroke: a dose-response meta-analysis of prospective studies, *International journal of cardiology* 174(3) (2014) 669-677.
- [89] R. Parker, S.-J. Kim, B. Gao, Alcohol, adipose tissue and liver disease: mechanistic links and clinical considerations, *Nature Reviews Gastroenterology & Hepatology* 15(1) (2018) 50.
- [90] L. Dautrebande, H. Beckmann, W. Walkenhorst, Lung deposition of fine dust particles, *Arch. Indust. Health* 16(3) (1957) 179-87.
- [91] X. Xu, J. Gao, J. Gao, Y. Chen, Air pollution and daily mortality in residential areas of Beijing, China, *Archives of Environmental Health: An International Journal* 49(4) (1994) 216-222.
- [92] C.K. Chan, X. Yao, Air pollution in mega cities in China, *Atmospheric environment* 42(1) (2008) 1-42.

- [93] X. Hu, Y. Zhang, Z. Ding, T. Wang, H. Lian, Y. Sun, J. Wu, Bioaccessibility and health risk of arsenic and heavy metals (Cd, Co, Cr, Cu, Ni, Pb, Zn and Mn) in TSP and PM_{2.5} in Nanjing, China, *Atmospheric Environment* 57 (2012) 146-152.
- [94] S. Charlesworth, E. De Miguel, A. Ordóñez, A review of the distribution of particulate trace elements in urban terrestrial environments and its application to considerations of risk, *Environmental geochemistry and health* 33(2) (2011) 103-123.
- [95] J. Zhang, K.R. Smith, Household air pollution from coal and biomass fuels in China: measurements, health impacts, and interventions, *Environmental health perspectives* 115(6) (2007) 848-855.
- [96] R. Pozzi, B. De Berardis, L. Paoletti, C. Guastadisegni, Inflammatory mediators induced by coarse (PM_{2.5-10}) and fine (PM_{2.5}) urban air particles in RAW 264.7 cells, *Toxicology* 183(1-3) (2003) 243-254.
- [97] M. Diociaiuti, M. Balduzzi, B. De Berardis, G. Cattani, G. Stacchini, G. Ziemacki, A. Marconi, L. Paoletti, The two PM_{2.5} (fine) and PM_{2.5-10} (coarse) fractions: evidence of different biological activity, *Environmental research* 86(3) (2001) 254-262.
- [98] Q. Li, Z. Kang, S. Jiang, J. Zhao, S. Yan, F. Xu, J. Xu, Effects of ambient fine particles PM_{2.5} on human HaCaT cells, *International journal of environmental research and public health* 14(1) (2017) 72.
- [99] H. Choi, D.W. Shin, W. Kim, S.-J. Doh, S.H. Lee, M. Noh, Asian dust storm particles induce a broad toxicological transcriptional program in human epidermal keratinocytes, *Toxicology letters* 200(1-2) (2011) 92-99.
- [100] D.E. Heck, D.R. Gerecke, A.M. Vetrano, J.D. Laskin, Solar ultraviolet radiation as a trigger of cell signal transduction, *Toxicology and applied pharmacology* 195(3) (2004) 288-297.
- [101] R. Shiroma, S. Uechi, T. Taira, M. Ishihara, S. Tawata, M. Tako, Isolation and characterization of fucoidan from *Hizikia fusiformis* (Hijiki), *Journal of Applied Glycoscience* 50(3) (2003) 361-365.
- [102] R. Shiroma, T. KoniShi, S. Uechi, M. TaKo, Structural study of fucoidan from the brown seaweed *Hizikia fusiformis*, *Food science and technology research* 14(2) (2008) 176-182.
- [103] Y.-S. Choi, S.-Y. Eom, I.-S. Kim, S.F. Ali, M.T. Kleinman, Y.-D. Kim, H. Kim, Fucoidan Extracted from Hijiki Protects Brain Microvessel Endothelial Cells Against Diesel Exhaust Particle Exposure-Induced Disruption, *Journal of medicinal food* 19(5) (2016) 466-471.
- [104] H.W. Lee, Functional food composition having effects of relieving alcohol-induced hangover symptoms and improving liver function, Google Patents, 2007.
- [105] J. Chale-Dzul, R. Moo-Puc, D. Robledo, Y. Freile-Pelegri, Hepatoprotective effect of the fucoidan from the brown seaweed *Turbinaria tricostata*, *Journal of applied phycology* 27(5) (2015) 2123-2135.
- [106] S. Meenakshi, S. Umayaparvathi, R. Saravanan, T. Manivasagam, T. Balasubramanian,

Hepatoprotective effect of fucoidan isolated from the seaweed *Turbinaria decurrens* in ethanol intoxicated rats, *International journal of biological macromolecules* 67 (2014) 367-372.

[107] S.M. Jung, H.Y. Cho, B.S. Hong, D.H. Shin, W.J. Jun, D.H. Lee, [P10-136] The Screening of Seaweeds which Enhance Ethanol Metabolizing Enzyme Activity and Liver Protection, *한국식품영양과학회 학술대회발표집* (2005) 491-491.

[108] M.-C. Kang, K.-N. Kim, W. Wijesinghe, X. Yang, G. Ahn, Y.-J. Jeon, Protective effect of polyphenol extracted from *Ecklonia cava* against ethanol induced oxidative damage in vitro and in zebrafish model, *Journal of functional foods* 6 (2014) 339-347.

[109] A. Jayachitra, S. Sreelatha, P. Padma, Antioxidant and hepatoprotective effects of *Clitoria ternatea* leaf extracts by using in vivo model, *International Journal of Medicinal and Aromatic Plants* 2(2) (2012) 323-332.

[110] S. Palanisamy, M. Vinosa, M. Manikandakrishnan, R. Anjali, P. Rajasekar, T. Marudhupandi, R. Manikandan, B. Vaseeharan, N.M. Prabhu, Investigation of antioxidant and anticancer potential of fucoidan from *Sargassum polycystum*, *International journal of biological macromolecules* 116 (2018) 151-161.

[111] C. Sarithakumari, G. Renju, G.M. Kurup, Anti-inflammatory and antioxidant potential of alginic acid isolated from the marine algae, *Sargassum wightii* on adjuvant-induced arthritic rats, *Inflammopharmacology* 21(3) (2013) 261-268.

[112] M.-J. So, B.-K. Kim, M.-J. Choi, K.-Y. Park, S.-H. Rhee, E.-J. Cho, Protective activity of fucoidan and alginic acid against free radical-induced oxidative stress under in vitro and cellular system, *Preventive Nutrition and Food Science* 12(4) (2007) 191-196.

[113] C. Sarithakumari, G.M. Kurup, Alginic acid isolated from *Sargassum wightii* exhibits anti-inflammatory potential on type II collagen induced arthritis in experimental animals, *International immunopharmacology* 17(4) (2013) 1108-1115.

[114] M. Dubois, K.A. Gilles, J.K. Hamilton, Pt. Rebers, F. Smith, Colorimetric method for determination of sugars and related substances, *Analytical chemistry* 28(3) (1956) 350-356.

[115] S. Bjornsson, Size-dependent separation of proteoglycans by electrophoresis in gels of pure agarose, *Analytical biochemistry* 210(2) (1993) 292-298.

[116] G. Li, X. Xing, Y. Luo, X. Deng, S. Lu, S. Tang, G. Sun, X. Sun, Notoginsenoside R 1 prevents H9c2 cardiomyocytes apoptosis against hypoxia/reoxygenation via the ERs/PI3K/Akt pathway, *RSC Advances* 8(25) (2018) 13871-13878.

[117] G. Lizard, S. Fournel, L. Genestier, N. Dhedin, C. Chaput, M. Flacher, M. Mutin, G. Panaye, J.P. Revillard, Kinetics of plasma membrane and mitochondrial alterations in cells undergoing apoptosis, *Cytometry Part A* 21(3) (1995) 275-283.

- [118] L. Zhang, H. Yu, Y. Sun, X. Lin, B. Chen, C. Tan, G. Cao, Z. Wang, Protective effects of salidroside on hydrogen peroxide-induced apoptosis in SH-SY5Y human neuroblastoma cells, *European journal of pharmacology* 564(1-3) (2007) 18-25.
- [119] M.-H. Pan, W.-L. Chang, S.-Y. Lin-Shiau, C.-T. Ho, J.-K. Lin, Induction of apoptosis by garcinol and curcumin through cytochrome c release and activation of caspases in human leukemia HL-60 cells, *Journal of agricultural and food chemistry* 49(3) (2001) 1464-1474.
- [120] S.-H. Lee, S.-M. Kang, C.H. Sok, J.T. Hong, J.-Y. Oh, Y.-J. Jeon, Cellular activities and docking studies of eckol isolated from *Ecklonia cava* (Laminariales, Phaeophyceae) as potential tyrosinase inhibitor, *Algae* 30(2) (2015) 163.
- [121] F. Nanjo, K. Goto, R. Seto, M. Suzuki, M. Sakai, Y. Hara, Scavenging effects of tea catechins and their derivatives on 1, 1-diphenyl-2-picrylhydrazyl radical, *Free Radical Biology and Medicine* 21(6) (1996) 895-902.
- [122] K. Hiramoto, H. Johkoh, K.-I. Sako, K. Kikugawa, DNA breaking activity of the carbon-centered radical generated from 2, 2'-azobis (2-amidinopropane) hydrochloride (AAPH), *Free radical research communications* 19(5) (1993) 323-332.
- [123] E. Finkelstein, G.M. Rosen, E.J. Rauckman, Spin trapping of superoxide and hydroxyl radical: practical aspects, *Archives of Biochemistry and Biophysics* 200(1) (1980) 1-16.
- [124] T. Mosmann, Rapid colorimetric assay for cellular growth and survival: application to proliferation and cytotoxicity assays, *Journal of immunological methods* 65(1-2) (1983) 55-63.
- [125] M.-C. Kang, K.-N. Kim, S.-M. Kang, X. Yang, E.-A. Kim, C.B. Song, J.-W. Nah, M.-K. Jang, J.-S. Lee, W.-K. Jung, Protective effect of dieckol isolated from *Ecklonia cava* against ethanol caused damage in vitro and in zebrafish model, *Environmental toxicology and pharmacology* 36(3) (2013) 1217-1226.
- [126] J. Chu, K.C. Sadler, New school in liver development: lessons from zebrafish, *Hepatology* 50(5) (2009) 1656-1663.
- [127] M.J. Passeri, A. Cinaroglu, C. Gao, K.C. Sadler, Hepatic steatosis in response to acute alcohol exposure in zebrafish requires sterol regulatory element binding protein activation, *Hepatology* 49(2) (2009) 443-452.
- [128] D. Gérard-Monnier, I. Erdelmeier, K. Régnard, N. Moze-Henry, J.-C. Yadan, J. Chaudiere, Reactions of 1-methyl-2-phenylindole with malondialdehyde and 4-hydroxyalkenals. Analytical applications to a colorimetric assay of lipid peroxidation, *Chemical research in toxicology* 11(10) (1998) 1176-1183.
- [129] F. Tietze, Enzymic method for quantitative determination of nanogram amounts of total and oxidized glutathione: applications to mammalian blood and other tissues, *Analytical biochemistry* 27(3) (1969) 502-522.

- [130] E.-A. Kim, S.-H. Lee, C.-i. Ko, S.-H. Cha, M.-C. Kang, S.-M. Kang, S.-C. Ko, W.-W. Lee, J.-Y. Ko, J.-H. Lee, Protective effect of fucoidan against AAPH-induced oxidative stress in zebrafish model, *Carbohydrate polymers* 102 (2014) 185-191.
- [131] I. Fernando, H.-S. Kim, K. Sanjeeva, J.-Y. Oh, Y.-J. Jeon, W.W. Lee, Inhibition of inflammatory responses elicited by urban fine dust particles in keratinocytes and macrophages by diphloretohydroxycarmalol isolated from a brown alga *Ishige okamurae*, *Algae* 32(3) (2017) 261-273.
- [132] M.C.R. de Souza, C.T. Marques, C.M.G. Dore, F.R.F. da Silva, H.A.O. Rocha, E.L. Leite, Antioxidant activities of sulfated polysaccharides from brown and red seaweeds, *Journal of applied phycology* 19(2) (2007) 153-160.
- [133] E. Bagheri, F. Hajiaghaalipour, S. Nyamathulla, N. Salehen, Ethanolic extract of *Brucea javanica* inhibit proliferation of HCT-116 colon cancer cells via caspase activation, *RSC Advances* 8(2) (2018) 681-689.
- [134] G. Ahn, W. Lee, K.-N. Kim, J.-H. Lee, S.-J. Heo, N. Kang, S.-H. Lee, C.-B. Ahn, Y.-J. Jeon, A sulfated polysaccharide of *Ecklonia cava* inhibits the growth of colon cancer cells by inducing apoptosis, *EXCLI journal* 14 (2015) 294.
- [135] D. Baskić, S. Popović, P. Ristić, N.N. Arsenijević, Analysis of cycloheximide-induced apoptosis in human leukocytes: fluorescence microscopy using annexin V/propidium iodide versus acridin orange/ethidium bromide, *Cell biology international* 30(11) (2006) 924-932.
- [136] R.C. Scaduto Jr, L.W. Grotyohann, Measurement of mitochondrial membrane potential using fluorescent rhodamine derivatives, *Biophysical journal* 76(1) (1999) 469-477.
- [137] P.F. Li, R. Dietz, R. von Harsdorf, p53 regulates mitochondrial membrane potential through reactive oxygen species and induces cytochrome c - independent apoptosis blocked by Bcl - 2, *The EMBO journal* 18(21) (1999) 6027-6036.
- [138] N.A. Thornberry, Y. Lazebnik, Caspases: enemies within, *Science* 281(5381) (1998) 1312-1316.
- [139] M.A. Barry, C.A. Behnke, A. Eastman, Activation of programmed cell death (apoptosis) by cisplatin, other anticancer drugs, toxins and hyperthermia, *Biochemical pharmacology* 40(10) (1990) 2353-2362.
- [140] L. Mooney, K. Al-Sakkaf, B. Brown, P. Dobson, Apoptotic mechanisms in T47D and MCF-7 human breast cancer cells, *British journal of cancer* 87(8) (2002) 909-917.
- [141] C. Weng, Y. Li, D. Xu, Y. Shi, H. Tang, Specific cleavage of Mcl-1 by caspase-3 in tumor necrosis factor-related apoptosis-inducing ligand (TRAIL)-induced apoptosis in Jurkat leukemia T cells, *Journal of Biological Chemistry* 280(11) (2005) 10491-10500.
- [142] S. Salakou, D. Kardamakis, A.C. Tsamandas, V. Zolota, E. Apostolakis, V. Tzelepi, P.

Papathanasopoulos, D.S. Bonikos, T. Papapetropoulos, T. Petsas, Increased Bax/Bcl-2 ratio up-regulates caspase-3 and increases apoptosis in the thymus of patients with myasthenia gravis, *In vivo* 21(1) (2007) 123-132.

[143] R.U. Jänicke, M.L. Sprengart, M.R. Wati, A.G. Porter, Caspase-3 is required for DNA fragmentation and morphological changes associated with apoptosis, *Journal of Biological Chemistry* 273(16) (1998) 9357-9360.

[144] W. Goessling, K.C. Sadler, Zebrafish: an important tool for liver disease research, *Gastroenterology* 149(6) (2015) 1361-1377.

[145] K. Howe, M.D. Clark, C.F. Torroja, J. Turrance, C. Bertelot, M. Muffato, J.E. Collins, S. Humphray, K. McLaren, L. Matthews, The zebrafish reference genome sequence and its relationship to the human genome, *Nature* 496(7446) (2013) 498.

[146] T.M. Donohue Jr, Alcohol-induced steatosis in liver cells, *World journal of gastroenterology: WJG* 13(37) (2007) 4974.

[147] K. Bambino, C. Zhang, C. Austin, C. Amarasiriwardena, M. Arora, J. Chu, K.C. Sadler, Inorganic arsenic causes fatty liver and interacts with ethanol to cause alcoholic liver disease in zebrafish, *Disease models & mechanisms* 11(2) (2018) dmm031575.

[148] M. Langheinrich, A privacy awareness system for ubiquitous computing environments, international conference on Ubiquitous Computing, Springer, 2002, pp. 237-245.

[149] A.J. Levine, J. Momand, C.A. Finlay, The p53 tumour suppressor gene, *nature* 351(6326) (1991) 453.

[150] R.-B. Ding, K. Tian, C.-W. He, Y. Jiang, Y.-T. Wang, J.-B. Wan, Herbal medicines for the prevention of alcoholic liver disease: a review, *Journal of Ethnopharmacology* 144(3) (2012) 457-465.

[151] H.R.B. Raghavendran, A. Sathivel, T. Devaki, Hepatoprotective nature of seaweed alcoholic extract on acetaminophen induced hepatic oxidative stress, *Journal of health science* 50(1) (2004) 42-46.

[152] M.-C. Kang, G. Ahn, X. Yang, K.-N. Kim, S.-M. Kang, S.-H. Lee, S.-C. Ko, J.-Y. Ko, D. Kim, Y.-T. Kim, Hepatoprotective effects of dieckol-rich phlorotannins from *Ecklonia cava*, a brown seaweed, against ethanol induced liver damage in BALB/c mice, *Food and chemical toxicology* 50(6) (2012) 1986-1991.

[153] E.-Y. Choi, H.-J. Hwang, I.-H. Kim, T.-J. Nam, Protective effects of a polysaccharide from *Hizikia fusiformis* against ethanol toxicity in rats, *Food and Chemical Toxicology* 47(1) (2009) 134-139.

[154] K.S. Kang, I.D. Kim, R.H. Kwon, J.Y. Lee, J.S. Kang, B.J. Ha, The effects of fucoidan extracts on CCl₄-induced liver injury, *Archives of pharmacal research* 31(5) (2008) 622.

[155] M. Wu, Y. Wu, M. Qu, W. Li, X. Yan, Evaluation of antioxidant activities of water-soluble

polysaccharides from brown alga *Hizikia fusiformis*, *International journal of biological macromolecules* 56 (2013) 28-33.

[156] Y.-L. Dai, Y.-F. Jiang, H.G. Lee, Y.-J. Jeon, M.-C. Kang, Characterization and screening of anti-tumor activity of fucoidan from acid-processed hijiki (*Hizikia fusiforme*), *International Journal of Biological Macromolecules* (2019).

[157] T. Miyashita, S. Krajewski, M. Krajewska, H.G. Wang, H. Lin, D.A. Liebermann, B. Hoffman, J.C. Reed, Tumor suppressor p53 is a regulator of bcl-2 and bax gene expression in vitro and in vivo, *Oncogene* 9(6) (1994) 1799-1805.

[158] D. Leal, B. Matsuhira, M. Rossi, F. Caruso, FT-IR spectra of alginic acid block fractions in three species of brown seaweeds, *Carbohydrate research* 343(2) (2008) 308-316.

[159] M. Akdis, A. Aab, C. Altunbulakli, K. Azkur, R.A. Costa, R. Cramer, S. Duan, T. Eiwegger, A. Eljaszewicz, R. Ferstl, Interleukins (from IL-1 to IL-38), interferons, transforming growth factor β , and TNF- α : Receptors, functions, and roles in diseases, *Journal of Allergy and Clinical Immunology* 138(4) (2016) 984-1010.

[160] J. Gao, C. Ma, S. Xing, L. Sun, L. Huang, A review of fundamental factors affecting diesel PM oxidation behaviors, *Science China Technological Sciences* 61(3) (2018) 330-345.

[161] H. Wang, Q. Song, Q. Yao, C.-h. CHEN, Experimental study on removal effect of wet flue gas desulfurization system on fine particles from a coal-fired power plant, *Proceedings-Chinese Society of electrical engineering* 28(5) (2008) 1.

[162] K. He, F. Yang, Y. Ma, Q. Zhang, X. Yao, C.K. Chan, S. Cadle, T. Chan, P. Mulawa, The characteristics of PM_{2.5} in Beijing, China, *Atmospheric Environment* 35(29) (2001) 4959-4970.

[163] X. Zhang, J. Sun, Y. Wang, W. Li, Q. Zhang, W. Wang, J. Quan, G. Cao, J. Wang, Y. Yang, Factors contributing to haze and fog in China, *Chinese Science Bulletin* 58(13) (2013) 1178-1187.

[164] F.Y. XIANG, The dust fall in Beijing, China on April 18, 1980, *Desert dust: Origin, characteristics, and effect on man* 186 (1981) 149.

[165] X. Zeng, X. Xu, X. Zheng, T. Reponen, A. Chen, X. Huo, Heavy metals in PM_{2.5} and in blood, and children's respiratory symptoms and asthma from an e-waste recycling area, *Environmental pollution* 210 (2016) 346-353.

[166] J.E. Gross, W.G. Carlos, C.S. Dela Cruz, P. Harber, S. Jamil, Sand and dust storms: Acute exposure and threats to respiratory health, *American journal of respiratory and critical care medicine* 198(7) (2018) P13-P14.

[167] I. Kim, Toxic compounds analysis and risk assessment for fine dust (PM_{2.5}) in Gwangju, *환경독성보건학회 심포지엄 및 학술대회* (2018) 139-153.

- [168] T. Schripp, M. Braun, T. Grein, P. Oßwald, Ambient Ultra-Fine Particle Exposure Assessment Based on Mobile and Stationary Monitoring during Fine Dust Season in Stuttgart, Germany, ISEE Conference Abstracts, 2018.
- [169] H. Wang, L. Qiao, S. Lou, M. Zhou, A. Ding, H. Huang, J. Chen, Q. Wang, S. Tao, C. Chen, Chemical composition of PM_{2.5} and meteorological impact among three years in urban Shanghai, China, *Journal of Cleaner Production* 112 (2016) 1302-1311.
- [170] H. Xu, J. Cao, J.C. Chow, R.-J. Huang, Z. Shen, L.A. Chen, K.F. Ho, J.G. Watson, Inter-annual variability of wintertime PM_{2.5} chemical composition in Xi'an, China: Evidences of changing source emissions, *Science of the Total Environment* 545 (2016) 546-555.
- [171] P. Chen, X. Bi, J. Zhang, J. Wu, Y. Feng, Assessment of heavy metal pollution characteristics and human health risk of exposure to ambient PM_{2.5} in Tianjin, China, *Particuology* 20 (2015) 104-109.
- [172] K. Bekki, T. Ito, Y. Yoshida, C. He, K. Arashidani, M. He, G. Sun, Y. Zeng, H. Sone, N. Kunugita, PM_{2.5} collected in China causes inflammatory and oxidative stress responses in macrophages through the multiple pathways, *Environmental toxicology and pharmacology* 45 (2016) 362-369.
- [173] X.-T. Jin, M.-L. Chen, R.-J. Li, Q. An, L. Song, Y. Zhao, H. Xiao, L. Cheng, Z.-Y. Li, Progression and inflammation of human myeloid leukemia induced by ambient PM_{2.5} exposure, *Archives of toxicology* 90(8) (2016) 1929-1938.
- [174] R. Hu, X.-Y. Xie, S.-K. Xu, Y.-N. Wang, M. Jiang, L.-R. Wen, W. Lai, L. Guan, PM_{2.5} exposure elicits oxidative stress responses and mitochondrial apoptosis pathway activation in HaCaT keratinocytes, *Chinese medical journal* 130(18) (2017) 2205.
- [175] Y. Zhang, L. Zheng, J. Tuo, Q. Liu, X. Zhang, Z. Xu, S. Liu, G. Sui, Analysis of PM_{2.5}-induced cytotoxicity in human HaCaT cells based on a microfluidic system, *Toxicology in Vitro* 43 (2017) 1-8.
- [176] C.K. Glass, K. Saijo, Nuclear receptor transrepression pathways that regulate inflammation in macrophages and T cells, *Nature Reviews Immunology* 10(5) (2010) 365.
- [177] N. Fujiwara, K. Kobayashi, Macrophages in inflammation, *Current Drug Targets-Inflammation & Allergy* 4(3) (2005) 281-286.
- [178] T.U. Jayawardena, K.A. Sanjeewa, I.S. Fernando, B.M. Ryu, M.-C. Kang, Y. Jee, W.W. Lee, Y.-J. Jeon, *Sargassum horneri* (Turner) C. Agardh ethanol extract inhibits the fine dust inflammation response via activating Nrf2/HO-1 signaling in RAW 264.7 cells, *BMC complementary and alternative medicine* 18(1) (2018) 249.
- [179] A.S. Pipal, P.G. Satsangi, Study of carbonaceous species, morphology and sources of fine (PM_{2.5}) and coarse (PM₁₀) particles along with their climatic nature in India, *Atmospheric Research* 154 (2015) 103-115.

- [180] X. Querol, A. Alastuey, S. Rodriguez, F. Plana, E. Mantilla, C.R. Ruiz, Monitoring of PM10 and PM2.5 around primary particulate anthropogenic emission sources, *Atmospheric Environment* 35(5) (2001) 845-858.
- [181] B.-j. Fu, X.-l. Zhuang, G.-b. Jiang, J.-b. Shi, Lu, Yi-he, Feature: environmental problems and challenges in China, ACS Publications, 2007.
- [182] H. Bové E. Bongaerts, E. Slenders, E.M. Bijnens, N.D. Saenen, W. Gyselaers, P. Van Eyken, M. Plusquin, M.B. Roeffaers, M. Ameloot, Ambient black carbon particles reach the fetal side of human placenta, *Nat Commun* (Accepted. 2019) 10 (2019).
- [183] W.F. Lever, *Histopathology of the Skin*, Histopathology of the skin. (1949).
- [184] S.-J. Heo, Y.-J. Jeon, Protective effect of fucoxanthin isolated from *Sargassum siliquastrum* on UV-B induced cell damage, *Journal of Photochemistry and Photobiology B: Biology* 95(2) (2009) 101-107.
- [185] T. Kawakami, M. Tsushima, Y. Katabami, M. Mine, A. Ishida, T. Matsuno, Effect of β , β -carotene, β -echinenone, astaxanthin, fucoxanthin, vitamin A and vitamin E on the biological defense of the sea urchin *Pseudocentrotus depressus*, *Journal of Experimental Marine Biology and Ecology* 226(2) (1998) 165-174.
- [186] K. Kanazawa, Y. Ozaki, T. Hashimoto, S.K. Das, S. Matsushita, M. Hirano, T. Okada, A. Komoto, N. Mori, M. Nakatsuka, Commercial-scale preparation of biofunctional fucoxanthin from waste parts of brown sea algae *Laminalia japonica*, *Food science and technology research* 14(6) (2008) 573-573.
- [187] S.-J. Heo, W.-J. Yoon, K.-N. Kim, G.-N. Ahn, S.-M. Kang, D.-H. Kang, C. Oh, W.-K. Jung, Y.-J. Jeon, Evaluation of anti-inflammatory effect of fucoxanthin isolated from brown algae in lipopolysaccharide-stimulated RAW 264.7 macrophages, *Food and Chemical Toxicology* 48(8-9) (2010) 2045-2051.
- [188] S.-J. Heo, S.-C. Ko, S.-M. Kang, H.-S. Kang, J.-P. Kim, S.-H. Kim, K.-W. Lee, M.-G. Cho, Y.-J. Jeon, Cytoprotective effect of fucoxanthin isolated from brown algae *Sargassum siliquastrum* against H₂O₂-induced cell damage, *European food research and technology* 228(1) (2008) 145-151.
- [189] K.-N. Kim, S.-J. Heo, S.-M. Kang, G. Ahn, Y.-J. Jeon, Fucoxanthin induces apoptosis in human leukemia HL-60 cells through a ROS-mediated Bcl-xL pathway, *Toxicology in vitro* 24(6) (2010) 1648-1654.
- [190] S.M. Kim, Y.-J. Jung, O.-N. Kwon, K.H. Cha, B.-H. Um, D. Chung, C.-H. Pan, A potential commercial source of fucoxanthin extracted from the microalga *Phaeodactylum tricornutum*, *Applied biochemistry and biotechnology* 166(7) (2012) 1843-1855.
- [191] A.W. Ha, S.J. Na, W.K. Kim, Antioxidant effects of fucoxanthin rich powder in rats fed with high fat diet, *Nutrition research and practice* 7(6) (2013) 475-480.

- [192] S.M. Jeon, H.J. Kim, M.N. Woo, M.K. Lee, Y.C. Shin, Y.B. Park, M.S. Choi, Fucoxanthin - rich seaweed extract suppresses body weight gain and improves lipid metabolism in high - fat - fed C57BL/6J mice, *Biotechnology journal* 5(9) (2010) 961-969.
- [193] A.W. Ha, W.K. Kim, The effect of fucoxanthin rich powder on the lipid metabolism in rats with a high fat diet, *Nutrition Research and Practice* 7(4) (2013) 287-293.
- [194] X. Yan, Y. Chuda, M. Suzuki, T. Nagata, Fucoxanthin as the major antioxidant in *Hijikia fusiformis*, a common edible seaweed, *Bioscience, biotechnology, and biochemistry* 63(3) (1999) 605-607.
- [195] N.S. Trede, A. Zapata, L.I. Zon, Fishing for lymphoid genes, *Trends in immunology* 22(6) (2001) 302-307.
- [196] L.-J. Wang, Y. Fan, R. Parsons, G.-R. Hu, P.-Y. Zhang, F.-L. Li, A Rapid Method for the Determination of Fucoxanthin in Diatom, *Marine drugs* 16(1) (2018) 33.
- [197] S.C. Foo, F.M. Yusoff, M. Ismail, M. Basri, S.K. Yau, N.M. Khong, K.W. Chan, M. Ebrahimi, Antioxidant capacities of fucoxanthin-producing algae as influenced by their carotenoid and phenolic contents, *Journal of biotechnology* 241 (2017) 175-183.
- [198] G. Rajauria, B. Foley, N. Abu-Ghannam, Characterization of dietary fucoxanthin from *Himanthalia elongata* brown seaweed, *Food Research International* 99 (2017) 995-1001.
- [199] T. Maoka, Y. Fujiwara, K. Hashimoto, N. Akimoto, Rapid Identification of carotenoids in a combination of liquid chromatography/UV-visible absorption spectrometry by photodiode-array detector and atmospheric pressure chemical ionization mass spectrometry (LC/PAD/APCI-MS), *Journal of Oleo Science* 51(1) (2002) 1-9.
- [200] K.-J. Yeum, R.M. Russell, Carotenoid bioavailability and bioconversion, *Annual review of nutrition* 22(1) (2002) 483-504.
- [201] A.R.-B. de Quirós, S. Frecha-Ferreiro, A. Vidal-Perez, J. López-Hernández, Antioxidant compounds in edible brown seaweeds, *European Food Research and Technology* 231(3) (2010) 495-498.
- [202] J. Terao, Antioxidant activity of β - carotene - related carotenoids in solution, *Lipids* 24(7) (1989) 659-661.
- [203] A. Subramoniam, V.V. Asha, S.A. Nair, S.P. Sasidharan, P.K. Sureshkumar, K.N. Rajendran, D. Karunakaran, K. Ramalingam, Chlorophyll revisited: Anti-inflammatory activities of chlorophyll a and inhibition of expression of TNF- α gene by the same, *Inflammation* 35(3) (2012) 959-966.
- [204] K.-N. Kim, S.-J. Heo, W.-J. Yoon, S.-M. Kang, G. Ahn, T.-H. Yi, Y.-J. Jeon, Fucoxanthin inhibits the inflammatory response by suppressing the activation of NF- κ B and MAPKs in lipopolysaccharide-induced RAW 264.7 macrophages, *European journal of pharmacology* 649(1-3) (2010) 369-375.

- [205] R.L. Siegel, K.D. Miller, A. Jemal, Cancer statistics, 2019, CA: a cancer journal for clinicians 69(1) (2019) 7-34.
- [206] A. Jemal, F. Bray, M.M. Center, J. Ferlay, E. Ward, D. Forman, Global cancer statistics, CA: a cancer journal for clinicians 61(2) (2011) 69-90.
- [207] P.T. James, Obesity: the worldwide epidemic, Clinics in dermatology 22(4) (2004) 276-280.
- [208] K. McColl, "Fat taxes" and the financial crisis, The Lancet 373(9666) (2009) 797-798.
- [209] Z. Yang, A.G. Hall, The financial burden of overweight and obesity among elderly Americans: the dynamics of weight, longevity, and health care cost, Health services research 43(3) (2008) 849-868.
- [210] R.C. Rossi, L.C.M. Vanderlei, A.C.C.R. Gonçalves, F.M. Vanderlei, A.F.B. Bernardo, K.M.H. Yamada, N.T. da Silva, L.C. de Abreu, Impact of obesity on autonomic modulation, heart rate and blood pressure in obese young people, Autonomic neuroscience 193 (2015) 138-141.
- [211] J. Cho, H.-S. Juon, Assessing overweight and obesity risk among Korean Americans in California using World Health Organization body mass index criteria for Asians, Preventing chronic disease 3(3) (2006) A79-A79.
- [212] P.L. Lutsey, L.M. Steffen, J. Stevens, Dietary intake and the development of the metabolic syndrome, Circulation 117(6) (2008) 754-761.
- [213] A. Shin, S.-Y. Lim, J. Sung, H.-R. Shin, J. Kim, Dietary intake, eating habits, and metabolic syndrome in Korean men, Journal of the American Dietetic Association 109(4) (2009) 633-640.
- [214] N.-H. Kim, J.-D. Heo, J.-R. Rho, M.H. Yang, E.J. Jeong, Anti-obesity Effect of Halophyte Crop, Limonium tetragonum in High-Fat Diet-Induced Obese Mice and 3T3-L1 Adipocytes, Biological and Pharmaceutical Bulletin 40(11) (2017) 1856-1865.
- [215] E. Rosen, J. Eguchi, Z. Xu, Transcriptional targets in adipocyte biology, Expert opinion on therapeutic targets 13(8) (2009) 975-986.
- [216] V. Gnanavel, S.M. Roopan, S. Rajeshkumar, Aquaculture: An overview of chemical ecology of seaweeds (food species) in natural products, Aquaculture (2019).
- [217] T. Woyengo, V. Ramprasath, P. Jones, Anticancer effects of phytosterols, European journal of clinical nutrition 63(7) (2009) 813.
- [218] K. Kazłowska, H.-T.V. Lin, S.-H. Chang, G.-J. Tsai, In vitro and in vivo anticancer effects of sterol fraction from red algae Porphyra dentata, Evidence-Based Complementary and Alternative Medicine 2013 (2013).
- [219] Z. Chen, J. Liu, Z. Fu, C. Ye, R. Zhang, Y. Song, Y. Zhang, H. Li, H. Ying, H. Liu, 24 (S)-Saringosterol from edible marine seaweed Sargassum fusiforme is a novel selective LXR β agonist,

Journal of agricultural and food chemistry 62(26) (2014) 6130-6137.

[220] S.-E.N. Ayyad, S.Z. Sowellim, M.S. El-Hosini, A. Abo-Atia, The structural determination of a new steroidal metabolite from the brown alga *Sargassum asperifolium*, *Zeitschrift für Naturforschung C* 58(5-6) (2003) 333-336.

[221] J.-H. Lee, J.-Y. Ko, C.Y. Kim, Y.-T. Kim, J. Kim, Y.-J. Jeon, Saringosterol Acetate from a Popular Edible Seaweed, *Hizikia Fusiformis* Attenuated Proliferation of Human Lung Adenocarcinoma Epithelial Cells (A549 Cells) via Apoptosis Signaling Pathway, (2019).

[222] C. Yokoyama, X. Wang, M.R. Briggs, A. Admon, J. Wu, X. Hua, J.L. Goldstein, M.S. Brown, SREBP-1, a basic-helix-loop-helix-leucine zipper protein that controls transcription of the low density lipoprotein receptor gene, *Cell* 75(1) (1993) 187-197.

[223] J.B. Kim, B.M. Spiegelman, ADD1/SREBP1 promotes adipocyte differentiation and gene expression linked to fatty acid metabolism, *Genes & development* 10(9) (1996) 1096-1107.

[224] J.A. Lee, Y.R. Cho, S.S. Hong, E.K. Ahn, Anti - Obesity Activity of Saringosterol Isolated from *Sargassum muticum* (Yendo) Fensholt Extract in 3T3 - L1 Cells, *Phytotherapy research* 31(11) (2017) 1694-1701.

[225] J.-H. Lee, J.-Y. Ko, K. Samarakoon, J.-Y. Oh, S.-J. Heo, C.-Y. Kim, J.-W. Nah, M.-K. Jang, J.-S. Lee, Y.-J. Jeon, Preparative isolation of sargachromanol E from *Sargassum siliquastrum* by centrifugal partition chromatography and its anti-inflammatory activity, *Food and chemical toxicology* 62 (2013) 54-60.

[226] D. Ribble, N.B. Goldstein, D.A. Norris, Y.G. Shellman, A simple technique for quantifying apoptosis in 96-well plates, *BMC biotechnology* 5(1) (2005) 12.

[227] I.S. Fernando, W.W. Lee, T.U. Jayawardena, M.-C. Kang, Y.-S. Ann, C.-i. Ko, Y.J. Park, Y.-J. Jeon, 3 β -Hydroxy- Δ 5-steroidal congeners from a column fraction of *Dendronephthya puetteri* attenuate LPS-induced inflammatory responses in RAW 264.7 macrophages and zebrafish embryo model, *RSC Advances* 8(33) (2018) 18626-18634.

[228] Y. Liu, *Sargassum fusiforme* (Harv.) Setch. 羊栖菜 (Yangqicai, Hijiki), *Dietary Chinese Herbs*, Springer2015, pp. 789-796.

[229] A.B. Awad, K.C. Chan, A.C. Downie, C.S. Fink, Peanuts as a source of β -sitosterol, a sterol with anticancer properties, *Nutrition and cancer* 36(2) (2000) 238-241.

[230] J.F. Carvalho, M.M.C. Silva, J.N. Moreira, S.r. Simões, M.L. Sá e Melo, Sterols as anticancer agents: synthesis of ring-B oxygenated steroids, cytotoxic profile, and comprehensive SAR analysis, *Journal of medicinal chemistry* 53(21) (2010) 7632-7638.

[231] K.K.A. Sanjeeva, I.P.S. Fernando, K.W. Samarakoon, H.H.C. Lakmal, E.-A. Kim, O.-N. Kwon,

M.G. Dilshara, J.-B. Lee, Y.-J. Jeon, Anti-inflammatory and anti-cancer activities of sterol rich fraction of cultured marine microalga *Nannochloropsis oculata*, *Algae* 31(3) (2016) 277-287.

[232] L.-L. Wang, Q.-L. Yu, L. Han, X.-L. Ma, R.-D. Song, S.-N. Zhao, W.-H. Zhang, Study on the effect of reactive oxygen species-mediated oxidative stress on the activation of mitochondrial apoptosis and the tenderness of yak meat, *Food chemistry* 244 (2018) 394-402.

[233] J. Liu, L. Cao, J. Chen, S. Song, I.H. Lee, C. Quijano, H. Liu, K. Keyvanfar, H. Chen, L.-Y. Cao, Bmi1 regulates mitochondrial function and the DNA damage response pathway, *Nature* 459(7245) (2009) 387.

[234] M.-C. Kang, Y. Ding, J. Kim, E.-A. Kim, I.S. Fernando, S.-J. Heo, S.-H. Lee, 3-Chloro-4, 5-dihydroxybenzaldehyde inhibits adipogenesis in 3T3-L1 adipocytes by regulating expression of adipogenic transcription factors and AMPK activation, *Chemico-biological interactions* 287 (2018) 27-31.

[235] A.E. Pollard, L. Martins, P.J. Muckett, S. Khadayate, A. Bornot, M. Clausen, T. Admyre, M. Bjursell, R. Fiadeiro, L. Wilson, AMPK activation protects against diet-induced obesity through Ucp1-independent thermogenesis in subcutaneous white adipose tissue, *Nature metabolism* 1(3) (2019) 340.

[236] Y. Lim, J. Sung, J. Yang, H.S. Jeong, J. Lee, Butein inhibits adipocyte differentiation by modulating the AMPK pathway in 3T3 - L1 cells, *Journal of Food Biochemistry* 42(1) (2018) e12441.

[237] F. Hu, *Obesity epidemiology*, Oxford University Press 2008.

[238] A. Must, J. Spadano, E.H. Coakley, A.E. Field, G. Colditz, W.H. Dietz, The disease burden associated with overweight and obesity, *Jama* 282(16) (1999) 1523-1529.

[239] S. Enerbäck, The origins of brown adipose tissue, *New England Journal of Medicine* 360(19) (2009) 2021-2023.

[240] J.-P. Despres, S. Moorjani, P.J. Lupien, A. Tremblay, A. Nadeau, C. Bouchard, Regional distribution of body fat, plasma lipoproteins, and cardiovascular disease, *Arteriosclerosis: An Official Journal of the American Heart Association, Inc.* 10(4) (1990) 497-511.

[241] K. Zieger, J. Weiner, K. Krause, M. Schwarz, M. Kohn, M. Stumvoll, M. Blüher, J.T. Heiker, Vaspin suppresses cytokine-induced inflammation in 3T3-L1 adipocytes via inhibition of NFκB pathway, *Molecular and cellular endocrinology* 460 (2018) 181-188.

[242] T. Garin-Shkolnik, A. Rudich, G.S. Hotamisligil, M. Rubinstein, FABP4 attenuates PPARγ and adipogenesis and is inversely correlated with PPARγ in adipose tissues, *Diabetes* 63(3) (2014) 900-911.

[243] M. Furuhashi, S. Saitoh, K. Shimamoto, T. Miura, Fatty acid-binding protein 4 (FABP4): pathophysiological insights and potent clinical biomarker of metabolic and cardiovascular diseases, *Clinical Medicine Insights: Cardiology* 8 (2014) CMC. S17067.

- [244] H. Miyoshi, S.C. Souza, H.-H. Zhang, K.J. Strissel, M.A. Christoffolete, J. Kovsan, A. Rudich, F.B. Kraemer, A.C. Bianco, M.S. Obin, Perilipin promotes hormone-sensitive lipase-mediated adipocyte lipolysis via phosphorylation-dependent and-independent mechanisms, *Journal of Biological Chemistry* 281(23) (2006) 15837-15844.
- [245] H. Wajant, The Fas signaling pathway: more than a paradigm, *Science* 296(5573) (2002) 1635-1636.
- [246] L.A. Tartaglia, The leptin receptor, *Journal of Biological Chemistry* 272(10) (1997) 6093-6096.
- [247] C.-S. Kong, J.-A. Kim, B.-N. Ahn, T.S. Vo, N.-Y. Yoon, S.-K. Kim, 1-(3' , 5' -dihydroxyphenoxy)-7-(2" , 4" , 6-trihydroxyphenoxy)-2, 4, 9-trihydroxydibenzo-1, 4-dioxin Inhibits Adipocyte Differentiation of 3T3-L1 Fibroblasts, *Marine biotechnology* 12(3) (2010) 299-307.
- [248] Y. Dagon, Y. Avraham, E.M. Berry, AMPK activation regulates apoptosis, adipogenesis, and lipolysis by eIF2 α in adipocytes, *Biochemical and biophysical research communications* 340(1) (2006) 43-47.

ACKNOWLEDGEMENT

I would like to express my deep and sincere gratitude to my supervisor, professor You-jin Jeon, for the kindly support of my Ph.D. course and research, for his patience, motivation, enthusiasm, and immense knowledge. His guidance helped me in all the time of research and writing of this thesis. His wide knowledge and logical way of thinking have been of great value to me I could not have imagined having a better supervisor and mentor for my Ph.D. study.

Second, I would like to express my heartfelt gratitude to Professor Yong Li, who recommended me to the Marine Bio-resource Technology Lab. Furthermore, I am also greatly indebted to the professors and teachers at the department of Marine Life Science: Professor Choon Bok Song, Professor Gi-young Kim, and Professor Moon-Soo Heo, who have instructed and helped me a lot in the past years. Special thanks go to Professor Min-cheol Kang, Korea Food Research Institute, for kindly review and comments of my research work.

Third, I would like to thank my lab mates, especially Dr. Yunfei Jiang and Dr. Yuan Lu, for the advices and help during the experiments and study in these years. Also, I would like to thank my teachers and colleagues in Changchun University of Chinese Medicine, Professor Shuying Liu, Professor Changbao Chen, Professor Rui-xue Men, Professor Hao Yue, and Professor Peng Yu, for their enthusiastic supports during my study abroad.

Last but not the least, I would like to thank my wife Chunyan Wu for her great patience and understanding at all times. And for my two babies, Qian and Elmer, I wish I would be a good father in front of you. Without my family's understanding and encouragement, it would have been impossible to finish my study. My parents have given me their great support throughout, as always, for which my mere expression of thanks likewise does not suffice.